6-2020

Selective Targeting of CYP3A5 Through Chemical and Genetic Approaches

William C. Wright
University of Tennessee Health Science Center

Selective Targeting of CYP3A5 Through Chemical and Genetic Approaches

Abstract

Cytochrome P450 enzymes function to catalyze a wide range of reactions important for various biological processes. In humans, the CYP3A subfamily is particularly critical for drug response. Within this family are CYP3A4 and CYP3A5, which collectively metabolize greater than half of all currently prescribed drugs. These promiscuous enzymes can bind a broad and structurally diverse array of compounds, in turn leading to an increased risk of their modulation via small molecules. In the case of CYP3A5, which is over-expressed in some cancers, this leads to chemoresistance. Such aberrant expression and corresponding drug resistance merit a need to selectively target CYP3A5. However, the significant overlap in sequence and structural identity with CYP3A4 as well as flexible and dynamic binding modes make development of a selective inhibitor challenging, and no progress has been made thus far. Moreover, the cancer-specific regulation of CYP3A5 remains unknown, removing the possibility of targeting a factor upstream of its transcription. While CYP3A4 regulation in liver is well-documented, these regulators don't control CYP3A5 in extra-hepatic contexts. This warrants further investigation in order to understand the biological basis of CYP3A5 over-expression in disease models. Here we present discovery of the first isoform-selective CYP3A5 inhibitor. We used high-throughput technology to identify clobetasol propionate as capable of selectively inhibiting CYP3A5 enzymatic activity without conferring CYP3A4 inhibition. We further demonstrate the in vitro ability of the compound using a clinically relevant cell model with CYP3A5 overexpression and CRISPR/Cas9-mediated full genetic deletion. Additionally, we explore the mechanism of selectivity, employing computational and biophysical techniques to illustrate how subtle active site differences allow the compound to adopt a tight heme-ligand coordination exclusively in CYP3A5 and serving as the basis of its selective inhibition.

Document Type

Dissertation

Degree Name

Doctor of Philosophy (PhD)

Program

Biomedical Sciences

Research Advisor

Taosheng Chen, Ph.D.

Keywords

Cellular biology

Subject Categories

Medical Sciences | Medicine and Health Sciences

UNIVERSITY OF TENNESSEE HEALTH SCIENCE CENTER

DOCTOR OF PHILOSOPHY DISSERTATION

Selective Targeting of CYP3A5 Through Chemical and Genetic Approaches

---

Author:
William C. Wright

Advisor:
Taosheng Chen, PhD

A Dissertation Presented for The Graduate Studies Council of
The University of Tennessee Health Science Center
in Partial Fulfillment of the Requirements for the
Doctor of Philosophy degree from
The University of Tennessee

in

Biomedical Sciences: Cancer and Developmental Biology
College of Graduate Health Sciences

June 2020

DEDICATION

To my beloved brother Zachary, who motivates me each day to be my best.

ACKNOWLEDGEMENTS

I express my deepest gratitude and appreciation to my mentor Dr. Taosheng Chen for allowing the opportunity to become a scientist under his guidance. The experiences I've gained in his laboratory enable me to do important and exciting research. His hands-off approach to mentoring allowed me the freedoms to succeed and to fail on my own, and I wholeheartedly consider this to be the most important part of my training. Dr. Chen has always been an incredible source of support and motivation for me, and constantly inspires me to do good science.

I am profoundly grateful to Dr. Len Lothstein, who is responsible for the start of my academic journey. He took a chance on me and facilitated my acceptance into his graduate program. The program was transformative, and his advice and guidance taught me the practical knowledge of how to become a good researcher. His teachings gave me a wealth of insight far beyond traditional academic learning and were critical for my development. Once I expressed interest in pursuing a Ph.D., Dr. Lothstein was my biggest supporter and was an instrumental part in my progression into the Chen lab. I will carry what I learned from him into all aspects of my future profession.

In addition to Dr. Chen and Dr. Lothstein, I'm thankful to have other brilliant scientists on my committee. Dr. Erin Schuetz who inspires me not only by the excellent caliber of her work, but by the excited and joyful tone she uses when discussing some very complex research. Dr. David Nelson who taught me the world of biochemistry, and whose passion for Cytochrome P450 enzymes was a wonderful source of motivation for my own work. Dr. Kirk Hevener who provided his valuable expertise to my computational chemistry endeavors, and whose feedback always gives me a sense that my work is well-respected. Dr. Marcus Fischer, an outstanding structural biologist who exercised great patience with me and met my plethora of questions with a calm and insightful attitude. I'm thankful to each member of my committee for their contribution to my research, and the time they took to guide me on my academic pursuit.

Finally, I acknowledge the tremendous help from all members of the Chen research lab. Over the few years I've been in the lab, I've only had good interactions with my lab mates, all of whom played critical roles in allowing me to reach the end of this journey. I'm particularly grateful to Dr. Jing Wu for training me in cell culture and for indirectly teaching me the value of kindness in a lab setting. I also recognize that without the collaborative opportunities afforded to me by Dr. Jesse Bake, Dr. Sergio Chai, Dr. Peter Oladimeji, and Dr. Andrew Huber, that I could not have gotten to the point I reached in the end. Each of these scientists took a risk by allowing a student to play major parts of their research, and I am extremely thankful for them.

ABSTRACT

Cytochrome P450 enzymes function to catalyze a wide range of reactions important for various biological processes. In humans, the CYP3A subfamily is particularly critical for drug response. Within this family are CYP3A4 and CYP3A5, which collectively metabolize greater than half of all currently prescribed drugs. These promiscuous enzymes can bind a broad and structurally diverse array of compounds, in turn leading to an increased risk of their modulation via small molecules. In the case of CYP3A5, which is over-expressed in some cancers, this leads to chemoresistance. Such aberrant expression and corresponding drug resistance merit a need to selectively target CYP3A5. However, the significant overlap in sequence and structural identity with CYP3A4 as well as flexible and dynamic binding modes make development of a selective inhibitor challenging, and no progress has been made thus far. Moreover, the cancer-specific regulation of CYP3A5 remains unknown, removing the possibility of targeting a factor upstream of its transcription. While CYP3A4 regulation in liver is well-documented, these regulators don't control CYP3A5 in extra-hepatic contexts. This warrants further investigation in order to understand the biological basis of CYP3A5 over-expression in disease models.

Here we present discovery of the first isoform-selective CYP3A5 inhibitor. We used high-throughput technology to identify clobetasol propionate as capable of selectively inhibiting CYP3A5 enzymatic activity without conferring CYP3A4 inhibition. We further demonstrate the *in vitro* ability of the compound using a clinically relevant cell model with CYP3A5 overexpression and CRISPR/Cas9-mediated full genetic deletion. Additionally, we explore the mechanism of selectivity, employing computational and biophysical techniques to illustrate how subtle active site differences allow the compound to adopt a tight heme-ligand coordination exclusively in CYP3A5 and serving as the basis of its selective inhibition.

In addition to directly targeting CYP3A5 itself, we also uncovered its upstream transcriptional regulators in the same cancer-specific context. We developed a computational pipeline capable of taking large and heterogenous expression data from patient tumors, and outputting co-expression networks. We leveraged the power of our tool to produce putative transcriptional regulators of a given target and applied it to CYP3A5. We screened all candidates experimentally and show that, when knocked down, our top hits completely ablate CYP3A5 expression. Interestingly, we show that a peptide and enzyme control CYP3A5 mRNA levels more strongly than our top transcription factor hit. This discovery highlights the utility of our tool and illuminates previously unreported targets, ultimately providing more insight into the biology of CYP3A5-expressing cancers.

TABLE OF CONTENTS

CHAPTER 1. INTRODUCTION 1

The CYP3A Family of Drug-Metabolizing Enzymes 1
Interplay Between CYP3A and Small Molecules 1
Roles Involving Endogenous Compounds 3
Important Exogenous Substrates and Metabolites 4
CYP3A Modulation by Small Molecules 5
Selective Catalysis and Substrate Recognition 9
Structural Insights 11
Secondary Structures and Flexibility 11
Contrasting Active Sites and Consequences Therein 12
Comparisons to Other Human CYPs 15
Further Perspectives 16
Hypothesis and Specific Aims 17
Aim 1: Small Molecule Selective Inhibition of CYP3A5 17
Aim 2: Characterizing Mechanism of Isoform-Selective Inhibition 17
Aim 3: Uncovering Transcriptional Regulators of CYP3A5 in Cancer 17

CHAPTER 2. SELECTIVE INHIBITION OF CYP3A5 18

Relevance of Selective Modulation 18
High-Throughput Screening Identifies Clobetasol as a Selective CYP3A5 Inhibitor 19
Pancreatic Cancer Is an Appropriate and Clinically Relevant Model for Studying Selective Modulation of CYP3A5 22
Clobetasol Selectively Inhibits CYP3A5 in Cells 22
Molecular Dynamics Simulations Predict the Mechanism of Selective Inhibition by Clobetasol 26
Differential Interaction of Clobetasol with the Heme in CYP3A4 and CYP3A5 32

CHAPTER 3. TRANSCRIPTIONAL REGULATION OF CYP3A5 36

Regulation of CYP3A5 in Pancreatic Cancer Remains Unknown 36
Development of a Novel Computational Method of Regulator Prediction 36
COLDSTaR Analysis of Pancreatic Tumors 41
COLDSTaR Captures Transcriptional Regulators of CYP3A5 42
Knockdown of Predicted Transcriptional Regulators Ablates CYP3A5 mRNA Expression 44

CHAPTER 4. METHODOLOGY 47

Compounds Used 47
CYP3A4 and CYP3A5 Biochemical Inhibition 47
Clobetasol Inhibition Profiling Against a Panel of Major Human CYPs 48
Data Mining to Profile CYP3A5 Expression Across Cancer Types 49
RNA Extraction and Sequencing 49
RNA-Seq Data Analysis 49

Cell Culture Method 50
Generation of Stable AsPC-1 Cells with Inducible Overexpression of CYP3A4 and CYP3A5 51
Western Blot Analysis 51
CRISPR/Cas9-Mediated Deletion of CYP3A5 52
LC-MS/MS Detection of Midazolam and 1-Hydroxymidazolam 52
Confluence Imaging 53
Ligand Docking and Molecular Dynamics Simulations 54
Cloning of CYP3A4 and CYP3A5 for Bacterial Protein Expression 55
Expression and Purification of CYP3A4 and CYP3A5 55
UV-Visible Absorbance Titrations with CYP3A4 and CYP3A5 57
EPR Spectroscopic Analysis of CYP3A4 and CYP3A5 57
Statistics for CYP Inhibition 57
COLDSTaR Development and Analysis of Pancreatic Cancer 58
NetBID Analysis of Pancreatic Cancer 58
siRNA Screening of Predicted CYP3A5 Regulators 59
qPCR-Based Validation of CYP3A5 Regulators 59

CHAPTER 5. DISCUSSION 61

LIST OF REFERENCES 67

VITA 84

LIST OF FIGURES

Figure 1-1. Protein sequence homology among CYP3A enzymes.....2

Figure 1-2. Effects of various compounds on CYP3A.....6

Figure 1-3. Promiscuity of the CYP3A ligand binding pocket. 13

Figure 1-4. Structural differences in CYP3A conformations. 14

Figure 2-1. Clobetasol propionate is a potent and selective inhibitor of CYP3A5. 21

Figure 2-2. CYP3A5 is over-expressed in pancreatic cancer models and AsPC-1 cells are ideal for studying CYP3A5 modulation.....23

Figure 2-3. Normalized expression of CYP3A4 and CYP3A5 across various cancer types. 24

Figure 2-4. Clobetasol selectively inhibits CYP3A5 *in vitro*.....25

Figure 2-5. Overlay of clobetasol docked into CYP3A4 and CYP3A5. 28

Figure 2-6. RMSD of CYP3A4 and CYP3A5 molecular dynamics simulations. 29

Figure 2-7. Molecular dynamics simulations suggest that clobetasol forms a heme-ligand coordination in CYP3A5 but not in CYP3A4. 30

Figure 2-8. Overlay of crystalized and simulated water-bound CYP3A4. 31

Figure 2-9. UV-Vis and EPR spectroscopy of clobetasol binding. 33

Figure 2-10. Spectral changes of CYP3A4 and CYP3A5 from various compounds. 34

Figure 3-1. Neither PXR nor HNF4α control CYP3A5 in AsPC-1 cells. 37

Figure 3-2. COLDSTaR analysis of pancreatic tumors. 40

Figure 3-3. COLDSTaR captures transcriptional regulators of CYP3A5. 43

Figure 3-4. Knockdown of predicted transcriptional regulators ablates CYP3A5 mRNA expression. 45

LIST OF ABBREVIATIONS

CHOL	Cholangiocarcinoma
Clobetasol	Clobetasol Propionate
CW	Continuous Wave
CYP3A	Cytochrome P450 3A Family
Dox	Doxycycline
HS	High Spin
Keto	Ketoconazole
LIHC	Liver and Hepatocellular Carcinoma
LS	Low Spin
MDZ	Midazolam
PDAC	Pancreatic Ductal Adenocarcinoma
RMSF	Root-Mean-Square Fluctuation
RNAi	RNA Interference
RNA-Seq	RNA Sequencing
TCGA	The Cancer Genome Atlas
1OH-MDZ	1′-Hydroxymidazolam
3A4OE	CYP3A4 Overexpression
3A5−/−	CYP3A5 Genetic Deletion
3A5OE	CYP3A5 Overexpression

CHAPTER 1. INTRODUCTION*

The CYP3A Family of Drug-Metabolizing Enzymes

The human cytochrome P450 3A (CYP3A) family is part of the broader CYP superfamily of heme-containing enzymes. The CYP3A enzymes are critical for metabolizing both endogenous and exogenous compounds, and they have been reported to metabolize more than half of all currently prescribed drugs.[1] Members of the CYP3A family include CYP3A4, CYP3A5, CYP3A7, and CYP3A43. These enzymes catalyze various reactions and have exceptionally broad substrate specificity. Because of their ability to interact with structurally diverse compounds, CYP3A enzymes have a high capacity for modulation to change drug responses. CYP3A4 and CYP3A5 are the best characterized members of the family and are reported to be mostly functionally redundant, but they do exhibit differences in their regulation and mRNA expression, as we have reviewed previously.[2] CYP3A4 is considered the most important drug-metabolizing enzyme in the body and is the most abundant isoform in the liver, whereas CYP3A5 is the primary source of extra-hepatic CYP3A. CYP3A7 is primarily expressed in fetal liver. [3,4] CYP3A43 remains poorly characterized but does have clinical significance stemming from its genetic variation.[5,6] CYP3A enzymes display high protein sequence homology (**Figure 1-1**), which is the basis of the functional redundancy assumptions made by many researchers. Although several differences in substrate specificity or catalytic efficiency have been reported within the CYP3A family,[7,8] one of the most striking differences was recently highlighted by evidence implicating CYP3A5 specifically in the progression of pancreatic ductal adenocarcinoma (PDAC).[9] Structural evidence has been obtained for both CYP3A4 and CYP3A5, enabling investigations of the subtle differences between their active sites. Detailed here are some of the differences in the drug metabolism and modulation profiles within the CYP3A family. Clinically relevant consequences of the differences between these enzymes are discussed, and structural perspectives are provided to further the understanding of isoform-selective effects.

Interplay Between CYP3A and Small Molecules

The CYP3A enzymes can interact with a vast array of small molecules. Accordingly, it's of no surprise that these molecules are of differing classes, come from different sources, and have different intended biological functions.

---

*Reprinted from final submission with permission. Lolodi, O., Wang, Y. M., Wright, W. C. & Chen, T. Differential Regulation of CYP3A4 and CYP3A5 and its Implication in Drug Discovery. Curr Drug Metab 18, 1095-1105, https://doi.org/10.1016/j.livres.2019.08.001%20 (2017) [2]

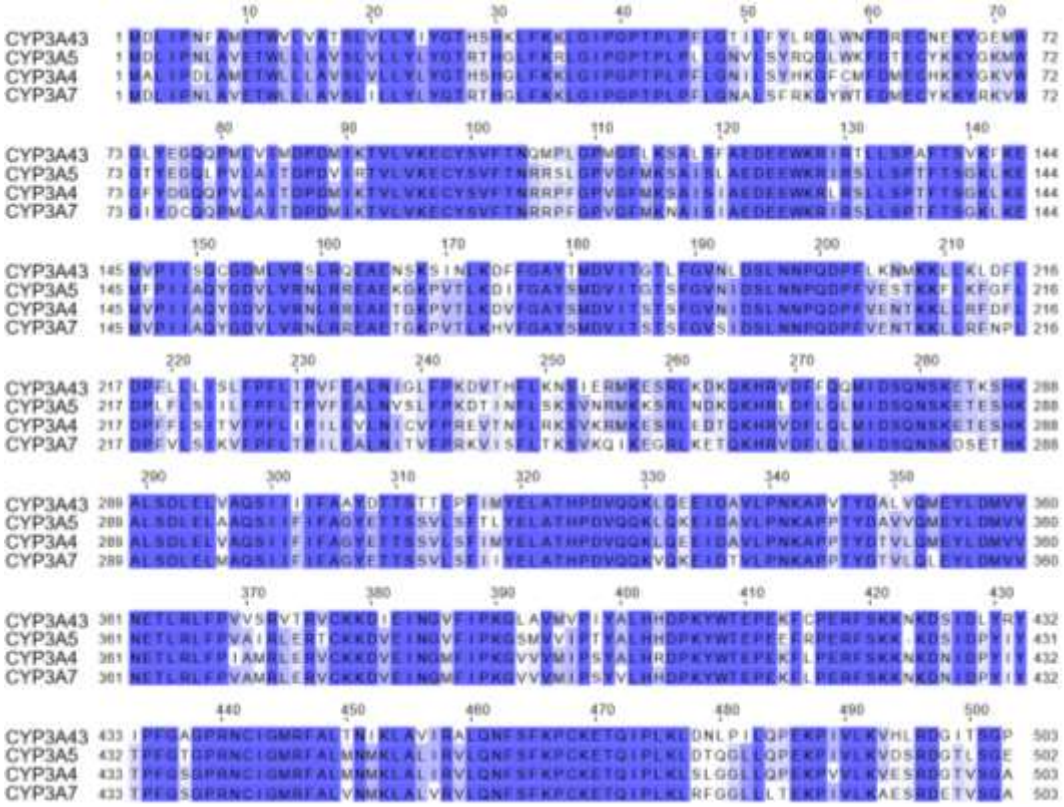

Figure 1-1. Protein sequence homology among CYP3A enzymes.

Members of the human CYP3A family were aligned and colored by protein sequence homology, with blue indicating a complete match and white indicating a residue deviation.

Roles Involving Endogenous Compounds

Most current research involving enzymes of the CYP3A family relates to their modulation by, or interactions with, exogenous compounds, primarily those intended for medicinal purposes. However, important and clinically relevant information has been obtained from studies of the endobiotic roles of these enzymes. Although CYP3A enzymes act on a wide range of structurally diverse compounds, most studies of these enzymes in the context of endogenous metabolism have focused on substrates with structural similarities. For example, CYP3A members play an important role in bile acid and steroid metabolism. CYP3A4, CYP3A5, and CYP3A7 selectively catalyze the 1β-hydroxylation of the secondary bile acid deoxycholic acid.[10] The 1β-hydroxydeoxycholic acid (1β-OHDCA) metabolite has been proposed as a urinary biomarker with which to assess potential CYP3A-mediated drug–drug interactions.[10] Cholesterol, another endogenous steroid, also has a metabolite produced by CYP3A4 and CYP3A5, which again demonstrates the clinical relevance of the CYP3A family. Mao *et al*. reported on the suitability of the metabolite 4β-hydroxycholesterol (4β-HC) for studying CYP3A inducers such as the well-established inducer rifampicin.[11,12] Knowledge of the CYP3A inducibility potential contributed by a given drug is key to understanding the response of that drug. Furthermore, several inducers of CYP3A members act on upstream regulators and have been implicated in drug-induced liver injury (DILI), as we previously reviewed.[13] Probing for an endogenous metabolite to compare its level to the baseline in the presence or absence of a drug is one way to detect the CYP3A induction potential of a compound. Measuring the plasma levels of 4β-HC is a cost-effective and minimally invasive approach to studying CYP3A4 and CYP3A5.[11,14] Measurement of this metabolite has also been used to compare the inducibility of CYP3A4 with various drugs, and it has even been applied as a guideline for dosing adjustments.[15] The plasma 4β-HC level has been reported to be a useful parameter for studying CYP3A interactions in nonhuman animals such as rats, mice, and dogs.[16]

Although there has been considerable research on deoxycholic acid and cholesterol metabolism, perhaps the most extensive body of knowledge concerning the role of the CYP3A family with respect to endogenous steroids has come from investigations of the sex hormone testosterone. Testosterone has several metabolic fates, but CYP3A enzymes are responsible for producing the 6β-hydroxy metabolite.[17] This catalysis is widely used to study the effects of potential CYP3A-interacting drugs, owing to the robustness and sensitivity of regioselective testosterone hydroxylation by these enzymes. More recently, plasma levels of 4β-hydroxycholesterol have been used for CYP3A activity probes.[18] Assays for measuring the levels of testosterone metabolites by comparison to those obtained with ketoconazole as a control inhibitor have been developed and optimized as a straightforward means of assessing CYP3A activity.[19] Importantly, CYP3A4 and CYP3A5 have both been shown to catalyze this reaction, although less metabolite is contributed from CYP3A5 when human liver samples are used, owing to the lower hepatic expression of CYP3A5.[20] Probing for 6β-hydroxytestosterone (6β-OHTST) is of particular value when examining samples with diverse populations of P450s, such as those from liver.[21]

Steroidal derivative endogenous substrates of the CYP3A family also exist. One example was reported by Gupta *et al.*, who demonstrated that CYP3A4 acts upon vitamin D.[22] Although nonselective, CYP3A4 catalyzes the 25-hydroxylation of 1α-hydroxyvitamin D_2 (1α-OHD_2), and, to a lesser extent, 1α-hydroxyvitamin D_3 (1α-OHD_3).[22] Before this finding, this 25-hydroxylation was reported as being catalyzed only by CYP24A1.[23] Although 1α-OHD_2 can be metabolized by CYP3A4, its capacity to act as a sensor of CYP3A activity should not be heavily relied upon, as the metabolite detected in serum does not correlate well with the established 4β-HC metabolite.[24]

Important Exogenous Substrates and Metabolites

Given the remarkable promiscuity of the CYP3A family, it is not surprising that a broad range of prescription medications can serve as their substrates. These enzymes can metabolize many different classes of compound, each comprising many structurally diverse subsets. The effects of CYP3A–drug interactions vary greatly according to the individual drug, and these consequences need to be studied carefully to address unintended side effects. Chemotherapeutics are one class of drug that is largely implicated in CYP3A interactions.[25] For example, the microtubule-destabilizing vinca alkaloids vincristine, vinblastine, and vindesine are substrates of CYP3A4, CYP3A5, and CYP3A7.[26,27] Other antimitotics of the same parent class, such as the taxanes paclitaxel and docetaxel, are also metabolized by these enzymes.[28,29] Although paclitaxel is subject to CYP3A-mediated hydroxylation at different sites, it has been demonstrated that the 6α product is the primary metabolite.[30] One consequence of this is a 30-fold loss in the cytotoxic activity of the drug.[30] Likewise, docetaxel is metabolized by CYP3A into completely inactive metabolites.[31] Another example within this subclass is cabazitaxel. Although this is a substrate for CYP2C8, CYP3A4 is reported to be primarily responsible for the substantial decrease in the oral bioavailability of the compound.[32] CYP3A-mediated inactivation of pharmaceuticals is clearly a problem with respect to drug efficacy; however, some consequences of CYP3A metabolism are more serious and pose significant health risks to patients via the generation of toxic metabolites.

Tyrosine kinase inhibitors (TKIs) have been adopted as useful compounds for treating various cancers and other diseases. Many approved drugs within this class are subject to CYP3A-mediated biotransformation as their primary metabolic pathway, as reviewed elsewhere.[33] Some TKI metabolites not only lessen the intended effects of the drug, but also exhibit considerable toxicity themselves. Adverse reactions resulting from these metabolites can lower the quality of life for the patient and often necessitate a reduction in the dosage of a drug, thus dampening its intended effect.[34] The Human epidermal growth factor receptor/proto-oncogene neu (EGFR/HER-2) inhibitor lapatinib is one example of a compound whose CYP3A4- and CYP3A5-catalyzed metabolites have been implicated in severe drug-induced hepatotoxicity and even in some fatalities.[35] Furthermore, the concentration of lapatinib can be dramatically influenced by the induction or inhibition of CYP3A4 activity—260% increases in the AUC have been reported when the CYP3A4 activity is inhibited with ketoconazole.[36] Thus, modulating the enzymes responsible can influence the concentrations of harmful metabolites.

Another example of CYP3A-mediated hepatotoxicity arising from TKI metabolism is associated with the BCR-ABL inhibitor dasatinib. CYP3A4 oxidizes this compound to produce at least two reactive intermediates with the capacity to covalently bind proteins.[37] Quinone-imine products are formed by further dasatinib oxidation and are partly responsible for the toxic effects. Interestingly, one of the metabolites is active and equipotent to dasatinib itself.[35] The EGFR inhibitor erlotinib is another approved medicine of this class that is a substrate of CYP3A4 and CYP3A5.[38] Erlotinib is approved for non–small cell lung cancer and pancreatic cancer, but its toxicity must be considered before it is given to patients. Skin-related adverse reactions and, more seriously, acute hepatotoxicity have been reported for this compound.[39] Although not explicitly reported as a function of any one metabolite, it is proposed that this toxicity occurs via reactive epoxide and electrophilic quinone-imine intermediates produced largely by CYP3A4.[40] Additionally, it is possible that TKI metabolites produced by the CYP3A pathway induce toxicity by altering gene expression. Microarray profiling has been used to investigate this effect in patients with PDAC who develop erlotinib-associated skin toxicity, possibly potentiated through CYP3A.[41]

Outside the realm of chemotherapeutics, opioids are another class of drugs that are partly metabolized by the CYP3A system. In particular, CYP3A4 has been reported to be a critical mediator of the efficacy of these compounds and of the patient response to many of them.[42] The use of opioids as pain-management tools for patients with cancer also requires careful thought regarding the extensive interplay between these drugs and CYP3A enzymes. The induction or inhibition of opioids by the responsible CYPs may drastically alter the intended analgesic effects. Administering compounds that result in CYP3A4 induction, for example, will markedly reduce the pain-alleviating effects and potentially require higher dosing than would otherwise be expected.[42] One commonly prescribed opioid substrate of CYP3A enzymes is alfentanil, a synthetic opioid that is metabolized by CYP3A4 and CYP3A5 into the primary metabolite noralfentanil.[43] Because of the extensive CYP3A-mediated metabolism of alfentanil, as with several other opioids, modulation of one of the enzymes responsible can produce drastic effects in the context of drug disposition. Indeed, it was reported that the induction of CYP3A4 with rifampicin produced a 3-fold increase in alfentanil clearance.[44] In addition to small molecule modulation, inherent expression differences among CYP3A enzymes resulting from interindividual variability also contribute to this highly variable drug clearance.[44]

CYP3A Modulation by Small Molecules

The clinical impact of modulating CYP3A enzymes is so significant that the Food and Drug Administration (FDA) recommends testing new drugs for potential CYP3A interactions and doing so by using two structurally unrelated substrates.[45] Moreover, the CYP3A family can be modulated by various compounds, including FDA-approved drugs, in some fashion – with both overlapping and distinct catalytic activities (**Figure 1-2**). Among the most potent and effective modulators of CYP3A4 and CYP3A5 are azole-containing antifungal compounds. Ketoconazole, a prototypical CYP3A inhibitor, has submicromolar IC_{50} values for CYP3A4.[46]

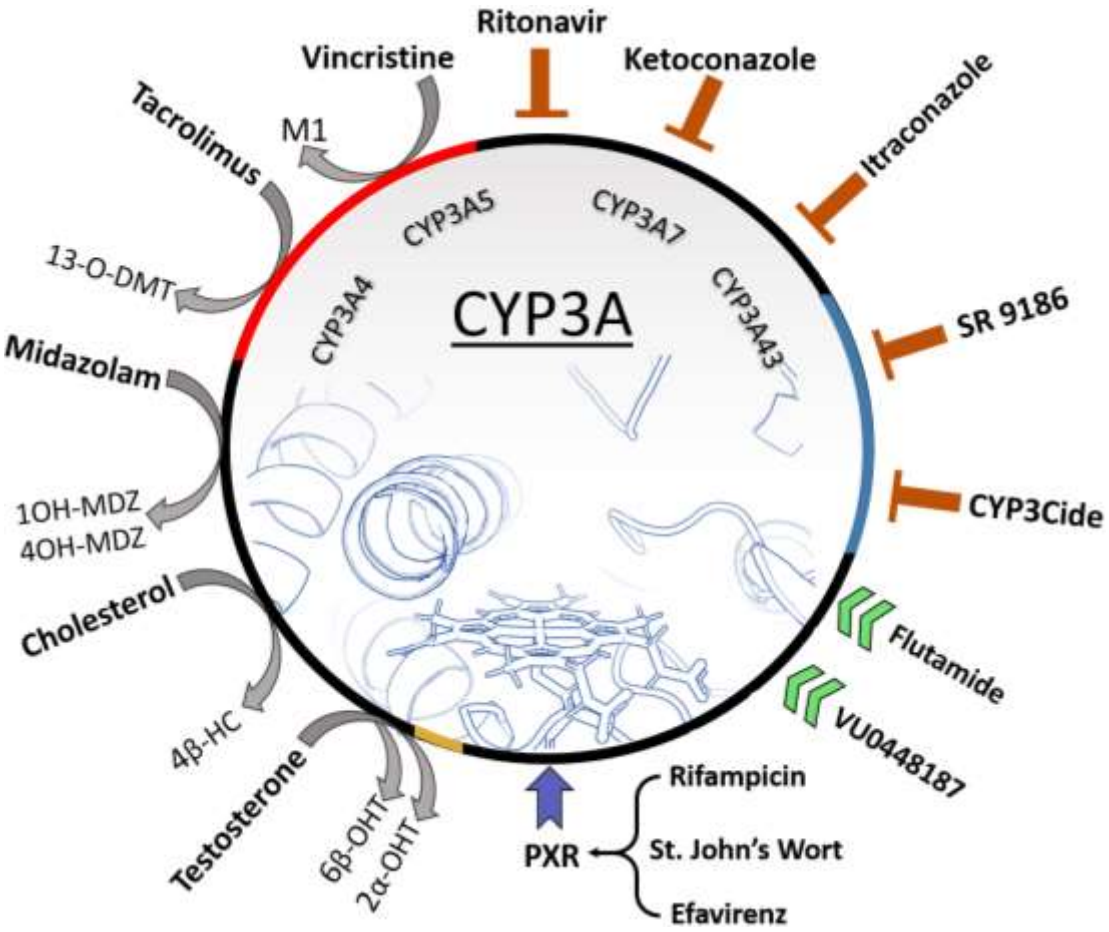

Figure 1-2. Effects of various compounds on CYP3A.

Several relevant endogenous compounds, pharmaceuticals, or tool compounds are indicated as substrates (gray curved arrows), inhibitors (orange flattened arrows), enzymatic activators (green double arrows), or inducers (purple arrow) of CYP3A. Known selectivity information is indicated along the circle as red (CYP3A5-selective), blue (CYP3A4-selective), yellow (CYP3A7-selective), or black (unknown or non-selective).

Concordantly, ketoconazole mediated CYP3A inhibition in patients dramatically reduces the metabolism of many drugs that are subject to hepatic clearance. The inhibitory effects of ketoconazole on CYP3A activity in patient populations have far-reaching consequences for drugs intended for various uses, such as diminishing metabolism of the antipsychotic risperidone,[47] the sedative midazolam,[48] the kinase inhibitors fostamatinib[49] and midostaurin,[50] and the contraceptive drospirenone,[51] among others. The antifungal isavuconazole is a more moderate inhibitor of CYP3A4 than is ketoconazole, but it still influences the metabolism of CYP3A substrates such as midazolam and norethindrone in patients.[52] Apart from the studies of antifungal effects in humans, several cell-based *in vitro* studies have also demonstrated the ability of these compounds to modulate CYP3A activity and have addressed the responses to specific isoforms by using recombinantly expressed enzymes. For example, Godamudunage *et al.* tested 13 different azole-containing drugs to evaluate their modulation of CYP3A4 versus CYP3A7.[53] Although some of the tested compounds demonstrated CYP3A7 inhibition, the inhibitory effect of these compounds on CYP3A4 was consistently more pronounced.[53] This is of particular clinical relevance because CYP3A4 is expressed in adult liver, whereas CYP3A7 is primarily expressed in neonates. Moreover, when testing nine antifungals for CYP3A4 and CYP3A5 inhibition, Niwa *et al.* reported that the commonly prescribed itraconazole, ketoconazole, and miconazole were more inhibitory than were other azole drugs.[54]

Antiretroviral drugs are an example of a class of compounds that contains both inducers and inhibitors of CYP3A. Some drugs in this class can directly bind to and inactivate CYP3A enzymes, whereas others interact with upstream transcription factors and induce CYP3A expression. CYP3A4 for example is inducible primarily via the Pregnane X Receptor (PXR), but also by other nuclear receptors like the Constitutive Androstane Receptor (CAR), Retinoid X Receptor (RXR), Vitamin D Receptor (VDR), and transcription factors like Hepatocyte Nuclear Factor 4 alpha (HNF4A).[55,56] Various antiretrovirals induce CYP3A4 by engaging its upstream regulators. For example, efavirenz is an antiretroviral that strongly induces the expression of CYP3A4 via activation of the human transcription factor pregnane X receptor (PXR),[54] whereas atazanavir inhibits CYP3A4.[57] Ritonavir is one of the strongest CYP3A inhibitors in this class, having an IC_{50} of 14 nanomolar, and is even used as a pharmacokinetic boosting agent for other similar compounds because it so effectively halts CYP3A catalysis.[58] Interestingly, the strong inhibitory effect of this antiretroviral can be exploited for other drug classes. For example, it has been proposed to use ritonavir in patients with cystic fibrosis (CF) to inhibit the metabolism of the anti-CF drug ivacaftor and thereby curtail the CYP3A-mediated adverse effects that would otherwise result in reduced efficacy of the latter drug.[59] Cobicistat is often used in a similar manner to ritonavir and acts as an inhibitor for and substrate of CYP3A4.[60] Although both of these drugs modulate CYP3A via potent inhibition, cobicistat has been reported to be more specific for CYP3A, having fewer interactions with other CYPs;[61] accordingly, it has been proposed as an important component of combination regimens for Human immunodeficiency virus (HIV) management.[62] Not all antiretroviral drugs modulate CYP3A enzymes equipotently, however: Although ritonavir is a preferential and potent inhibitor of CYP3A4 and CYP3A5, its inhibition of CYP3A7 is weaker.[63] This information may prove beneficial

when treating infants with these compounds. The varying effects and wide potential for CYP3A-mediated adverse interactions when antiretrovirals are used in combination with other medications necessitates careful consideration when prescribing these drugs.

Apart from conventional medications that act as small molecule modulators of CYP3A, natural products present in common foods can also exert such effects. The best-known example was discovered nearly 30 years ago when it was reported that grapefruit juice changed the bioavailability of the antihypertensives felodipine and nifedipine.[64] It is now accepted that more than 80 commonly prescribed drugs interact unfavorably with grapefruit juice, resulting in serious adverse reactions such as rhabdomyolysis, myelotoxicity, nephrotoxicity, and respiratory depression.[65] The observed consequences are a direct result of potent inhibition of CYP3A enzymes (primarily CYP3A4, according to reports), which results in a failure to metabolize these compounds and, thus, in the accumulation of toxic concentrations in the body. Bergamottin is the furanocoumarin in grapefruit that is responsible for CYP3A4 inhibition; importantly, it causes mechanism-based (or "suicide") inactivation.[66] This irreversible inhibition is caused by covalent modification of CYP3A4 and contributes more substantially to a reduction in the available enzyme when compared to a reversible inhibitor.[67] In addition to the unfavorable increase in the bioavailability of many drugs, grapefruit juice also inhibits the metabolic activation of CYP3A prodrugs—two examples thus affected are the blood thinners clopidogrel and prasugrel.[68,69] Other natural products originating from fruits and vegetables have been reported as modulators of CYP3A enzymes. Cabbage and onion juices, for example, were reported to be inhibitors of CYP3A4 activity in both biochemical- and cell-based experiments.[70] Bael fruit,[71] evodia fruit,[70] goji berry,[72] and starfruit[73] all contain small molecule CYP3A inhibitors that lead to various adverse drug interactions. Studies have also implicated CYP3A enzymes in herb-drug interactions. These studies help to explain some of the toxicities associated with traditional medicines and modern drugs. Cat's claw and peppermint oil are examples of highly potent CYP3A4 inhibitors that may interfere with prescription medications.[74] *Schisandra chinensis* (magnolia vine) is a plant used in traditional Chinese medicine that contains CYP3A4 and CYP3A5 inhibitors that lead to dramatically higher bioavailability profiles of certain CYP3A-interacting drugs.[75] Furthermore, natural products from foods and herbs can also be inducers of CYP3A enzymes. St. John's wort is one such example; hyperforin, a component of St. John's wort, acts as a potent inducer of CYP3A4 expression by activating its upstream transcriptional regulator PXR.[76,77] The use of this herb in patients taking prescription medications presents a serious safety concern because of the high potential for interactions.[78] The routine consumption of food products containing CYP3A modulators may account for observed differences in drug efficacy and toxicity, beyond what can be explained by interindividual variability.

One interesting form of CYP3A modulation is that of direct enzymatic activation, whereby a compound binds to an enzyme and induces a level of enzymatic activity that is higher than the basal levels. Modulators in this category are generally considered to be allosteric regulators that bind outside or distal from the classical heme-containing active site in a manner that structurally enables increased catalysis. A few researchers have hypothesized the existence of peripheral ligand-binding sites for CYP3A4.[79–80] The

compound 5-(4-fluorobenzyl)-2-((3-fluorophenoxy)methyl)-4,5,6,7-tetrahydropyrazolo[1,5-a]pyrazine (hereafter referred to as VU0448187) is an activator of CYP3A4 and CYP3A5 that increases midazolam hydroxylation activity by more than 100-fold compared to the baseline level.[81] Interestingly, the activity of VU0448187 is reportedly substrate dependent; it affects the hydroxylation of midazolam, but not that of testosterone and progesterone. [82] As VU0448187 is intended as a ligand of metabotropic glutamate receptor 5 ($mGlu_5$), there is a possibility of drug–drug interactions.[81] Similarly, the prescription androgen receptor antagonist flutamide and its metabolite 2-hydroxyflutamide are also CYP3A heterotropic activators.[83] Flutamide can induce CYP3A4 and CYP3A5 midazolam hydroxylation activity that is more than 100% higher than the basal level and can result in a dramatic increase in the CYP3A substrates nifedipine and amiodarone.[83] A particularly interesting case of CYP3A activation involves the platelet aggregation inhibitor ticagrelor. This compound exhibits an intriguing bimodal modulation of CYP3A activity, whereby the hydroxylation of midazolam to 4-hydroxymidazolam is mildly inhibited but the conversion to 1-hydroxymidazolam is mildly increased.[84] This may contribute to the adverse effects seen when patients are given ticagrelor with CYP3A inducers.[82] Progesterone has also been proposed as a CYP3A4 allosteric activator,[85] but little work has been done to investigate its effect on drug–drug interactions as a direct result. Isoform-selective allosteric activation was reported with the TKI icotinib, which appears to activate CYP3A5 but not CYP3A4.[86] Small molecule enzymatic activators of CYP3A family members represent yet another potential source of drug–drug interactions. The unintended increase in CYP3A metabolic activity (and, thus, the unintended increase in CYP3A-mediated metabolism of drugs) means that caution is warranted when drugs are taken alongside these activators.

Selective Catalysis and Substrate Recognition

Members of the CYP3A family are commonly regarded as having enough overlapping substrate specificity to justify considering them as a single enzyme. Indeed, many research studies do not differentiate between the isoforms and frequently use annotations such as “CYP3A4/5.” The tissue-specific expression and overall abundance of each enzyme in the CYP3A family is occasionally taken into account, but the individual metabolic capabilities of these enzymes receive much less consideration. However, several isoform-specific or isoform-preferential reactions are known to occur within the CYP3A family, and some have clinical relevance. In recent years, important tool compounds have been developed that exploit subtle differences between CYP3A4 and CYP3A5, enabling evidence of isoform-specific catalytic activities to be obtained. In 2012, two separate groups published the first reports of CYP3A4-selective inhibitors. SR-9186 is a CYP3A4 inhibitor demonstrating 1000-fold selectivity over CYP3A5,[87] whereas CYP3cide is a mechanism-based (irreversible) CYP3A4-selective inhibitor.[88] At present, there is no selective CYP3A5 inhibitor available. Although there is a clear need for an isoform-selective CYP3A5 inhibitor, it has been suggested that the development of such a compound presents a considerable challenge. [9,89,90] This is probably based on the observation that when a compound tends to inhibit both CYP3A4 and CYP3A5, it is

almost always CYP3A4 that is more potently inhibited. However, a probe compound for selectively measuring CYP3A5 does exist. In 2014, the N-oxide metabolite of the phosphodiesterase inhibitor T-1032 (hereafter referred to as T5NO) was the first compound to be identified as a highly selective metabolite catalyzed by CYP3A5, demonstrating greater than 100-fold selectivity over CYP3A4.[91] Although T-1032 is metabolized by CYP3A4, CYP3A5, and CYP2C8, the T5NO metabolite is produced almost exclusively by CYP3A5. These tool compounds have proved instrumental in the delineation of the discrete contributions of CYP3A isoforms.

Vincristine was one of the earliest compounds reported to be catalyzed preferentially by a CYP3A isoform. Dennison *et al.*[7] tested various recombinantly expressed CYPs and showed that vincristine oxidation was significantly more efficient in the context of CYP3A5 as compared to CYP3A4. In a subsequent study, the same authors further characterized the CYP3A5-mediated 14-fold metabolite increase, reporting that genetic polymorphisms of CYP3A5 play major roles in the biotransformation of this compound.[92] Moreover, when CYP3A5 is inactive because of genetic polymorphisms, vincristine-induced toxicity is heightened, further suggesting that CYP3A5 is critical for the clearance of this drug.[93] Importantly, there is evidence that the CYP3A5 genotype is not the only causative factor associated with vincristine toxicity.[94] No structure for CYP3A5 bound with vincristine has yet been solved, but molecular dynamics simulations have been employed to help explain its preferential catalysis,[95] and the researchers who conducted those simulations hypothesized that vincristine binds to CYP3A5 in an orientation different from that of CYP3A4, enabling it to interact more tightly with critical active-site residues. Another well-characterized association between CYP3A5 and selective catalysis is that observed with the immunosuppressant tacrolimus. Patients receiving organ transplants are prescribed this drug to suppress their immune systems to avoid rejection of the transplant. Both CYP3A4 and CYP3A5 can metabolize tacrolimus into 13-O-tacrolimus, but the catalytic efficiency is 64% higher for CYP3A5.[96] As with vincristine, genetic polymorphisms of CYP3A5 (particular those that classify patients as "expressors" versus "non-expressors") contribute dramatically to the efficacy of the drug and provide the basis for dosing adjustments.[97] Because tacrolimus is one of the few drugs that is catalyzed preferentially by CYP3A5, the expression levels of the functional CYP3A5 isoform of a patient must be carefully considered when prescribing this drug. Naturally, nonselective inhibition of CYP3A5 via ketoconazole or cyclosporine A also affects tacrolimus biotransformation and, thus, the proper dosage.[8]

When panels of compounds are tested for their CYP3A4 and CYP3A5 inhibitory potential, the general pattern is that if a compound inhibits CYP3A4 then it probably also inhibits CYP3A5.[98] Similarly, most substrates of CYP3A4 are also substrates of CYP3A5. Although the potencies usually differ (with most compounds being more potent for or more efficiently catalyzed by CYP3A4 than CYP3A5), changes greater than 2- to 5-fold are not commonly observed. Because CYP3A4 is the primary CYP3A enzyme expressed in liver, side-by-side comparisons with CYP3A5, using recombinantly expressed enzymes, have been only infrequently conducted. However, one CYP3A4-selective compound was reported in 2016, when it was demonstrated that gomisin A is metabolized nearly 13 times more efficiently by CYP3A4 than by CYP3A5.[99] CYP3A4

preferentially catalyzes the hydroxylation of this natural compound to 8-hydroxygomisin A, and this product was not detected when other human CYPs were tested. Interestingly, gomisin A is also reported to be an inhibitor of CYP3A4.[100] Compounds serving as substrates that are also inhibitors at clinically relevant concentrations may help to provide insights into modes of isoform-selective catalysis and/or inhibition of the human CYP3A family. Moreover, gomisin A is of additional interest because of its hepatoprotective effects, which may be directly related to interplay with CYP3A4.[101,102] Another important example of a compound that is selectively catalyzed by CYP3A4 is luciferin-IPA, which has been developed by Promega for use in drug-development assays.[103] This is a "pro-luciferin" that is selectively metabolized into D-luciferin by CYP3A4, with very minimal cross-reactivity from other CYP3A members and none from various other human CYPs.[103] Adding luciferase to the system yields a luminescent signal, and this technique has been routinely used as a robust measure of various biological processes, such as cytotoxicity.[104] Leveraging this in the context of CYP3A, the signal from luciferin-IPA being converted to D-luciferin (and ultimately luminescence) is directly proportional to the CYP3A4 activity, making this method suitable for high-throughput drug-development screens.[105] In systems that express multiple CYP3A family members, isoform-selective substrates such as these are important tools for uncovering the individual roles of a given isozyme.

Structural Insights

With the recent progress in crystallization of CYP3A5, new insights have been gained into the slight differences between CYP3A4. Such nuances in secondary structures provide details into discrete modes of binding and catalysis.

Secondary Structures and Flexibility

Several crystal structures of human CYP3A4 have been solved and deposited in the Protein Data Bank (PDB, https://www.rcsb.org). These structures serve as informative tools with which to further the understanding of the enzymatic function of this molecule. The flexibility of CYP3A4 has been well established and is an essential part of its ability to so promiscuously recognize and bind compounds.[106] The ligand-accessible volume of the CYP3A4 binding pocket is estimated to be very large at 520 $Å^3$.[107] It can bind a greatly diverse set of ligands (i.e., compounds that bind to the CYP3A4 binding pocket) and even exhibits multiple conformations itself.[108] CYP3A4 and CYP3A5 have been described as having the highest catalytic promiscuity among the major human CYPs.[109] Some of the structural diversity of the compounds that bind to CYP3A4 can be observed in the various crystal structures. Although structurally diverse, these ligands also have varying functions. Compounds that exemplify the structural and functional diversity of CYP3A4-binding ligands, as determined using x-ray crystallography, include the endogenous hormone progesterone,[110] the antibiotic erythromycin,[111] the antifungal ketoconazole,[111] the antiretroviral ritonavir,[112] the

dopamine promoter bromoergocryptine,[109] and the sedative midazolam (**Figure 1-3**).[113] Interestingly, the cavity can adapt to accommodate multiple ligands at once, as seen with ketoconazole and ritonavir. It can also adopt a conformation that may present a noncanonical binding site (as seen with progesterone). The most striking differences in flexibility when binding various ligands occur in the F–F′ region.[114] This change is apparent when the ligand-free states of CYP3A4 (in the absence of ligand or coordinated to a water molecule) are compared with the structure that has two molecules of ketoconazole bound and an expanded active site (**Figure 1-4**). [111, 115-116] The F–F′ region is expanded outward as a result of the inherent flexibility of the secondary structure lining the roof of the pocket. This culminates in an expanded state that can accommodate two molecules of ketoconazole. The ability of CYP3A4 to conform to diverse molecules is a direct function of this secondary structure flexibility.

Only one crystal structure has been solved for CYP3A5. In 2018, Hsu *et al.* were the first to crystalize CYP3A5, bound with the potent inhibitor ritonavir. [117] This was the first concrete evidence that although CYP3A4 and CYP3A5 have largely homologous overall secondary structures, certain residues lining the binding pocket of CYP3A5 do indeed confer a unique shape. Amino acid residues in the F–F′ region are positioned slightly differently in the two enzymes. Consequently, the CYP3A4 binding pocket has a comparatively shorter and more horizontal shape when compared to the CYP3A5 binding pocket, whereas the roof of the latter pocket is higher and narrower than that of the CYP3A4 pocket.[117] Subtle changes such as these probably contribute to the differences that constitute the basis for isoform-selective inhibition and catalysis, where observed. On comparing the CYP3A5 structure to CYP3A4 crystallized with the same ligand,[118] it is apparent that ritonavir can extend into the roof of the CYP3A5 binding pocket but is blocked by the position of F213 in CYP3A4 (**Figure 1-4b**). It is, therefore, reasonable to suppose that compounds that extend into this available region of CYP3A5 could be developed as selective substrates or inhibitors. This structure presents an opportunity to exploit key differences between these two enzymes to further understand their selectivity.

Contrasting Active Sites and Consequences Therein

The in-depth exploration of active-site differences of CYP3A enzymes and the resulting biological consequences is just beginning. At present, no crystal structure exists for CYP3A7 or CYP3A43. However, kinetic analyses and *in silico* studies can provide insights into the selectivity of these enzymes and other CYP3A family members. It was previously reported that these enzymes exhibit regioselective and stereoselective differences in testosterone metabolism.[119] It is well established that CYP3A family members are responsible for testosterone metabolism.[17] Interestingly, however, Kandel *et al.* investigated the apparent differences in the production of 6β-hydroxytestosterone (6β-OHT), 2α-hydroxytestosterone (2α-OHT), and 2β-hydroxytestosterone (2β-OHT) and proposed that active-site differences between CYP3A4/5 and CYP3A7 contribute to testosterone binding in a position that favors the 2α-OHT metabolite.[120] The differences in the binding mode and resulting metabolite suggest that the 2α-OHT product is

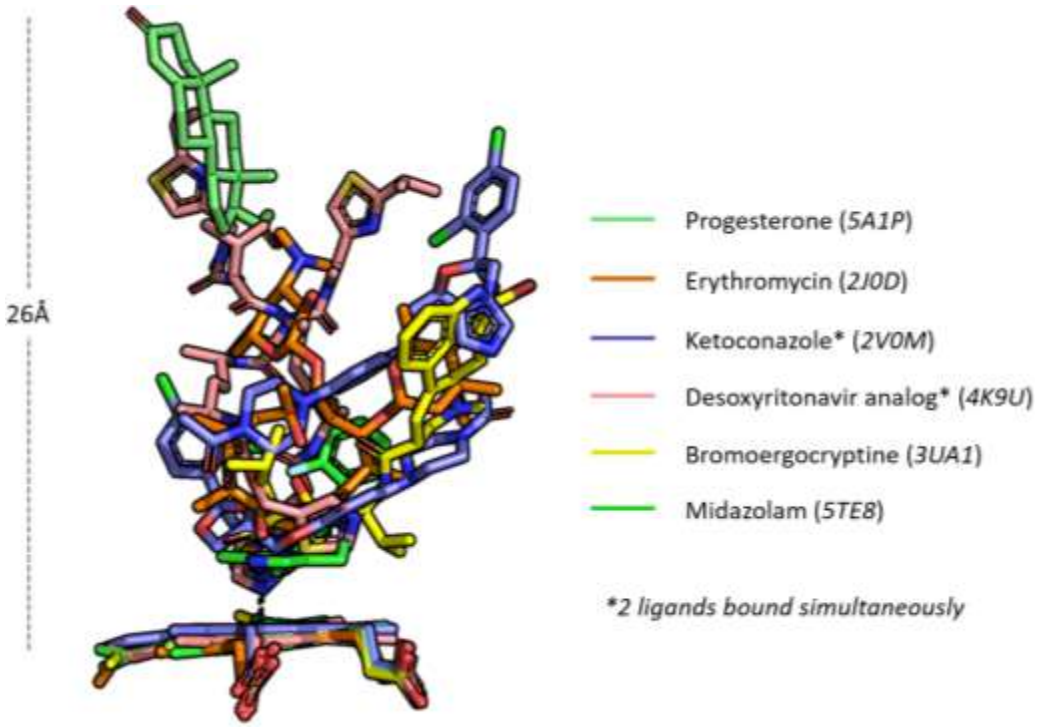

Figure 1-3. Promiscuity of the CYP3A ligand binding pocket.

The crystal structures of CYP3A4 were obtained from PDB and aligned to illustrate the structural diversity of ligands capable of binding to CYP3A4. Progesterone (PDB : 5A1P) is shown in light green, Eerythromycin (PDB: 2J0D) in orange, Kketoconazole (PDB : 2V0M) in blue, Rritonavir analog (PDB : 4K9U) in pink, Bbromoergocryptine (PDB: 3UA1) in yellow, and Mmidazolam (PDB : 5TE8) in green. Asterisks (*) indicates that two molecules of the same ligand are bound in the respective structures.

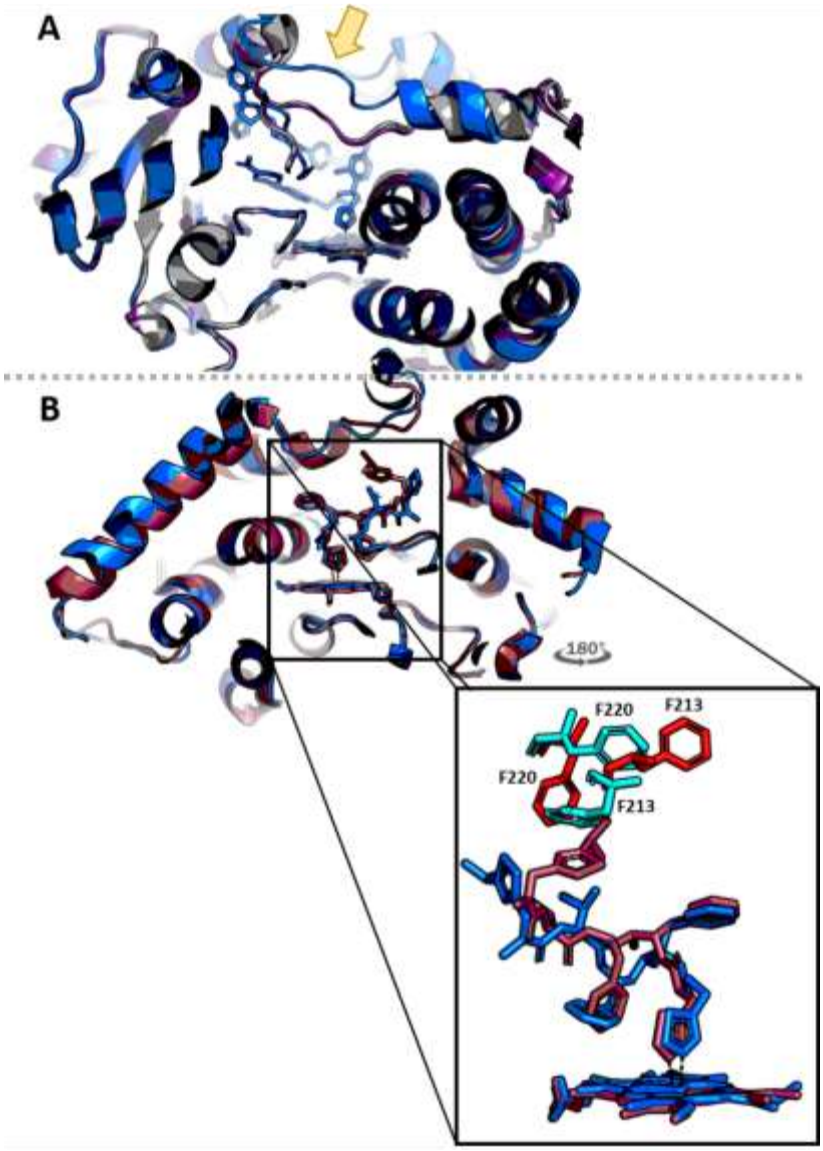

Figure 1-4. Structural differences in CYP3A conformations.

(A) CYP3A4 demonstrates flexibility in the active site. Ketoconazole-bound (PDB : 2V0M) (blue), water-bound (PDB : 4I3Q) (purple), or ligand-free (PDB : 1TQN) (gray) structures of CYP3A4 are overlaid. The flexibility of the F–F′ region at the roof of the binding pocket in the ketoconazole-bound structure is indicated by the yellow arrow. (B) Differences in key active-site residues in CYP3A4 and CYP3A5 contribute to the differential binding modes of ritonavir. Ritonavir-bound CYP3A4 (PDB : 3NXU) (blue) superimposed with ritonavir-bound CYP3A5 (PDB : 5VEU) (raspberry) demonstrates slightly different ligand-binding poses. The magnified panel shows the residues responsible for this difference in CYP3A4 (cyan) versus CYP3A5 (red).

important in the fetal environment, as CYP3A7 is the primary fetal CYP3A enzyme. This could also serve as an example of how subtle differences between CYP3A catalytic sites confer different and potentially biologically relevant activities. Another example of differential effects among CYP3A enzymes that result from differences in their active sites is seen with the lignan compounds gomisin C and gomisin G.[75] The inhibition profiles of these compounds appear to be different for CYP3A4 versus CYP3A5, with consequent varying effects on the substrates midazolam, testosterone, and nifedipine. This is intriguing because gomisin C and gomisin G share high structural similarity and have the same molecular weight. When *in silico* modelling studies were performed, docking of these compounds revealed an interesting CYP3A5-exclusive hydrogen-bonding interaction.[75] Importantly, these compounds also showed different capacities for interaction with heme groups. It is plausible that the minor differences between CYP3A active sites, which were previously considered trivial, are responsible for how certain molecules fit and interact differently within these enzymes and, thus, elicit differing biological consequences.

Comparisons to Other Human CYPs

Although the CYP3A family comprises the CYPs that metabolize the widest range of compounds, other enzymes in this superfamily also play critical roles in drug metabolism and response to stimuli. Humans have 18 distinct CYP families, and it is accepted that the most abundant and biologically relevant members hail from CYP1, CYP2, CYP3, and CYP4.[120] These families do share some redundancy, but specific roles in metabolism and disease progression have been reported for various enzymes within them. Moreover, differences in their tissue-specific expression patterns have provided clues to their intended functions and clinical relevance. The CYP1 family is one of the primary CYP families expressed in lung.[121] Interestingly, CYP3A5—but not CYP3A4—is expressed in lung with the CYP1 family.[121] Within the CYP1 family, CYP1A1, CYP1A2, and CYP1B2 catalyze the activation of polycyclic aromatic hydrocarbons,[122] and they have recently been reported to possess pro-cancer effects.[123] The inhibition of CYP1B1 has recently been reported to have anti-angiogenic activities, and it has been suggested to be an important target for anticancer strategies.[123,124] Unlike the CYP3A family, which is transcriptionally regulated by PXR, CYP1 is controlled the aryl hydrocarbon receptor (AHR).[125] The CYP2 family includes some of the primary CYPs expressed in endothelium, myocardium, and kidney,[126] but members can be found in other tissues too. CYP2B6 is among the most clinically relevant CYP2 enzymes; it is proposed to metabolize around 2% to 10% of clinically prescribed drugs.[127] CYP2B6 is the primary CYP inhibited by drugs such as artemisinin, bupropion, cyclophosphamide, and ketamine.[128] The constitutive androstane receptor (CAR), which is known to have overlapped regulation and function with PXR, transcriptionally controls the expression of this enzyme. Like the members of the CYP3A family, CYP2B6 is highly polymorphic and displays population disparities in its genotype.[128] The CYP4 family comprises 13 members that are primarily implicated in the metabolism of eicosanoids and fatty acids, most notably through their ω-hydroxylase activity.[129] This family has been specifically implicated in the progression of fatty acid–linked diseases and certain cancers, and its

members represent an important class of drug targets.[130] Like all CYPs, these enzymes have a heme group that is important for catalytic activity. However, CYP4 enzymes generally prefer to covalently bind their heme group, whereas the CYP3A enzymes catalyze a reaction and turn over the product, leaving them ready to repeat the process.[131] CYP4F2 and CYP4F12 are expressed in liver and are currently being investigated as biomarkers for hepatocellular carcinoma.[132]

Further Perspectives

It is clear that CYP3A enzymes are critical for endogenous metabolism, xenobiotic response, the mediation of drug–drug interactions, and other important biological processes. Less clear however, has been the discrete role that a given enzyme in this family might play and whether that role was of any biological importance. The recent efforts to delineate isoform-selective roles of CYP3A enzymes have shown that interesting and clinically relevant functions exist within the vast overlap. CYP3A enzymes are affected in different ways by various compounds, ranging from endogenous metabolites used as biomarkers to inducers that weaken intended drug effects. Comparing these enzymes in the context of structure, expression, substrate recognition, activity modulation, and catalytic efficiency has yielded insights into the most important differences. It has now been shown that the active sites of CYP3A4 and CYP3A5 have different shapes. It is likely that many compounds can be recognized by both isoforms because their active sites can usually conform to fit the various shapes. However, certain compounds demonstrate that there are scenarios in which compounds bind and confer either preferential catalysis or (in the case of CYP3A4) selective inhibition. These compounds appear to exploit key differences to elicit the observed selectivity. The identification of isoform-selective inhibitors of CYP3A4 suggests that it might also be possible to selectively inhibit CYP3A5, although given the generally higher inhibition potential of CYP3A4, this is likely to be a challenge. Nevertheless, examples such as vincristine and tacrolimus prove that at least some small molecules can be *metabolized* preferentially by CYP3A5, which is good news in the context of developing a selective CYP3A5 inhibitor. The preferential catalysis of 2α-hydroxytestosterone by CYP3A7 suggests that the latter enzyme may play important roles in development and perhaps even in disease progression. The distinct functions and drug-interaction profiles of CYP3A4, CYP3A5, and CYP3A7 warrant a further characterization of the metabolic capability of CYP3A43, which has been little studied so far. Furthermore, and beyond the scope of this review, genetic polymorphisms within the CYP3A family may represent an extra layer of regulation by changing the substrate recognition or inhibition potential of these enzymes. Elaboration on what has been reported so far regarding CYP3A selectivity is warranted to obtain a more complete understanding of the biological contributions of each enzyme and how they can be exploited in medicine

Hypothesis and Specific Aims

Differential expression and tissue distribution of CYP3A4 and CYP3A5 suggest that these enzymes may have discrete functions, particularly in disease, and thereby have the potential to be differentially modulated by small molecules. While these homologs share a breadth of substrates encompassing large and structurally diverse chemical matter, progress in selective CYP3A4 inhibition and identification of a few CYP3A5-selective substrates suggests that small molecule isoform-selective inhibition of CYP3A5 may be possible. Furthermore, the selective over-expression of CYP3A5 in certain cancers points to a distinct regulatory system of transcriptional control independent of CYP3A4 regulators.

We hypothesize that CYP3A5 catalytic activity can be chemically inhibited using a small molecule which does not inhibit CYP3A4 activity. We further hypothesize that CYP3A5 is under transcriptional regulation in cancer by factors independent of CYP3A4 regulation, and this presents another point by which CYP3A5 can be targeted. To validate our hypothesis, we propose the following specific aims:

Aim 1: Small Molecule Selective Inhibition of CYP3A5

To use high-throughput screening with an appropriate biochemical assay to test compounds for selective CYP3A5 inhibition, and to further validate the inhibition potential in cell-based systems.

Aim 2: Characterizing Mechanism of Isoform-Selective Inhibition

To make use of computational and biophysical techniques to understand the basis of selectivity between CYP3A4 and CYP3A5, detailing the small molecule-mediated discrimination of their catalytic activities.

Aim 3: Uncovering Transcriptional Regulators of CYP3A5 in Cancer

To develop a novel method for predicting putative transcriptional regulators of CYP3A5, and to test them by measuring CYP3A5 mRNA levels upon their RNAi-mediated knockdown.

CHAPTER 2. SELECTIVE INHIBITION OF CYP3A5*

Relevance of Selective Modulation

The cytochrome P450 (CYP) superfamily of heme-containing enzymes is responsible for catalyzing a wide range of biological processes. The heme group is critical for the catalytic activity of CYPs, with a highly reactive heme iron-oxo species (compound I) being responsible for the oxidation of CYP substrates bound close to the heme iron[133,134]. The 3A subfamily of CYPs (CYP3A) is critical for xenobiotic clearance in humans and is reported to metabolize more than half of all currently prescribed drugs[135,136]. Although the members of this family include CYP3A4, CYP3A5, CYP3A7, and CYP3A43, it is CYP3A4 and CYP3A5 that are the primary CYP enzymes expressed in adults[137,138]. These enzymes are promiscuous and have exceptionally broad substrate specificity. They metabolize various pharmaceuticals, natural products, and endogenous small molecules. This is possible, in part, because of their ability to bind diverse, structurally unrelated compounds within their large active sites (as we recently reviewed[139]). Such indiscriminate binding is the basis for many compounds being able to modulate CYP3A, thereby decreasing drug efficacy or drug–drug interactions[140-143]. Ligand promiscuity of CYP3A4 and CYP3A5 homologs is one reason why these enzymes are considered functionally redundant[120]. Compared to CYP3A5, CYP3A4 is more predominantly expressed in the normal liver, the primary site of drug metabolism, which explains why CYP3A4 is regarded as the representative member of the CYP3A family[137]. Furthermore, the US Food and Drug Administration (FDA) recommends testing potential pharmaceuticals for CYP3A inhibition and does not differentiate between CYP3A4 and CYP3A5[144,145]. For these reasons, the enzymes are ubiquitously grouped together as "CYP3A4/5" in most expression- and metabolism-related studies.[146-150] However, emerging evidence suggests that these isozymes are not as redundant as previously thought.

CYP3A5 is reportedly overexpressed in pancreatic ductal adenocarcinoma (PDAC) and mediates chemoresistance in different subtypes of this cancer[9]. Importantly, RNA interference (RNAi)-mediated knockdown of CYP3A5 re-sensitizes the drug-resistant PDAC cells, confirming the role of elevated CYP3A5 levels in drug resistance[9]. Although this is the first evidence that selectively inhibiting CYP3A5 might be clinically significant, previous reports have discussed the need for a CYP3A5-selective inhibitor as a tool compound with which to differentiate CYP3A5 from CYP3A4[90]. The challenge of finding such a tool compound is intensified by CYP3A4 being generally more catalytically active, although this property aided the development of CYP3A4-selective

---

*Reprinted from final submission with permission. Wright, W. C. et al. Clobetasol Propionate Is a Heme-Mediated Selective Inhibitor of Human Cytochrome P450 3A5. J Med Chem 63, 1415-1433, https://doi.org/10.1021/acs.jmedchem.9b02067 (2020).[180]

inhibitors[87,88]. Interestingly, among the numerous overlapping substrates, a few compounds, including the anticancer drug vincristine and the immunosuppressant tacrolimus have been reported which characterize the selective catalytic activity of CYP3A5[7,92,96,151]. These compounds are metabolized to a greater extent by CYP3A5 than by CYP3A4. Moreover, the *N*-oxide metabolite of the phosphodiesterase inhibitor T-1032 has been reported to be catalyzed almost exclusively by CYP3A5, further demonstrating the distinct function of the enzyme[91]. Unsurprisingly, each of these compounds has a different chemical structure, upending the notion that this selective activity is chemotype-dependent. The demonstration that CYP3A5 selectively metabolizes certain compounds, however few, suggests that CYP3A5 plays a discrete role which might potentially be selectively targeted. A compound capable of selectively inhibiting CYP3A5 will be important for circumventing the inaccurate assignment of cumulative enzymatic activity to CYP3A4 alone, as well as for delineating between the two homologs. Such an inhibitor could prove especially beneficial in cases in which CYP3A5 is the target (e.g., when extrahepatic CYP3A5 is elevated and causes drug resistance) but CYP3A4 inhibition should be avoided (e.g., so as not to alter normal drug metabolism in the liver).

Here, we exploited high-throughput screening techniques to identify a selective inhibitor of CYP3A5. The compound we identified, clobetasol propionate (abbreviated hereafter as clobetasol), can potently block CYP3A5 catalytic activity without inhibiting CYP3A4 or other major CYPs. We further identified pancreatic cancer cell lines as suitable models for studying the selective modulation of CYP3A5 *in vitro*. Clobetasol proved to be a nontoxic, potent, and selective inhibitor of CYP3A5 in these cells. We leveraged molecular dynamics (MD) simulations to predict the potential mechanism of CYP3A5-selective inhibition. Our simulations suggested that clobetasol resides closely to the heme group in CYP3A5 but binds to CYP3A4 too distally from the heme in that protein for effective clobetasol–heme interaction to occur. This computational prediction is consistent with the essential role of heme in the catalytic activity of CYPs, and it was further supported experimentally with multiple biophysical techniques, including UV–visible spectroscopy and electron paramagnetic resonance (EPR) analyses, which can detect the heme-dependent interactions with compounds. Although it has been suggested that identifying a CYP3A5-selective inhibitor would be challenging because of the high structural similarity between CYP3A4 and CYP3A5[9,90], our work demonstrates that it is indeed feasible. We anticipate that the structural basis and mechanistic insights revealed by this work will aid in the further development of CYP3A5-selective inhibitors, facilitate further investigations of the structural and functional regulation of CYP3A4 and CYP3A5, and enable exploration of the therapeutic potential of targeting CYP3A5.

High-Throughput Screening Identifies Clobetasol as a Selective CYP3A5 Inhibitor

The high degree of structural similarity between CYP3A4 and CYP3A5 makes it challenging to use a structure-based approach to design a CYP3A5-selective inhibitor. Therefore, to search for potential selective CYP3A5 inhibitors, we first used a luminescence-based enzymatic assay to screen and identify inhibitors of the catalytic

function of CYP3A5. We then eliminated those compounds which also inhibited CYP3A4. The assay we used leverages the ability of CYP3A5 to metabolize a "pro-luciferin" substrate into D-luciferin, which is then converted into luminescence when luciferase is added to the system. For the primary screen, we used the St. Jude bioactive compound library of 11,200 total compounds, which contains FDA-approved drugs, drug candidates, and other compounds with known activity[152,153]. The propensity of a given small molecule to inhibit CYP3A5 was clear; hundreds of compounds showed greater than 50% inhibition at the final tested concentration of 5 μM (**Figure 2-1a**). To confirm the CYP3A5-inhibitory activity and determine which of these compounds were selective for CYP3A5, we chose compounds from the primary screen that conferred at least 60% CYP3A5 inhibition and evaluated them in dose-response analyses. The 252 chosen compounds were then screened against CYP3A4 and CYP3A5 in parallel, using the exact same conditions for each (described in the Methods section). As a demonstration of nonselective inhibition, we tested the antiretroviral compound ritonavir—a known inhibitor of the CYP3A family[63] and the only compound to have been co-crystalized with both CYP3A4[154] and CYP3A5[117]. Ritonavir-mediated inhibition aligned with values reported in the literature[58,155], and the inhibitory curves demonstrated high potency for each enzyme (**Figure 2-1b**). A systematic comparison of all the dose-response curves led to the identification of clobetasol propionate (clobetasol) as a potent and selective CYP3A5 inhibitor. Clobetasol showed the greatest selective inhibition, having IC_{50} values of 0.206 μM for CYP3A5 and 15.6 μM for CYP3A4 (**Figure 2-1b**). While a few other compounds from the screen demonstrated comparatively marginal selective inhibition, none could match the approximately 76-fold CYP3A4/CYP3A5 IC_{50} ratio of clobetasol. Interestingly, clobetasol contains a four-ring steroid scaffold that is analogous to several known substrates of CYP3A5 within the same drug class[156] (**Figure 2-1c**).

To further demonstrate the CYP3A5-selective inhibition of clobetasol, we compared the effect to CYP3A4 using clobetasol at a concentration of 1.8 μM (the IC_{90} concentration for CYP3A5) and used the same concentration of ketoconazole (the gold-standard pan-CYP3A inhibitor[157] that served as a normalization control in our biochemical assays). At 1.8 μM, clobetasol inhibited CYP3A5 by 90%, but no inhibition of CYP3A4 was observed (**Figure 2-1d**). As expected, the same concentration of ketoconazole completely inhibited both enzymes (**Figure 2-1d**). Although clobetasol demonstrated remarkable selectivity for CYP3A5 as compared to CYP3A4, we wanted to test whether it inhibited the catalytic activity of other major human CYPs. We screened clobetasol against CYP3A4 and a panel of six other human CYPs (CYP1A2, 2B6, 2C8, 2C9, 2C19, and 2D6) recommended by the FDA for drug–drug interaction testing for candidate pharmaceuticals[144,145]. Each of these enzymes was tested for catalytic inhibition by directly measuring the formation of product derived from its own substrate. In the case of CYP3A4, we tested the two structurally unrelated substrates midazolam and testosterone, as recommended by the FDA[144,145]. Not only was CYP3A4-mediated catalysis of these substrates uninhibited by 1.8 μM clobetasol but other major CYPs also showed little or no inhibition (**Figure 2-1e**). Taken together, these data suggest that clobetasol is a potent and selective inhibitor of CYP3A5 in biochemical systems.

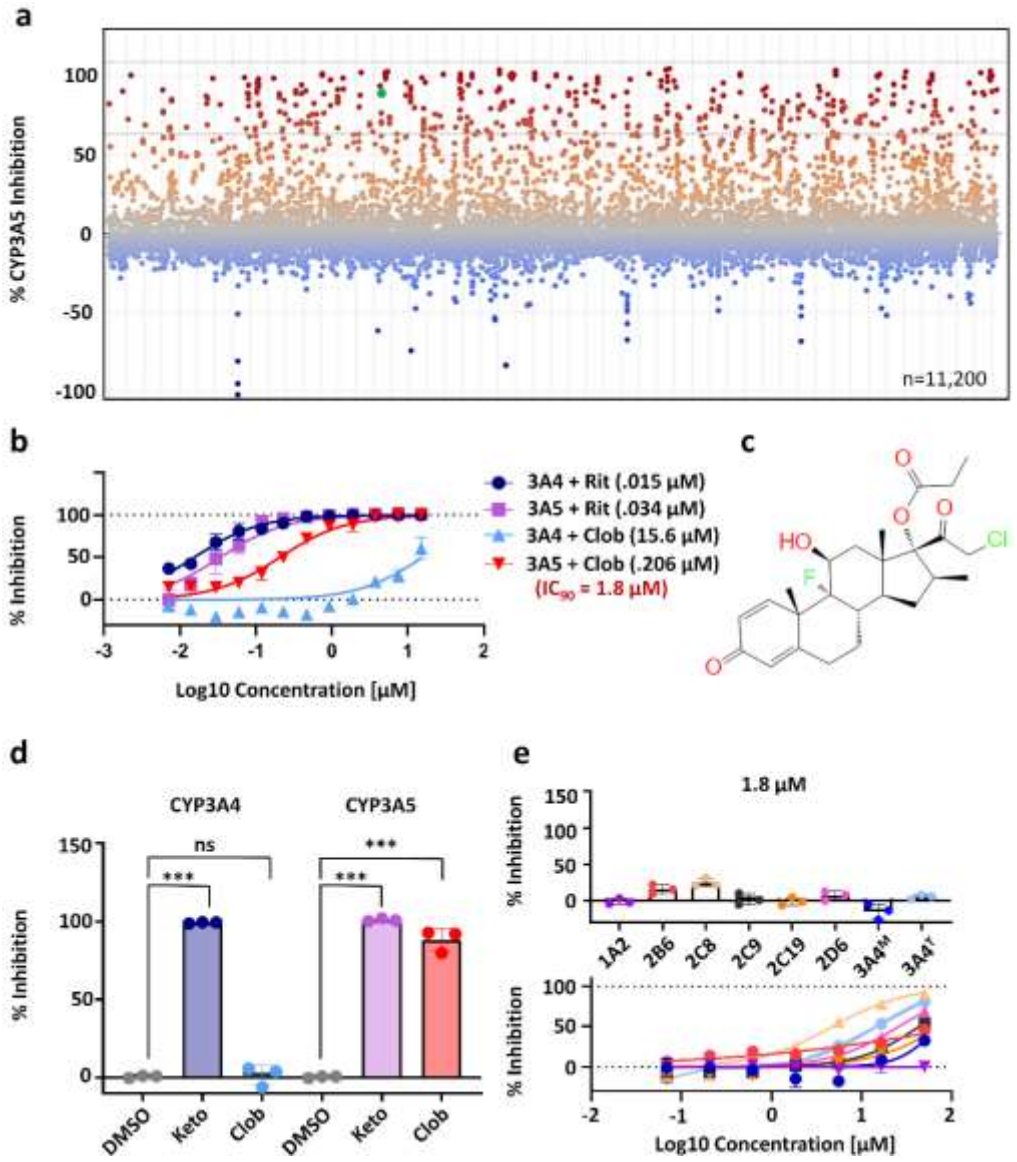

Figure 2-1. Clobetasol propionate is a potent and selective inhibitor of CYP3A5.

(a) CYP3A5 inhibition profile of the St. Jude bioactive library when screened at a concentration of 5 µM. Compounds selected for downstream dose-response testing (those having ≥60% CYP3A5 inhibition) are shown between the gray dotted lines. The green circle indicates clobetasol. (b) Dose-response curves for CYP3A4 and CYP3A5 with ritonavir (Rit) or clobetasol (Clob). IC50 values for each curve are shown in parenthesis. The IC90 for clobetasol–CYP3A5 are shown in red text. (c) Chemical structure of clobetasol. (d) Inhibition of CYP3A4 or CYP3A5 by using 1.89 µM ketoconazole (Keto) or clobetasol (Clob). The DMSO concentration is 0.1%. *** $P \leq 0.0001$, ns = not significant ($P \geq 0.05$); one-way analysis of variance (ANOVA). (e) Inhibition profile of 1.85 µM clobetasol against a panel of major human CYPs.

Pancreatic Cancer Is an Appropriate and Clinically Relevant Model for Studying Selective Modulation of CYP3A5

After validating clobetasol as a CYP3A5-selective inhibitor in biochemical assays, we next sought to determine whether this selectivity was maintained in cell-based systems. Hepatocellular carcinoma serves as a widely used model for studying CYP-related biology, including that of the CYP3A family[158-162]. However, although CYP3A5 is expressed appreciably in hepatocellular carcinoma, the (often higher) expression of CYP3A4 makes delineation between these homologs complex and arduous. Accordingly, we needed a model system that expressed CYP3A5 but lacked CYP3A4 expression. To this end, we turned to the PanCancer analysis project from The Cancer Genome Atlas (TCGA), which hosts RNA-seq datasets derived from more than 10,000 tumor samples spanning 33 different cancer types[163]. We reanalyzed all data from this project by using our in-house pipeline (our stepwise protocol is made available in Protocol Exchange[164]) and ranked each cancer type according to the level of CYP3A5 expression. As expected, the liver and hepatocellular carcinoma (LIHC) cohort exhibited the highest CYP3A5 expression, followed by the bile duct (CHOL) and pancreatic (PAAD) cancer cohorts (**Figure 2-2a**). Conversely, CYP3A4 expression was primarily contained within the LIHC and CHOL cancers (**Figure 2-3a**). In view of the apparent selective overexpression of CYP3A5 in pancreatic cancer, we decided to pursue our studies using cell models of this type. Moreover, CYP3A5 has been reported to be overexpressed in pancreatic adenocarcinoma and to mediate its chemoresistance[9], adding a clinical significance to studying CYP3A5-mediated drug metabolism in this cancer type.

Clobetasol Selectively Inhibits CYP3A5 in Cells

To determine whether clobetasol inhibited CYP3A5 in a cell-based context, we modulated the expression of CYP3A5 and/or CYP3A4 in parental AsPC-1 cells (referred to as wild-type, or WT), which express high levels of endogenous CYP3A5 but no detectable CYP3A4. To further elevate CYP3A5 levels, we produced doxycycline (Dox)-inducible CYP3A5 overexpression in AsPC-1 parental cells (hereafter referred to as "WT + $3A5^{OE}$" cells). We also used CRISPR/Cas9 technology to knock out CYP3A5 from the parental AsPC-1 cells (a total *CYP3A5* genetic deletion). In these AsPC-1$^{CYP3A5-/-}$ cells (hereafter abbreviated as $3A5^{-/-}$ cells), we also produced doxycycline inducible CYP3A4- and CYP3A5-overexpression systems (referred to as "$3A5^{-/-}$ + $3A4^{OE}$" and "$3A5^{-/-}$ + $3A5^{OE}$" cells, respectively). We validated each cell line by measuring and quantifying the relevant protein expression. As expected, the results (**Figure 2-4a**) demonstrated (1) that the $3A5^{-/-}$ cells had no detectable CYP3A5 protein, (2) that "WT + $3A5^{OE}$" cells could be induced to express a higher level of CYP3A5, (3) that "$3A5^{-/-}$ + $3A5^{OE}$" cells could be induced to express CYP3A5 at a level comparable to that in "WT + $3A5^{OE}$" cells, and (4) that CYP3A4 could be successfully overexpressed in the $3A5^{-/-}$ cells upon induction ("$3A5^{-/-}$ + $3A4^{OE}$" cells). To probe for CYP3A4 or CYP3A5 catalytic activity, we treated these cell lines with midazolam and measured the

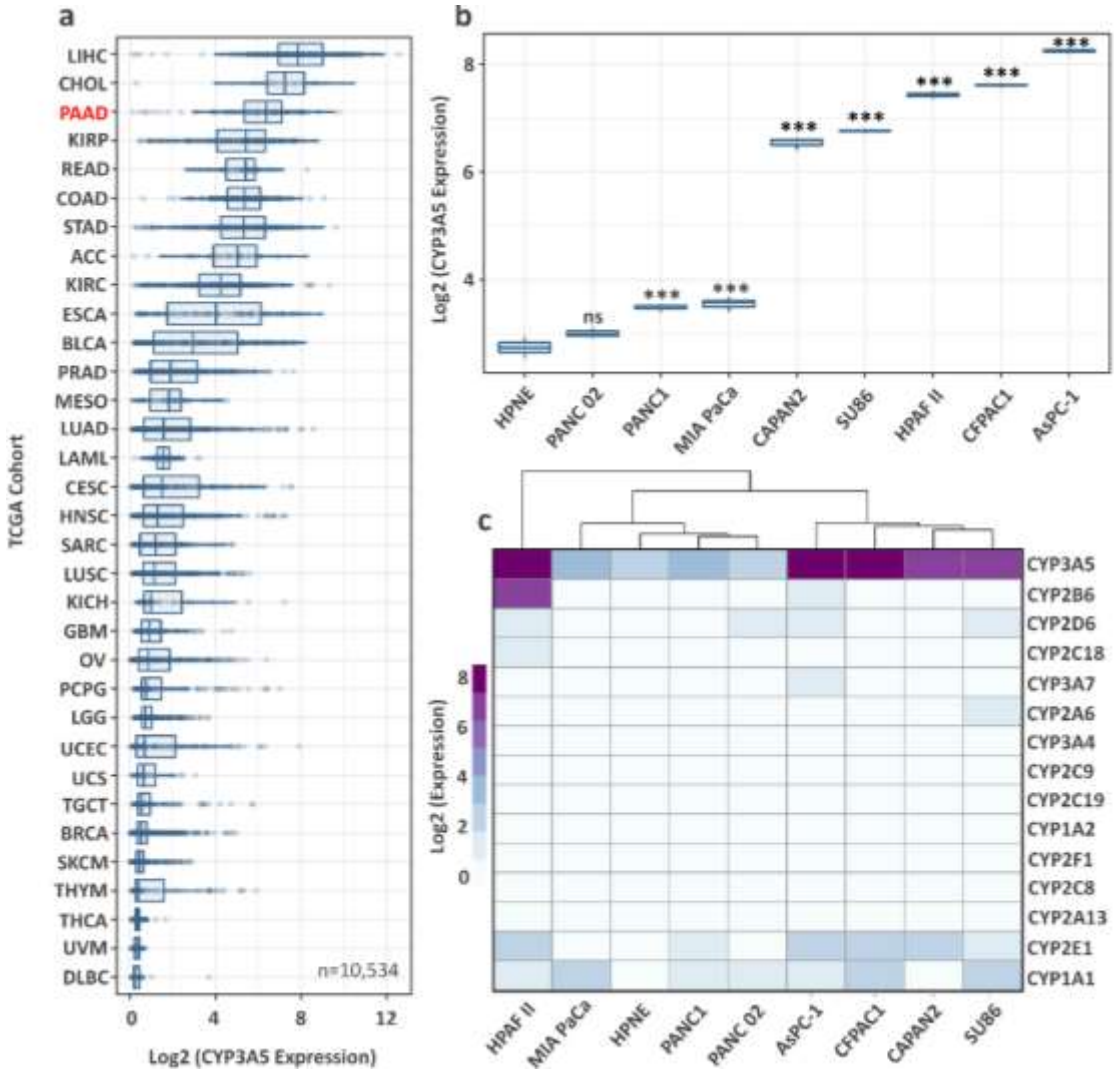

Figure 2-2. CYP3A5 is over-expressed in pancreatic cancer models and AsPC-1 cells are ideal for studying CYP3A5 modulation.

(a) Expression of CYP3A5 across all cancers within the PanCancer dataset from The Cancer Genome Atlas (TCGA). Expression is derived from 10,534 tumor samples across 33 cancers and is ranked by median values. The pancreatic adenocarcinoma cohort (PAAD) is highlighted in red. (b) CYP3A5 expression in pancreatic adenocarcinoma cell lines compared to that in the noncancerous pancreatic cell line HPNE. *** $P \leq 0.0001$, ns = not significant ($P \geq 0.05$); t statistic–derived P values adjusted by the Benjamini-Hochberg false discovery rate. (c) Expression of the xenobiotic-metabolizing CYPs from all pancreatic adenocarcinoma and control cell lines. Units of expression for all panels are log2 (normalized CPM+1).

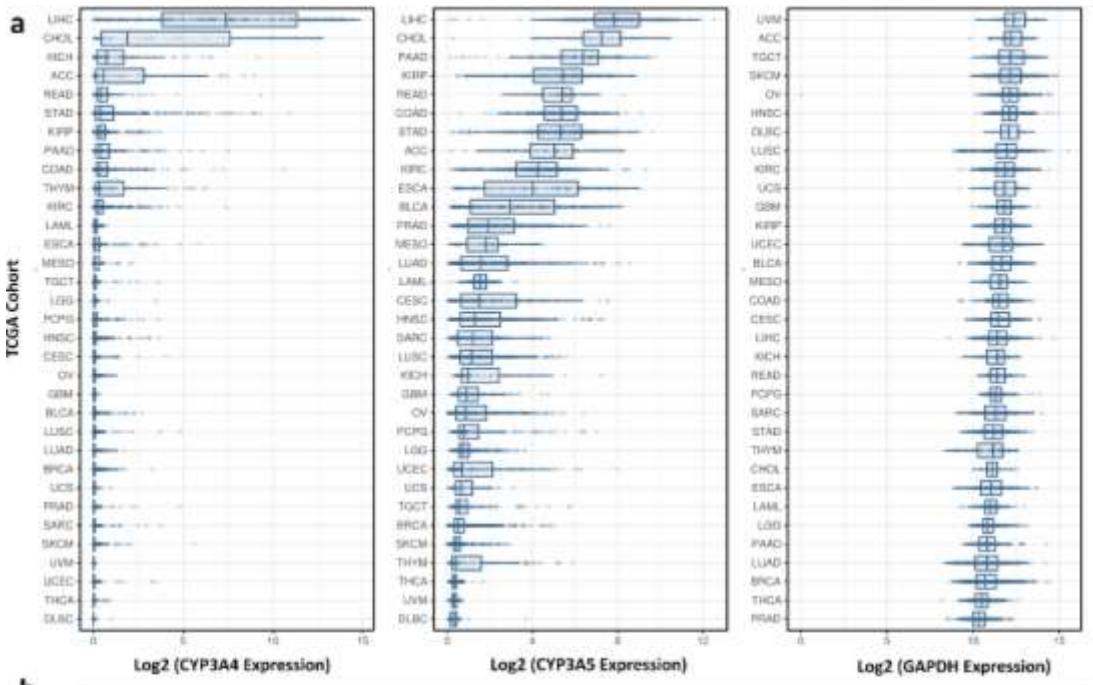

b

TCGA PanCancer Cohorts	
ACC : Adrenocortical carcinoma	LUAD : Lung adenocarcinoma
BLCA : Bladder Urothelial Carcinoma	LUSC : Lung squamous cell carcinoma
BRCA : Breast invasive carcinoma	MESO : Mesothelioma
CESC : Cervical squamous carcinoma & endocervical adenocarcinoma	OV : Ovarian serous cystadenocarcinoma
CHOL : Cholangio carcinoma	PAAD : Pancreatic adenocarcinoma
COAD : Colon adenocarcinoma	PCPG : Pheochromocytoma & Paraganglioma
DLBC : Lymphoid Neoplasm Diffuse Large B-cell Lymphoma	PRAD : Prostate adenocarcinoma
ESCA : Esophageal carcinoma	READ : Rectum adenocarcinoma
GBM : Glioblastoma multiforme	SARC : Sarcoma
HNSC : Head and Neck squamous cell carcinoma	SKCM : Skin Cutaneous Melanoma
KICH : Kidney Chromophobe	STAD : Stomach adenocarcinoma
KIRC : Kidney renal clear cell carcinoma	TGCT : Testicular Germ Cell Tumors
KIRP : Kidney renal papillary cell carcinoma	THCA : Thyroid carcinoma
LAML : Acute Myeloid Leukemia	THYM : Thymoma
LGG : Brain Lower Grade Glioma	UCEC : Uterine Corpus Endometrial Carcinoma
LIHC : Liver hepatocellular carcinoma	UCS : Uterine Carcinosarcoma
	UVM : Uveal Melanoma

Figure 2-3. Normalized expression of CYP3A4 and CYP3A5 across various cancer types.

(a) CYP3A4 (left) and CYP3A5 (right) expression across all TCGA PanCancer cohort types, with GAPDH (right) shown as a housekeeping example. All data were normalized according to our RNA-seq reprocessing protocol (available in the protocol exchange: http://doi.org/10.21203/rs.2.16081/v1). (b) TCGA PanCancer cohort abbreviations.

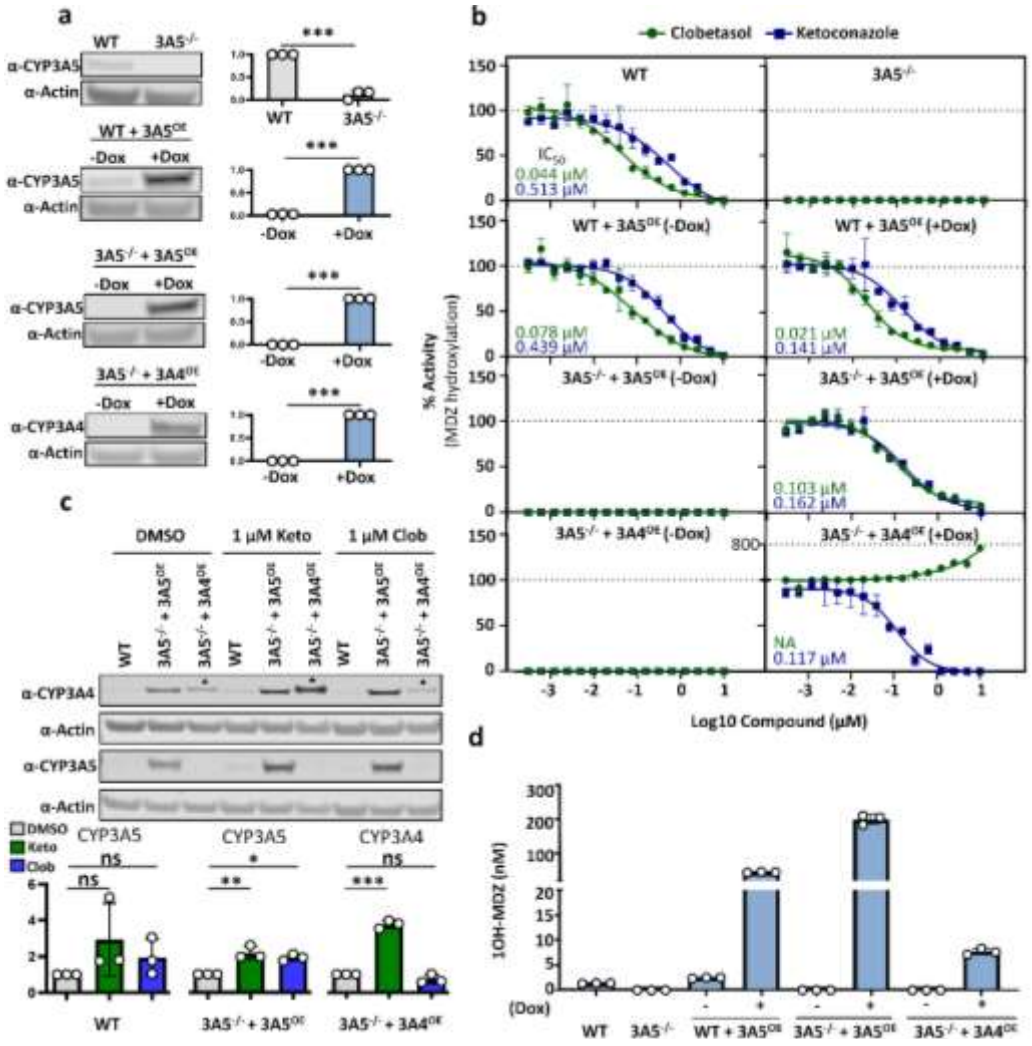

Figure 2-4. Clobetasol selectively inhibits CYP3A5 *in vitro*.

(a) Representative Western blots of CYP3A5 (top 3 panels) or CYP3A4 (bottom panel). Corresponding quantifications are shown to the right. Quantification was derived from triplicate experiments. *** $P \leq 0.0001$; unpaired two-tailed t-test. The relative intensity of WT, WT + 3A5OE (+Dox), 3A5−/− + 3A5OE (+Dox) and 3A5−/− + 3A4OE (+Dox) was set as 1.0, as indicated in each panel. Dox, doxycycline (100 ng/mL). (b) CYP3A4 or CYP3A5 activity measured by 1-hydroxymidazolam formation. All panels were normalized to the DMSO control as 100% activity. (c) Western blot of CYP3A4 or CYP3A5 expression after 24 h treatment with DMSO (left), 1 μM ketoconazole (Keto, middle), or 1 μM clobetasol (Clob, right). CYP3A4 is indicated by the slightly higher bands (star icon); the antibody is known to also detect CYP3A5. Quantification is shown below the gel images, with DMSO treatment set as 1.0. *** $P \leq 0.0001$, ** $P \leq 0.005$, * $P \leq 0.05$, and ns = not significant ($P \geq 0.05$); One way ANOVA with Tukey adjustment. (d) CYP3A-mediated activity across all cell lines, showing the relative catalytic contribution; all samples were treated with the same concentration of DMSO for 24 h.

product formation via liquid chromatography with tandem mass spectrometry (LC-MS/MS). Midazolam is a well-established substrate of CYP3A4 and CYP3A5[144], and the CYP3A-catalyzed 1-hydroxymidazolam product (1OH-MDZ) is readily amenable to detection by LC-MS/MS[81,165,166]. Furthermore, because no other enzyme has been reported to catalyze the formation of 1OH-MDZ, the presence of this product is generally attributed directly to CYP3A activity. In experiments using parental AsPC-1 (WT) cells, which have high endogenous CYP3A5 expression but no CYP3A4 expression, clobetasol produced a sigmoidal dose-response inhibition curve (**Figure 2-4b**, upper left). Surprisingly, clobetasol was even slightly more potent at inhibiting CYP3A5 activity than was the control compound, ketoconazole (a gold-standard, nonselective pan-CYP3A inhibitor). When we probed for activity in the $3A5^{-/-}$ cells, we found CYP3A5 activity to be totally abolished, as indicated by the absence of detectable 1OH-MDZ formation (**Figure 2-4b**, upper right), thus providing evidence that CYP3A5 was completely knocked out, and indeed no other enzyme is able to catalyze the formation of 1OH-MDZ in the $3A5^{-/-}$ cells. When CYP3A5 was induced (+Dox) to overexpress in either WT or $3A5^{-/-}$ cells, midazolam metabolism occurred, and both clobetasol and ketoconazole inhibited the CYP3A5 activity (**Figure 2-4b**, middle panels). Having demonstrated clobetasol to be a potent inhibitor of CYP3A5 catalytic activity in cells, we sought to test its selectivity by repeating the experiment using $3A5^{-/-}$ cells overexpressing CYP3A4. As expected, ketoconazole proved to be a potent and nonselective inhibitor, whereas clobetasol displayed remarkable selectivity and completely avoided CYP3A4 inhibition (**Figure 2-4b**, bottom right). Interestingly, at higher tested concentrations, clobetasol appeared to increase the enzymatic activity of CYP3A4, producing higher levels of 1OH-MDZ than were present at baseline (**Figure 2-4b**, bottom right). Although this phenomenon occurred only with higher concentrations of clobetasol, we found the result interesting and followed it up by examining whether clobetasol increased CYP3A4 protein levels. As shown in **Figure 2-4c**, clobetasol did not increase the protein level of CYP3A4 (note that the anti-CYP3A4 antibody detects both CYP3A4 [marked with a star] and CYP3A5). Interestingly, ketoconazole at a concentration of 1 μM increased CYP3A4 protein expression, but this had no effect on our activity assay because the tested concentration of 1 μM completely abolished CYP3A4 activity. The compounds used did not affect cell growth in any cell line that we tested. Moreover, we tested the catalytic activity of each DMSO-treated cell line by monitoring the generation of 1OH-MDZ in the absence of compound treatment. Our results showed that the actual catalytic activity of CYP3A4 in the "$3A5^{-/-} + 3A4^{OE}$" cells was less than 10% of that of CYP3A5 in the "$3A5^{-/-} + 3A5^{OE}$" cells (**Figure 2-4d**). Together, these data demonstrate that clobetasol is a potent and selective inhibitor of CYP3A5 in the context of relevant cell models.

Molecular Dynamics Simulations Predict the Mechanism of Selective Inhibition by Clobetasol

We next asked how clobetasol achieved selectivity between such highly homologous enzymes as CYP3A4 and CYP3A5. We hypothesized that the selectivity of clobetasol was in part due to the subtle differences in their active site shapes which were recently reported[167]. Furthermore, we reasoned that clobetasol probably interacted in

some way with the heme moiety of CYP3A5, but not with that of CYP3A4. Catalytic activation of CYPs occurs through single electron reduction of the CYP heme iron to its ferrous state, enabling binding of dioxygen. A further reduction and two subsequent protonation reactions facilitate the production of the reactive iron-oxo species compound I, which oxidatively attacks the bound substrate to form the product[168]. CYPs can also be inhibited by the binding of inhibitors that coordinate to the CYP heme iron[169]. Prototypical inhibitors such as ketoconazole function by forming tight, direct interactions with the heme iron and by blocking access to potential substrates[154,111,170,171]. To obtain insight into whether this might be the mechanism underlying the CYP3A5 selectivity of clobetasol, we used molecular dynamics (MD) simulations. We started by docking clobetasol into CYP3A4 and CYP3A5. Fortunately, both enzymes have been crystalized with the same ligand (ritonavir[154,117]), which provided us with a solid starting point for our *in silico* studies. As expected, superimposing the two structures revealed no significant differences in their secondary structure (**Figure 2-5**, upper panels). Interestingly, docking results produced only one pose of clobetasol for both CYP3A4 and CYP3A5; however, the ligand adopted a different orientation within their active sites (**Figure 2-5**, lower panels). To circumvent any bias in binding estimation as a result of starting structures being forced into low-energy, non-physiologically relevant conformations, we ran MD simulations independently for the CYP3A4–clobetasol and CYP3A5–clobetasol structures and ensured that each system had properly equilibrated by monitoring the root mean squared deviation (RMSD) (**Figure 2-6**). Additionally, we solvated the systems in the same water-based solvent model, ran 200-nanosecond (ns) simulations for each, and kept all other parameters the same between systems to enable direct comparisons (as detailed in the Methods section).

Our simulations showed clear differences between the interactions of clobetasol with CYP3A4 and its interactions with CYP3A5. Clobetasol could bind to CYP3A4, but it preferred an area of the active site too distant from the heme group to be considered a classical inhibitor (**Figure 2-7a**, upper panel). Remarkably, clobetasol was stabilized at a sufficient distance from the heme in CYP3A4 for water to enter the cavity from the solvent, and we observed a water molecule become stabilized on the heme iron in the distal position (**Figure 2-7a**, upper panel). A water molecule coordinated in this way is representative of the resting state of the enzyme[53,172,173], and our MD-derived CYP3A4–clobetasol structure closely matched the published crystal structure of water-bound CYP3A4[116] (**Figure 2-8**). Conversely, clobetasol interacted with the active site in closer proximity to the heme in CYP3A5 than to that in CYP3A4 (**Figure 2-7a**, lower panel). Moreover, we observed this heme-ligand interaction as stable and able to be maintained over the course of the simulation.

To predict the residues with which clobetasol might be interacting inside the active site of CYP3A4 or CYP3A5, we quantified the percentage interaction across both simulations and looked at the interaction types (**Figure 2-7b**). We also measured the binding stability of clobetasol itself as a function of relative movement by using the root mean squared fluctuation (RMSF) metric. Quantifying the RMSF showed that most atoms of clobetasol fluctuated less in CYP3A5 than in CYP3A4; these included the

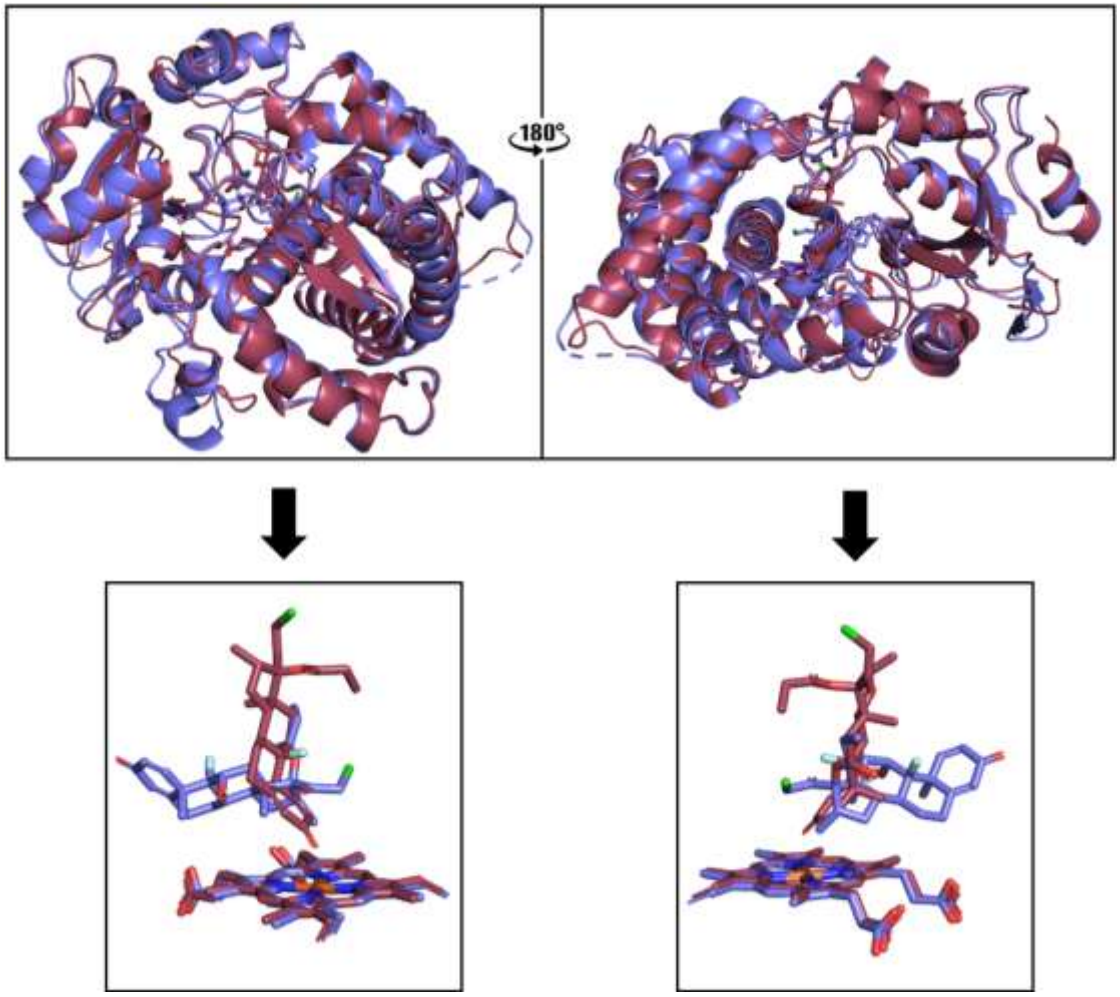

Figure 2-5. Overlay of clobetasol docked into CYP3A4 and CYP3A5.

Overlay of secondary structures for CYP3A4 (slate) and CYP3A5 (raspberry) illustrating the similarity of the structures (upper panels) and the differing binding orientations of clobetasol (lower panels).

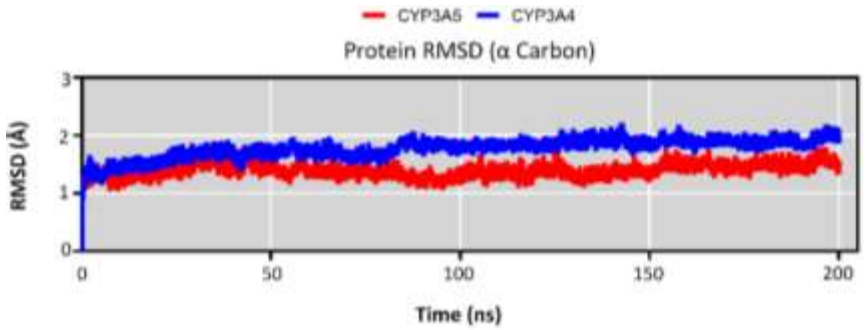

Figure 2-6. RMSD of CYP3A4 and CYP3A5 molecular dynamics simulations.

Root mean square deviation (RMSD) in Ångstroms of the CYP3A4 (blue) and CYP3A5 (red) molecular dynamics simulations. RMSD was measured based on α-carbon atoms.

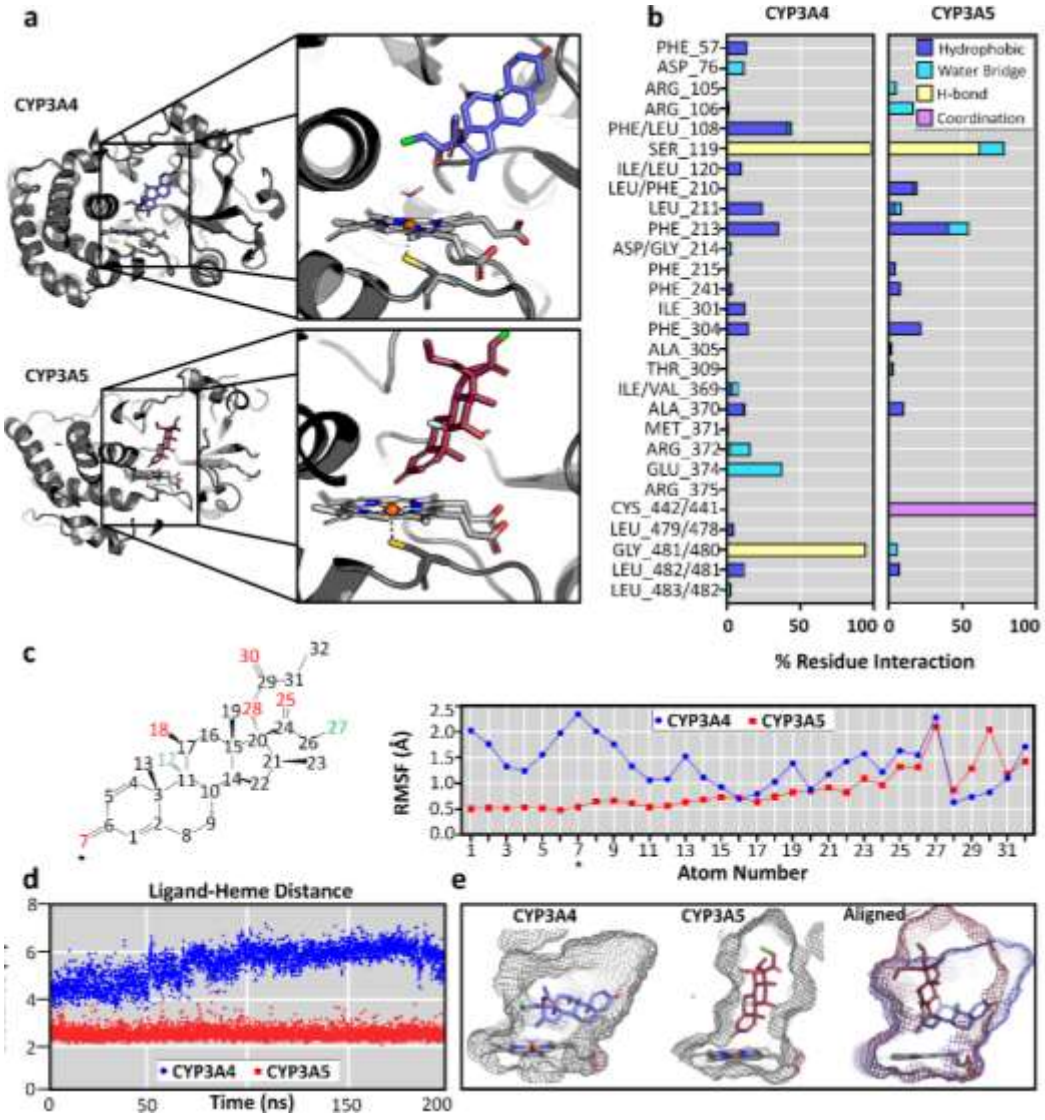

Figure 2-7. Molecular dynamics simulations suggest that clobetasol forms a heme-ligand coordination in CYP3A5 but not in CYP3A4.

(a) Snapshots from stable segments of simulations showing clobetasol bound to 3A4 (top) or 3A5 (bottom). (b) % residue interaction diagram demonstrating the residues interacting with clobetasol in 3A4 (left) or 3A5 (right). Only residues with a combined 3A4+3A5 interaction of ≥1% over the simulation course are shown. (c) The root mean squared fluctuation (RMSF) of clobetasol for 3A4 (blue) or 3A5 (red) simulations.Star (*) represents the carbonyl oxygen closest to the heme. (d) Distance measurement of the closest non-hydrogen atom of clobetasol to the heme iron of 3A4 (blue) or 3A5 (red) over simulations. (e) Docked poses of clobetasol in the 3A4 (left) or 3A5 (middle) active sites, with 5-Å binding sites shown in gray mesh. The superimposed structures are rotated to show the active site differences (right), which are shown in slate gray (for 3A4) or raspberry red (for 3A5) mesh.

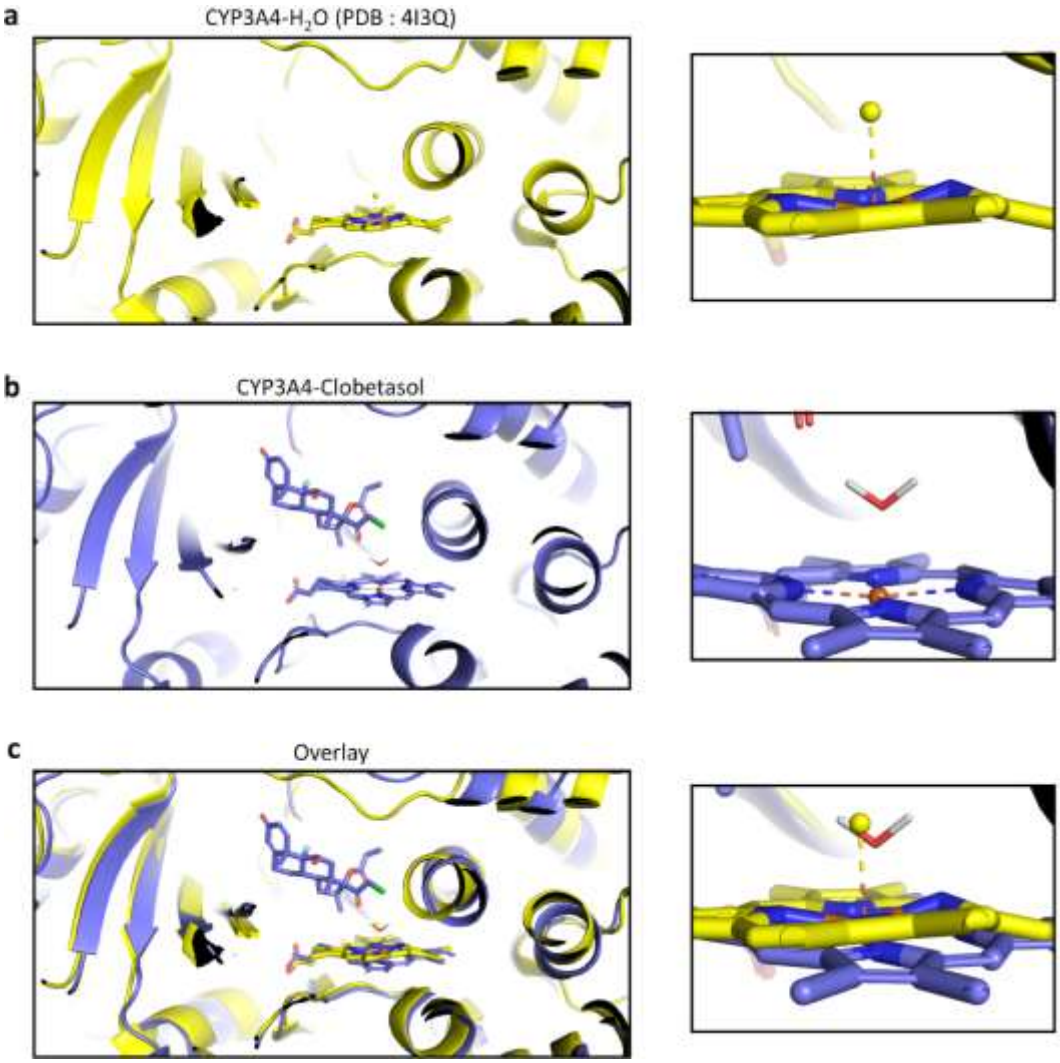

Figure 2-8. Overlay of crystalized and simulated water-bound CYP3A4.

(a) CYP3A4 bound to a water molecule from a published crystal structure (PDB:4I3Q). (b) The molecular dynamics simulation of CYP3A4 bound to clobetasol. (c) The two structures superimposed.

Carbonyl-(C=O) oxygen atoms, closest to the heme iron in CYP3A5 (Figure 2-7c). This finding can be attributed to clobetasol binding more stably (or moving less) in CYP3A5 than in CYP3A4. Additionally, we wanted to measure the clobetasol–heme distance in both simulations, since proximity to the heme group is such a hallmark of effective substrates and inhibitors[174-176]. We measured the clobetasol–heme distance for every frame of the simulation and observed that clobetasol was closer to the heme in CYP3A5 than in CYP3A4 (Figure 2-7d). The ability of clobetasol to preferentially and stably coordinate with the heme iron of CYP3A5 but not that of CYP3A4, thereby blocking solvent access and presumably serving as the mechanism of selective inhibition, was puzzling. We investigated why this might occur by examining the active site shapes of each enzyme. As reported when the crystal structure of CYP3A5 was first solved, its active site is slightly taller and narrower than that of CYP3A4[117,167]. Indeed, this difference was sufficient to permit clobetasol to adopt a vertical binding orientation in CYP3A5, as compared to its more horizontal orientation in CYP3A4 (Figure 2-7e, left and middle). Furthermore, neither active site could reciprocate its homolog's conformation to clobetasol, since the ligand would clash with the ceiling of the cavity of CYP3A4 or with the wall of the cavity of CYP3A5 (Figure 2-7e, right). Collectively, our *in silico* data have presented a model providing predictive insights into how and why clobetasol selectively inhibits CYP3A5.

Differential Interaction of Clobetasol with the Heme in CYP3A4 and CYP3A5

To determine experimentally the direct interaction of clobetasol with CYP3A4 and CYP3A5, we performed UV-visible spectroscopic analysis of clobetasol with each of these CYPs and compared the results to those obtained with their bona fide inhibitor ketoconazole[157] and substrate midazolam[177] using the recombinant purified enzymes. CYPs possess a prosthetic heme *b* group that is essential for their catalytic activity. Ligand interactions involving the heme in CYPs can be monitored by UV–visible spectroscopy, based on the ability of the ligands to induce either a type I Soret shift (blue shift), reflecting the conversion of the low-spin (LS) heme iron to the high-spin (HS) state through binding of a substrate, resulting in the displacement of the axial water ligand; or a type II Soret shift (red shift), typically occurring through the binding of an inhibitor that displaces the axial water ligand and coordinates to the heme iron (**Figure 2-9** upper panels). The titration of clobetasol and midazolam with CYP3A5 in both cases produced a typical type I CYP spectral shift with a Soret band shift from 417 nm (LS) to approximately 395 nm (HS) (**Figure 2-9c** and **Figure 2-10**). As expected, titration of ketoconazole with CYP3A5 produced a typical type II (LS) spectrum with a Soret band shift from 417 nm to 424 nm (**Figure 2-9b**). To determine the dissociation constant, the changes in the absorbance spectra of the heme-bound complex for both the clobetasol and ketoconazole titrations were determined by absorbance difference spectral titrations (**Figure 2-10**). Spectral data were obtained by successive additions of clobetasol or ketoconazole until no further heme absorbance change was observed. Thereafter, in each case, absorbance difference spectra were generated by subtracting the initial (ligand-free) spectrum from each successive spectrum, and then identifying the absorbance maximum (peak) and minimum (trough) values. The peak minus trough values were determined

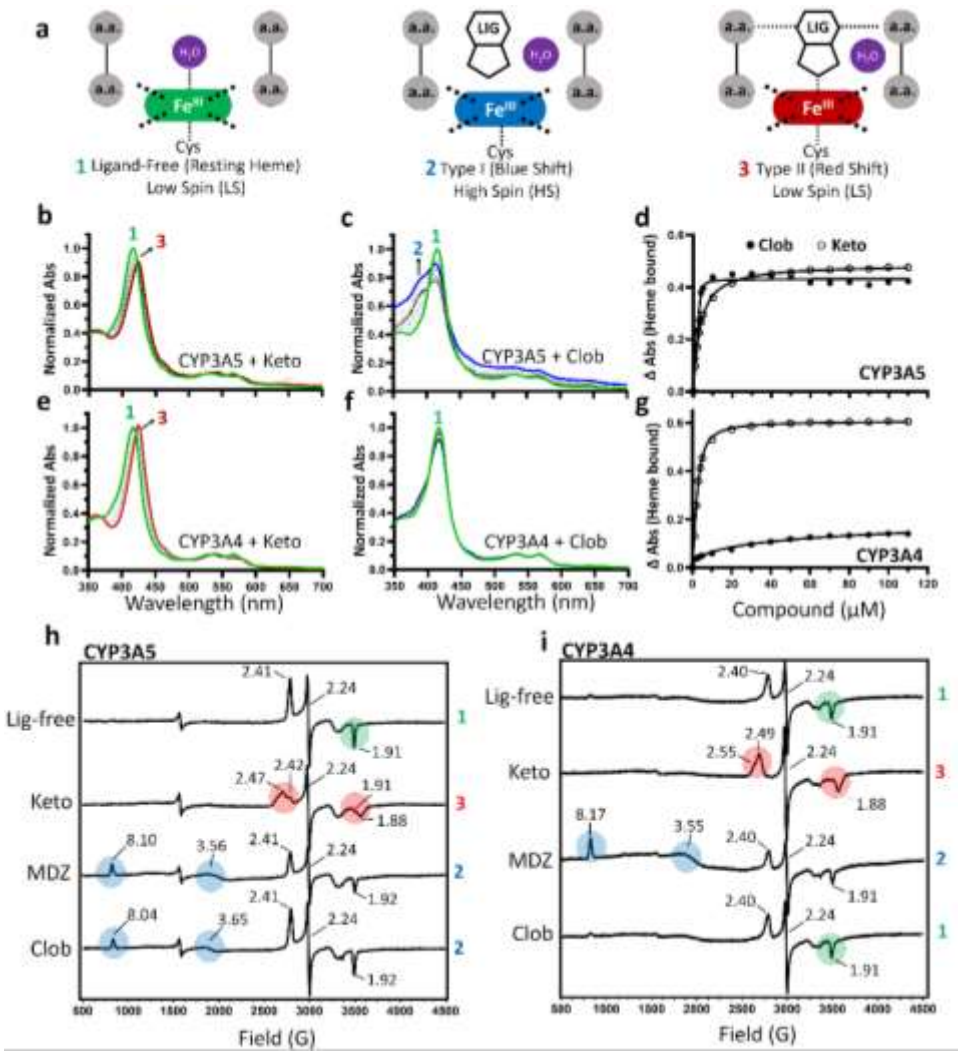

Figure 2-9. UV-Vis and EPR spectroscopy of clobetasol binding.

(a1–3) Schematic representation of ligand-induced CYP heme ferric iron (Fe^{III}) transition spin states from resting (green) to either high spin (blue) or low spin (red) states. (b,c,e,f) UV-Vis titrations of ketoconazole (Keto) (b,e) and clobetasol (Clob) (c,f) on 3A5 and CY3A4, respectively. All titrations were normalized (normalized Abs) for easy comparison. Green, blue or red line and numbering corresponds to the heme state in a1-3. (d) Plot of clobetasol (Clob) (ΔAbs 386 nm – 418 nm) and ketoconazole (Keto) (ΔAbs 432 nm – 410 nm) induced heme absorption change (ΔAbs of Heme Bound) in 3A5 versus ligand concentration and data fitted with equation 2 (methods) to give a Kd of 0.1 ± 0.3 μM and 3.1 ± 0.5 for clobetasol and keto, respectively. (g) Plot of the maximal clobetasol (ΔAbs 388 nm – 418 nm) and keto (ΔAbs 432 nm – 410 nm) induced heme absorption change (ΔAbs of Heme Bound) in 3A4 versus ligand concentration. A Kd of 0.9 ± 0.2 μM was calculated for keto. (h,i) EPR spectra for 3A5 and 3A4 in their ligand-free forms and for their complexes with ketoconazole, midazolam, and clobetasol with colored number labels corresponding to the heme ferric iron (Fe^{III}) state as in a1–3.

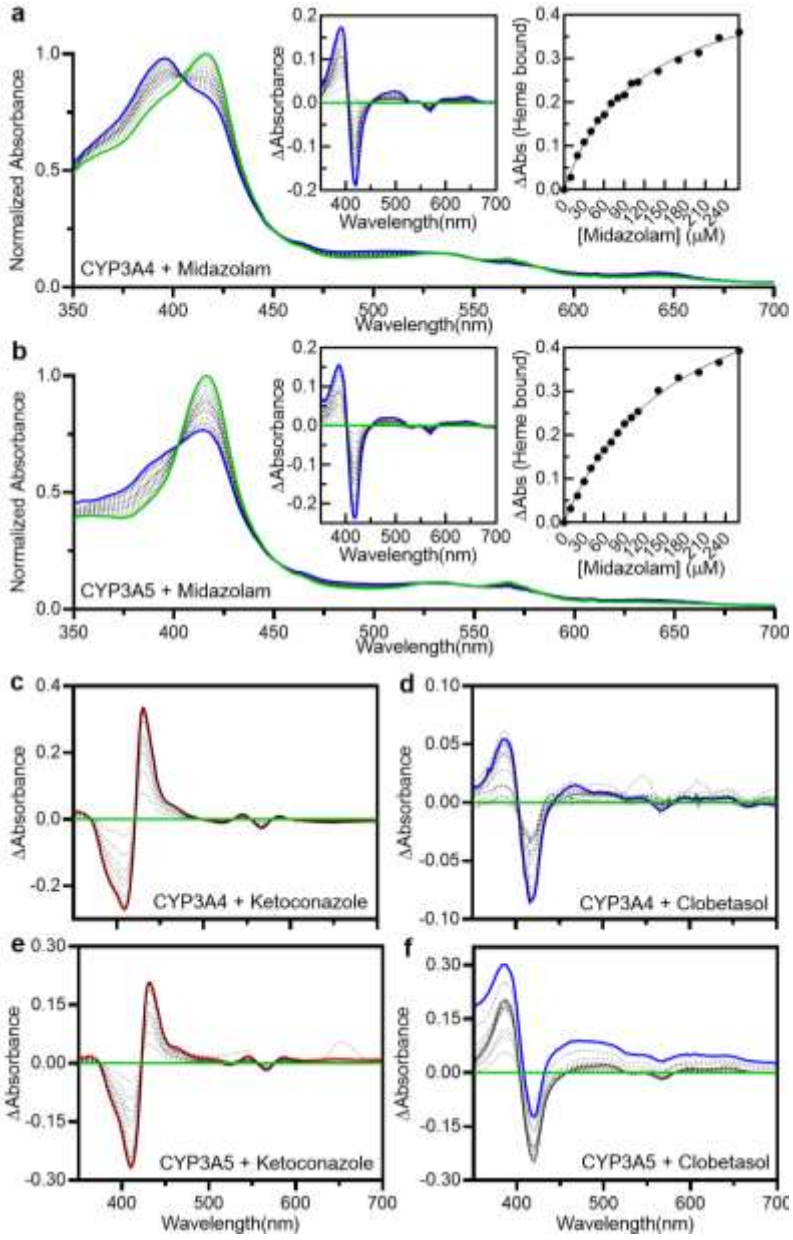

Figure 2-10. Spectral changes of CYP3A4 and CYP3A5 from various compounds.

(a,b) Spectral changes upon titrating midazolam into 5 μM of CYP3A4 (a) and CYP3A5 (b). Absorbance values were normalized to the maximum value in the spectra. Left insets: Difference spectra showing absorbance changes between the ligand-free and midazolam-bound states. Right insets: Titration plots fitted to a hyperbola equation. (c–f) Difference spectra showing absorbance changes between the ligand-free and compound-bound states for 3A4 and 3A5 proteins. Color scheme: The UV–Vis spectrum for the ligand-free (resting) state is in green, whereas the spectra for the last titration point are in blue (type II blue shift) or red (type I red shift).

from each difference spectrum, and these values were plotted against the relative ligand concentration, enabling the production of ligand-binding curves, leading to the generation of the respective dissociation constants (K_d) of 0.1 ± 0.3 μM for clobetasol binding to CYP3A5 and a K_d of 3.1 ± 0.5 μM for ketoconazole binding to CYP3A5. In addition, a similar degree of conversion to the ligand bound form was achieved in titrations with both clobetasol and ketoconazole where both showed a near complete conversion to the high-spin or inhibitor bound forms respectively albeit at different concentrations of ligand (**Figure 2-9d**). In contrast, titrating clobetasol with CYP3A4 produced only a 416 nm. Similar to CYP3A5, ketoconazole induced a type II spectral shift in CYP3A4 with a K_d value of 0.9 ± 0.2 μM (**Figure 2-9e-g** and **Figure 2-10**). These data clearly suggest a selective heme iron interaction by clobetasol, particularly for CYP3A5.

To further confirm the selective heme interaction of clobetasol with CYP3A5 versus CYP3A4, continuous wave (CW) X-band electron paramagnetic resonance (EPR) spectra were generated with ligand-free CYP3A4 and CYP3A5 and with these CYPs in complex with clobetasol, midazolam, and ketoconazole. Ligand-free CYP3A5 produced a rhombic LS EPR spectrum with g-values of 2.41 (g_z), 2.24 (g_y), and 1.91 (g_x), respectively, indicative of a single dominant ferric heme species coordinated by a proximal cysteine thiolate ligand and a weakly coordinated axial water ligand (**Figure 2-9a-h**). In ligand-free CYP3A4, a small signal was seen for an HS species with g-values apparent at 8.17 and 3.56 (the g-values were not labeled in the spectrum), while in CYP3A5 no such small HS signal was seen in the resting form of the enzyme. The EPR spectra for CYP3A5 in complex with clobetasol or midazolam revealed spectral signals consistent with the formation of a five-coordinate HS ferric heme iron state (which usually indicates the ligand-dependent displacement of the CYP3A5 distal water ligand) with HS g-values of 8.04/3.65 (with clobetasol) and 8.10/3.56 (with midazolam) (**Figure 2-9a-h**). A proportion of the LS ferric signals was retained, indicative of the retention of a water coordinated state in the absence of substrate, with g-values of 2.41/2.24/1.92 for both clobetasol and midazolam. In contrast, CYP3A4 revealed no new HS formation with clobetasol; the spectra were consistent with the corresponding LS ligand-free form with g-values of 2.40/2.24/1.91, indicating the retention of the axial water ligand in the presence of clobetasol in CYP3A4. However, an HS signal was induced by midazolam when the compound was bound to the enzyme with HS g-values of 8.17/3.55 and LS g-values of 2.40/2.24/1.91. As expected, both CYP3A4 and CYP3A5 produced new LS species when bound to ketoconazole, with g-values of 2.55, 2.49/2.24/1.88 for CYP3A4 and 2.47, 2.42/2.24/1.88 for CYP3A5, which are typical signals seen for a CYP enzyme with an azole inhibitor bound (**Figure 2-9h,i**). These data provide further evidence of the selectivity of clobetasol for CYP3A5.

CHAPTER 3. TRANSCRIPTIONAL REGULATION OF CYP3A5

Regulation of CYP3A5 in Pancreatic Cancer Remains Unknown

It is known that CYP3A4 and CYP3A5 are controlled by common regulators in the widely studied hepatocellular carcinoma model HepG2[178]. Due to heightened risk of drug-drug interactions, the subject of CYP3A regulation has been intensely researched in this context. Pregnane X Receptor (PXR) is a ligand-inducible transcription factor and serves as the primary regulator of CYP3A in liver - and its induction can lead to markedly higher expression of these enzymes[179]. However, the regulation of CYP3A has not been delineated in extra-hepatic models. CYP3A5 is expressed outside of the liver in several tissues such as kidney, prostate, intestine, and lung[2]. The recent report of selective CYP3A5 over-expression[180] and contribution to chemoresistance in pancreatic cancer[9] signifies that this enzyme is controlled in a different manner. Based on the only presently-available report, it is suggested that outside of PXR it's possible that CYP3A5 is regulated in this cancer by hepatocyte nuclear factor alpha (HNF4α)[9]. We investigated this by testing CYP3A5 mRNA and protein levels upon RNAi-mediated knockdown of PXR and HNF4α. We used the high CYP3A5-expressing pancreatic cancer model AsPC-1 and show that neither PXR nor HNF4α control CYP3A5 levels (**Figure 3-1a, b**). Additionally, we generated a CRISPR/Cas9-mediated genetic PXR mutant cell line and sequenced its RNA, along with a wild-type cell line of the same background. It was evident that the PXR functional mutation had a global effect on transcription, but CYP3A5 was completely unaffected (**Figure 3-1c**). Collectively, these data strengthen the evidence that neither PXR nor HNF4α transcriptionally regulate CYP3A5, and that its true regulators in this cancer model remain unknown. While we have identified the first selective CYP3A5 inhibitor which can be used as a means of target validation, there is a lot of room for improvement before it can be of potential clinical use (its current intended target is glucocorticoid receptor, for example). Outside of direct inhibition however exists the possibility of targeting CYP3A5 upstream. This warrants elucidation of its true transcriptional regulators, both for targeting CYP3A5 and for gaining more insight into the biology of CYP3A5-expressing cancers.

Development of a Novel Computational Method of Regulator Prediction

Several approaches are available to researchers needing to find which factors control the expression of a given target. Spanning both computational and experimental techniques, each has its own set of benefits and limitations. Among the most exhaustive of experimental approaches is knockdown of the entire genome one-by-one using expression modulation techniques like RNAi or CRISPR/Cas9. Screening at this scale requires an assay with target readout and signal window robust enough to be suitable for high-throughput. By that point the scientific question needs to merit the time and resources required for a project of such magnitude. Additionally, whole-genome screens are typically conducted in a single model, limiting the ability to capture regulation

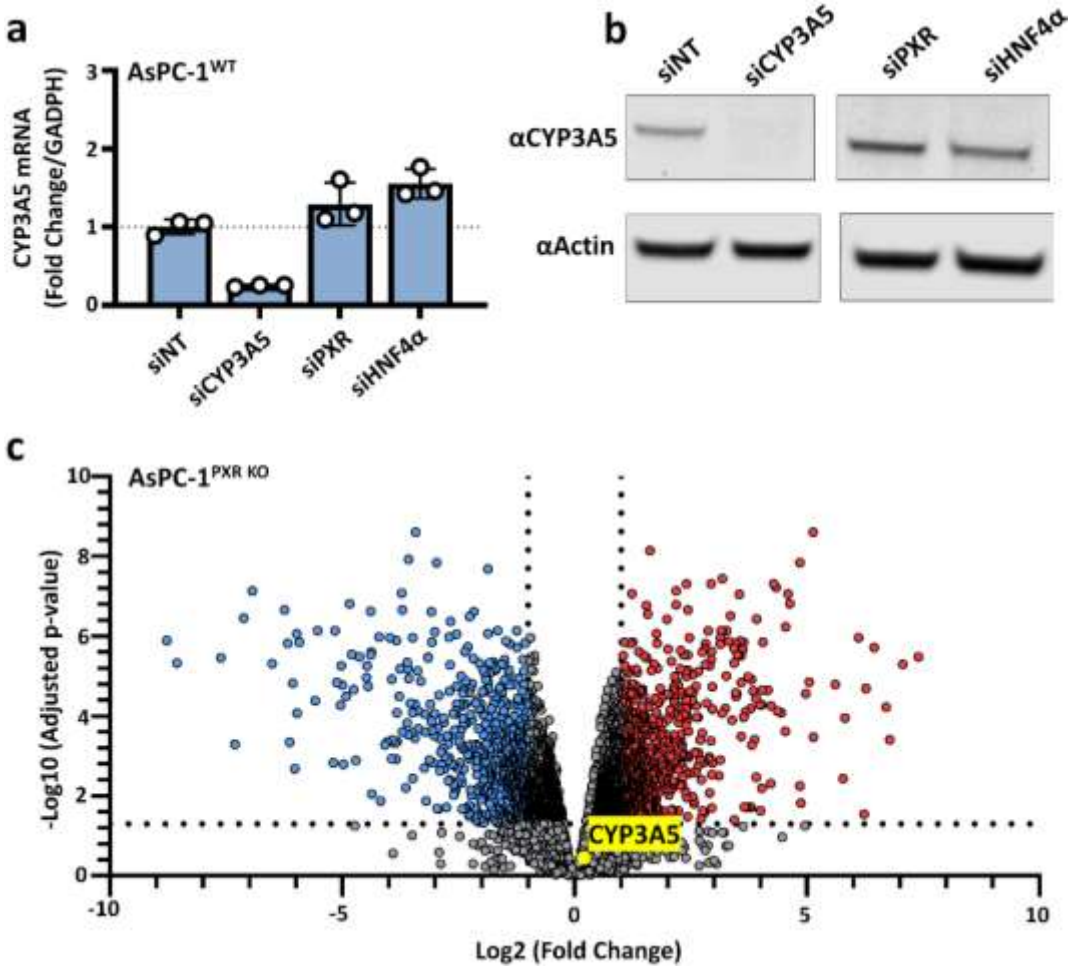

Figure 3-1. Neither PXR nor HNF4α control CYP3A5 in AsPC-1 cells.

(a) CYP3A5 mRNA and (b) protein levels upon RNAi-mediated knockdown of PXR or HNF4α. (c) Volcano plot of transcriptome-wide effects of gene expression mediated by PXR knockout. CRISPR/Cas9 technology was used to generate a PXR functional knockout, and data are compared to AsPC-1 WT.

mechanisms representative of the complex and heterogenous disease. A more casual option would be to search repositories of ChIP-seq experiments (such as the ENCODE database[181]), reverse-querying the data to see if DNA of the target has been bound by any known proteins. This option is easy to perform and often combines tissue/disease states for added robustness. However, these databases limit researchers to nucleic acid-associated proteins such as transcription factors, when any number of other non-DNA-binding proteins in a pathway may ultimately regulate a target. Furthermore, ChIP-seq data is rarely context-specific, and thus interpretation of putative regulators will be skewed if the target of interest is different across contexts. For example, a ChIP-seq query for proteins found to bind the CYP3A5 promoter may return PXR as a hit due to the samples being averaged across tissue and disease. While this may be indicative of hepatocellular carcinoma for example, it doesn't hold true in pancreatic cancer.

Experimental approaches that test knockdown of only a subset of genes are reasonable if the readout is appropriate. For example, if the aim is to search for regulators of a target's transcription, post-transcription readouts such as protein imaging or measuring its downstream function with luminescence (if an enzyme) may not be appropriate since mRNA, protein, and function do not always correlate. This is especially the case if the mRNA plays any non-canonical biological role. Another important consideration is how to come up with the initial list of candidate genes for knockdown. Choosing curated commercially available siRNA or CRISPR libraries like transcription factors or cancer-specific genes can drastically reduce the screening size compared to whole-genome. The downside of this is that each library limits researchers based on *a priori* knowledge, whereby genes of unknown or uncharacterized function are excluded. Computational methods exist to identify putative transcriptional regulators from sequencing data, potentially outputting a reasonable quantity of gene candidates to test. The benefits of these methods are that they start from a source of typically heterogenous data, such as expression data from several cell lines or patient tumor samples. The limitation is that most stem from inference algorithms which are fundamentally designed to uncover drivers of a disease, or essential genes – not the specific regulator(s) of a single target. One such example is the popular Algorithm for the Reconstruction of Accurate Cellular Networks (ARACNe)[182]. This method and others (such as Network-based Bayesian Inference of Drivers or NetBID) successfully address important topics in disease such as uncovering proteins that drive a given cancer[183] or characterize disease-specific transcriptional activity[184]. Obtaining regulators of a single target is only a byproduct of these techniques however and is flawed due the techniques themselves being designed to address different questions. Additionally, one of the highlights of using inference is to *infer* relationships based on known gene functions and/or existing experimental data. While sometimes helping to narrow down large hit lists, this precludes these methods from being unbiased.

There is a clear need for a computational method capable of agnostically predicting transcriptional regulators without inference. Ideally, one would want to know the pairwise relationships of all genes across all samples within a dataset. Theoretically, the mathematical operation to calculate these relationships is trivial; Spearman or Pearson correlations are among the most popular to detect the linear relationships of gene

products. In practice however, such a brute force approach on a transcriptome-wide level is challenging due to the substantial computational strain. Non inference-based methods to understand pairwise relationships of data do exist, such as the tool Weighted Gene Correlation Network Analysis (WGCNA)[185]. However, they often take shortcuts either by heavily filtering the starting data, only considering known transcription factors, avoiding statistical significance measurements altogether, or modifying expression results to achieve faster calculations. No current tool is available to overcome all of these limitations.

We developed a computational pipeline capable of intaking large expression data, and quickly computing transcriptome-wide pairwise correlations and co-expression networks to agnostically predict transcriptional regulators of a given target. The resulting tool is named **C**orrelations **O**f **L**arge **D**atasets to **S**earch for **Tra**nscriptional **R**egulators or COLDSTaR. Co-expression derived from pairwise correlations represents a useful means to understand how genes behave together across a population[186,187]. This type of data can be leveraged for the purpose of predicting which correlated genes may transcriptionally control a given target. Simplified, co-expression networks generally represent four possible interpretations. Relative to the gene of interest, a co-expressed gene could be transcriptionally upstream, transcriptionally downstream, co-regulated with the gene, or just noise and not truly co-expressed (**Figure 3-2a**). We incorporate several steps in the COLDSTaR workflow, which are explained in detail within our methodology. We also make our code publicly-available in our GitHub repository (github.com/wcharleswright). A graphical representation of the general workflow can be found in **Figure 3-2b**.

COLDSTaR takes in large expression data and automatically performs several steps for normalization. The resulting data are then prepared and filtered for downstream processes. Of note, no gene is filtered out unless completely unexpressed across 100% of samples in a set. This is different from other pipelines which often filter genes whose expression is low in the majority of samples for the purpose of gaining speed and decreasing workload. Our rationale was that the expression of a given transcriptional regulator may only need to be very lowly expressed in order to efficiently control its target. Such relaxed filtering criteria keeps tens of thousands more genes which would otherwise be discarded. The next step is to calculate the correlations and corresponding statistical significance. The calculations themselves are straightforward, and we take advantage of the Spearman rank correlation coefficient (ρ or "rho") due to its resistance to outliers when dealing with gene expression data[188]. The difficulty comes from the amount of calculations needed. Computing all-by-all correlations requires producing a matrix of n^2 values, where n is equal to the number of genes. A typical number of genes passing our relaxed filtering criteria is around 35,000, which would require $35{,}000^2$ (1.2 billion) calculations each of rho and p-values. This far exceeds the processing and memory limitations of even large, dedicated computer servers. We overcome this obstacle by expanding upon block-wise computation to create very large correlation matrices. Previous research has been conducted for computing such large matrices through the R framework in a block-wise fashion.[189] This method fills a large preallocated empty matrix with temporary submatrix 'blocks' at their corresponding positions, and ultimately accesses the blocks as they are completed to stitch them into the

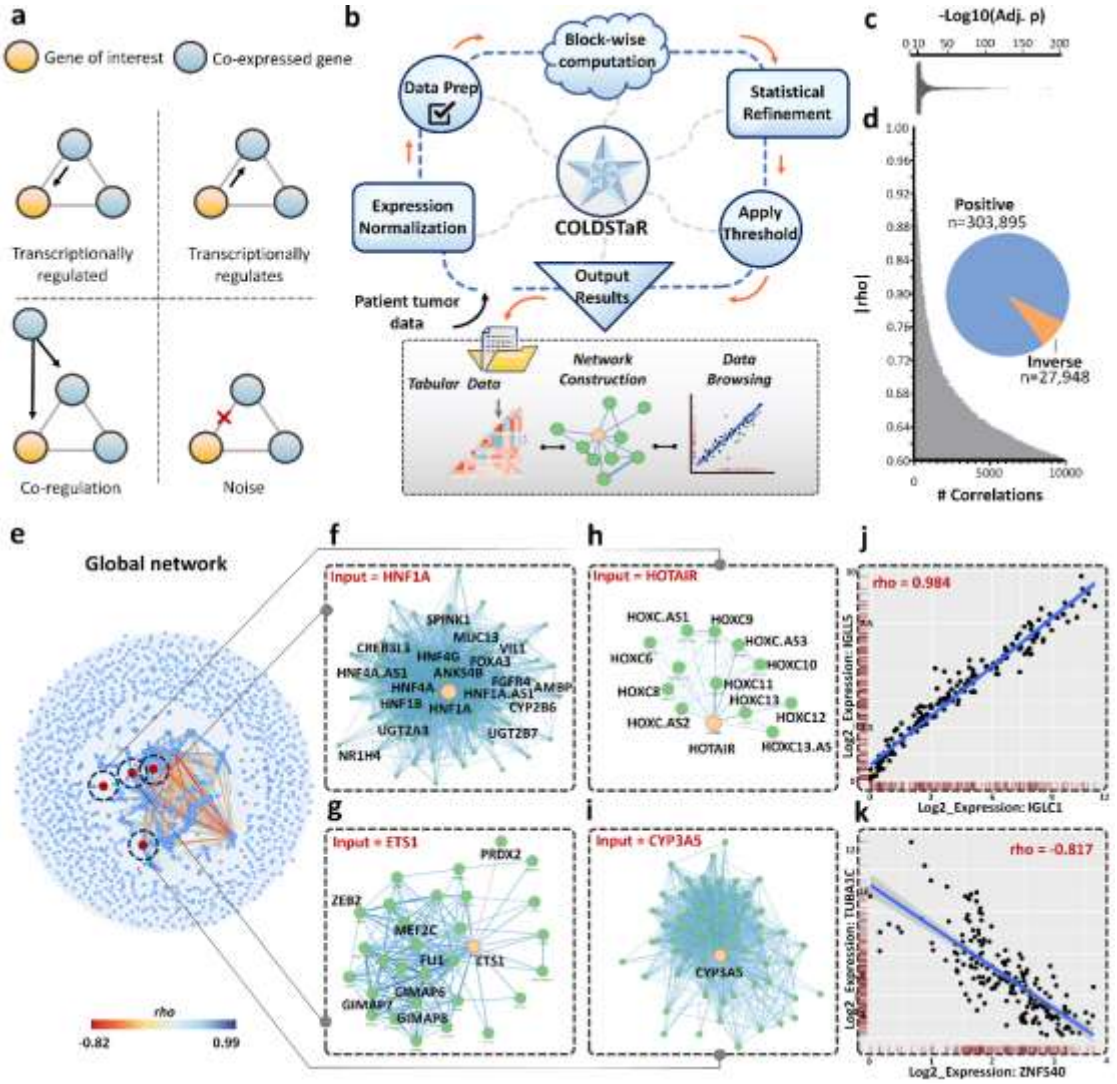

Figure 3-2. COLDSTaR analysis of pancreatic tumors.

(a) Diagram of typical types of information gained from co-expression networks. (b) General overview of the COLDSTaR pipeline for automated generation of co-expression networks based on tumor expression data. (c) Overview of the adjusted p-value distribution and (d) Spearman's rho value resulting from the pancreatic adenocarcinoma cohort of TCGA (n= 183 tumor samples) analyzed by COLDSTaR. (e) Global co-expression network of all threshold-passing correlations. (f-h) Extracted subnetworks of select transcriptional regulators, and their experimentally validated targets (i) Extracted subnetwork of CYP3A5. (j) Strongest positive and (k) inverse correlations from the network. Dots represent Log2(Normalized CPM+1) expression corresponding to a tumor sample. Regression lines are shown in blue and 95% confidence intervals in gray.

final matrix. We exploited this technique, modifying it to serve our purpose by simultaneously calculating Spearman correlations and p-values of our large gene sets. The next step is to apply a statistical adjustment to the resulting p-values. Statistical testing in gene expression suffers from the multiple hypothesis problem, which can dramatically skew statistical significance and lead to misinterpretation[190]. COLDSTaR applies a Bonferroni p-value adjustment. This type of correction dramatically lessens the statistical significance of any given p-value, and is considered to be among the most conservative of commonly-used corrections[191]. The rationale for using this method relates to the ultimate goal of selecting the most likely transcriptional regulators of a given target. While some correlations which may be biologically true are regarded as statistically insignificant due to this step, the top results (and thus most likely to be true) are retained. After statistical refinement, the tool then applies thresholds to the data. Thresholds are an important part of the workflow to discard co-expression results which are likely irrelevant. Spearman correlations on an absolute scale (|rho|) range from 0-1, where higher values indicate tighter correlations and values closer to zero are more suggestive of there being no linear relationship. While there is no strict rule for a cutoff as being biologically accurate[192], we chose a moderately stringent threshold for the purpose of keeping a reasonable number of likely true hits, based on empirical testing. The applied threshold is defined as those correlations of $|rho| \geq 0.6$ and adjusted p-value ≤ 0.05. Following threshold application, COLDSTaR exports the results as tabular data (a CSV file) which can be easily searched for a gene of interest. COLDSTaR results can also answer questions of which genes are most tightly co-expressed (either positively or inversely) across the entire transcriptome. This is a unique capability, afforded by the brute force all-by-all computation approach. Finally, we transform the tabular data into a co-expression network. This is achieved by our network calculation and visualization tool COLDNet (also available in our GitHub repository). Resulting networks can be generated easily to see not only all co-expressed genes relative to a gene of interest, but the relationship to themselves as well. This provides valuable insight especially in the context of hit selection.

COLDSTaR Analysis of Pancreatic Tumors

To begin our search for predicted CYP3A5 regulators in pancreatic cancer, we first obtained gene expression data from 183 pancreatic cancer tumors sequenced by The Cancer Genome Atlas (TCGA)[163]. We analyzed all data with the COLDSTaR pipeline and inspected the results. Greater than 300,000 statistically significant threshold-passing correlations were obtained (**Figure 3-2c, d**). Most of the correlations were positive, although a subset was inverse. This may represent transcriptional repression. Since correlation data were calculated on a transcriptome-wide level, a global network could be plotted from which to extract subnetworks of interest (**Figure 3-2e**). While no synthetic data can be constructed for transcriptional regulation to test the validity of our tool, we found it reasonable to inspect networks for known examples of regulators and their target genes as a means of sanity checks. HNF1A is widely implicated in pancreatic cancer[193-195]. We extracted the HNF1A subnetwork and found several examples of genes known to be under HNF1A regulation such as MUC13[196], FOXA3[197], SPINK1[193], and HNF4α [197]

among others(**Figure 3-2f**). We also extracted the subnetwork for ETS1, a well-established proto-oncogene transcription factor[198] and found examples of known downstream targets such as MEF2C[199], PRDX2[200], and ZEB2[201] (**Figure 3-2g**). We were curious about known non-transcription factor regulators, and decided to extract the subnetwork of the long noncoding RNA HOTAIR, which is known to transcriptionally regulate HOX gene clusters[202,203]. Interestingly, all but one gene in the resulting HOTAIR network belonged to the HOX family (**Figure 3-2h**). These networks suggested that COLDSTaR may be able to predict a list of regulators for CYP3A5. Indeed, we were able to extract the CYP3A5 subnetwork and obtain various co-expressed gene candidates along with it (**Figure 3-2i**). As previously mentioned, one distinguishing feature of our tool is the resulting all-by-all correlations, which can be used to simply browse which two genes are most tightly correlated among data spanning hundreds of thousands of correlations. We found the pancreatic cancer cohort to most tightly co-express IGLC1 and its paralog IGLL5, which are part of the immunoglobulin lambda chain (**Figure 3-2j**). The strongest inverse correlation was from ZNF540 and TUBA1C (**Figure 3-2k**). When ZNF540 expression is high, TUBA1C is low. Interestingly, ZNF540 is a known transcriptional repressor[204], and TUBA1C is reported as an oncogene[205], although no studies have tied them together. Collectively, COLDSTaR identified known regulator-target relationships, showed interesting connections between co-expressed genes, and suggested there could be promise for identifying transcriptional regulators of CYP3A5.

COLDSTaR Captures Transcriptional Regulators of CYP3A5

While COLDSTaR is able to overcome various limitations of other tools, it remained unvalidated experimentally and was not directly compared to other methods. To this end, we analyzed the exact same pancreatic cancer expression dataset using two other methods. NetBID is a systems biology algorithm which measures gene relationships across samples based on mutual information, and has successfully identified driver genes and their functions[183]. cBioPortal is another tool capable of calculating pairwise correlations without inference[206]. Like COLDSTaR, cBioPortal can measure Spearman correlation values across TCGA data to generate pairwise correlations. This repository is popular, accessible, and easy to use. Unlike COLDSTaR however, cBioPortal does not re-normalize expression data, cannot calculate all-by-all correlations (and thus only returns co-expressed results for one gene of interest at a time), and cannot produce co-expression networks. We removed these features from COLDSTaR in an effort to reproduce the cBioPortal method, only differing by applying the COLDSTaR threshold since cBioPortal's results are not subject to any cutoffs and would produces thousands of hits. We refer to this modified cBioPortal method as 'Correlation only'.

Each method was tested for its ability to predict transcriptional regulators of CYP3A5. All 3 methods returned candidate genes with corresponding commercially-available siRNAs that could be experimentally tested downstream. NetBID produced 173 candidates, Correlation only method produced 40, and COLDSTaR produced 60 (**Figure 3-3**a). Interestingly, there was relatively low overlap in predicted CYP3A5 regulators between the three methods, highlighting their differences in design. We inspected the

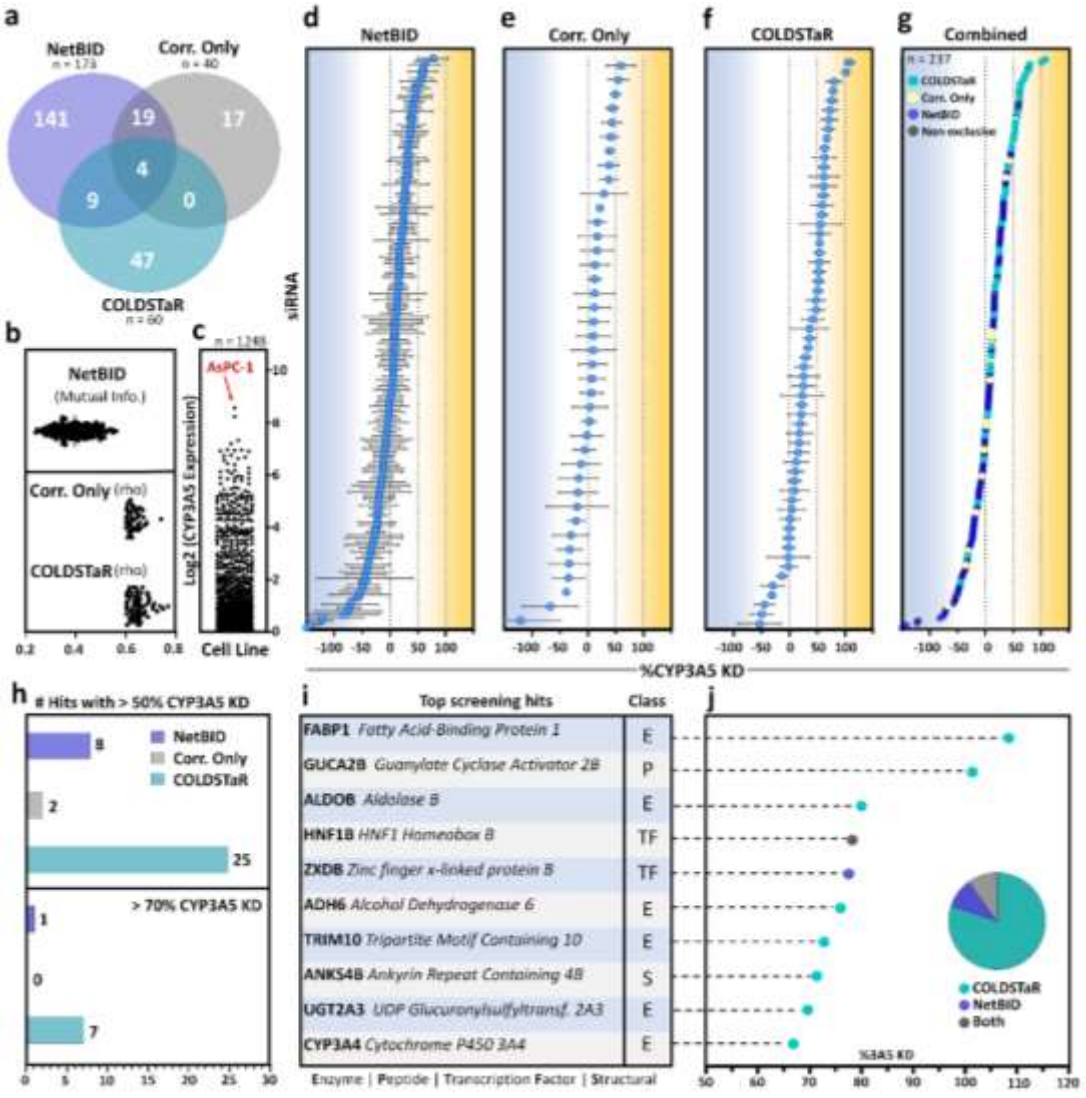

Figure 3-3. COLDSTaR captures transcriptional regulators of CYP3A5.

(a) Venn diagram of predicted CYP3A5 transcriptional regulators produced by the inference algorithm NetBID, correlation only method, and COLDSTaR. Hits displayed are those with commercially available siRNAs. (b) The distribution of predicted regulators in units of mutual information (for NetBID) or Spearman's rho (corr. only and COLDSTaR). (c) CYP3A5 expression across 1,248 cell lines obtained from depmap (depmap.org). Units are Log2(TPM+1). (d-g) mRNA-based screen of predicted regulators from each of the three methods, performed in AsPC-1 cells. Assay normalized to siCYP3A5 and siNT. Each assay performed in triplicate. (h) Number of hits with >50% or >70% CYP3A5 KD by prediction method. (i) Top 10 hits from screen (all methods combined) with their corresponding protein class and (j) %CYP3A5 KD and method origin.

distribution of these predictions among the three methods and saw they spanned various scores, either for mutual information (NetBID) or Spearman's rho (Corr only and COLDSTaR) (**Figure 3-3b**). This suggests that in cases where numbers of candidates are produced beyond validation capabilities, the lists could be ranked to narrow selections. For our purposes we wanted to exhaustively test our method against others and decided to continue with 100% of hits identified from each method. We then searched for an appropriate cell model in which to screen candidate CYP3A5 regulators. We searched the largest repository of RNA-seq data for cell lines, DepMap portal[207]. Of the 1,248 cell lines AsPC-1 cells had the highest CYP3A5 expression (**Figure 3-3c**), which we chose to continue forward with. We next knocked down all candidates using siRNA in these cells and measured the resulting effect on CYP3A5 mRNA. All three methods produced hits which both increased and decreased CYP3A5 levels **(Figure 3-3d-f**). When all 237 siRNA were combined and assigned the method they were derived from, COLDSTaR hits were enriched as the best in terms of CYP3A5 knockdown (**Figure 3-3g**). When evaluating hits in the categories of > 50% or > 70% CYP3A5 knockdown, COLDSTaR remained the best (**Figure 3-3h**). We inspected the top 10 screening hits (regardless of which method identified them) and noticed that the majority of them were not transcription factors (**Figure 3-3i**). These hits spanned from 68% CYP3A5 knockdown to > 100% (better than siCYP3A5) and were all exclusively identified by COLDSTaR, with the exception of HNF1B (identified by NetBID and COLDSTaR) and ZXDB (identified exclusively by NetBID). These results highlighted the utility of our new tool and showed promise for potentially identifying CYP3A5 transcriptional regulators.

Knockdown of Predicted Transcriptional Regulators Ablates CYP3A5 mRNA Expression

Results obtained from screening-level experiments can be spurious and need to be validated. To this end we tested the top 10 putative hits (**Figure 3-3i**) using pooled siRNA in AsPC-1 cells. Some of the hits showed very promising results, even approaching total knockdown (**Figure 3-4a**). We were interested to see that siCYP3A4 also decreased CYP3A5, but this is likely attributed to off-target effects considering the high homology between the homologs. We next decided to pursue the hits which decreased CYP3A5 levels ≥ 50% by deconvoluting them in an effort to decrease off-target effects and increase knockdown (**Figure 3-4b**). Each of the 4 hits showed striking CYP3A5 knockdown (**Figure 3-4b**) and were statistically significant compared to the siNT control (**Figure 3-4c**). Interestingly, the top two hits were not transcription factors. GUCA2B is a peptide ligand of the Guanylate Cyclase 2C receptor[208], and FABP1 is a fatty acid-binding enzyme[209]. Remarkably, these two hits displayed complete CYP3A5 knockdown and serve as indication that they tightly control CYP3A5 transcription. Furthermore, these hits were identified exclusively by COLDSTaR and also highlight the importance of considering non-DNA-binding candidates. Finally, we tested the ability of our hits to decrease 3A5 protein levels. While this is not the goal of our tool, we were interested to probe protein levels as an added layer of information. The top 2 hits which completely ablate CYP3A5 mRNA expression also drastically decrease CYP3A5 protein (**Figure 3-4d**). The other two hits didn't show much effect on protein knockdown,

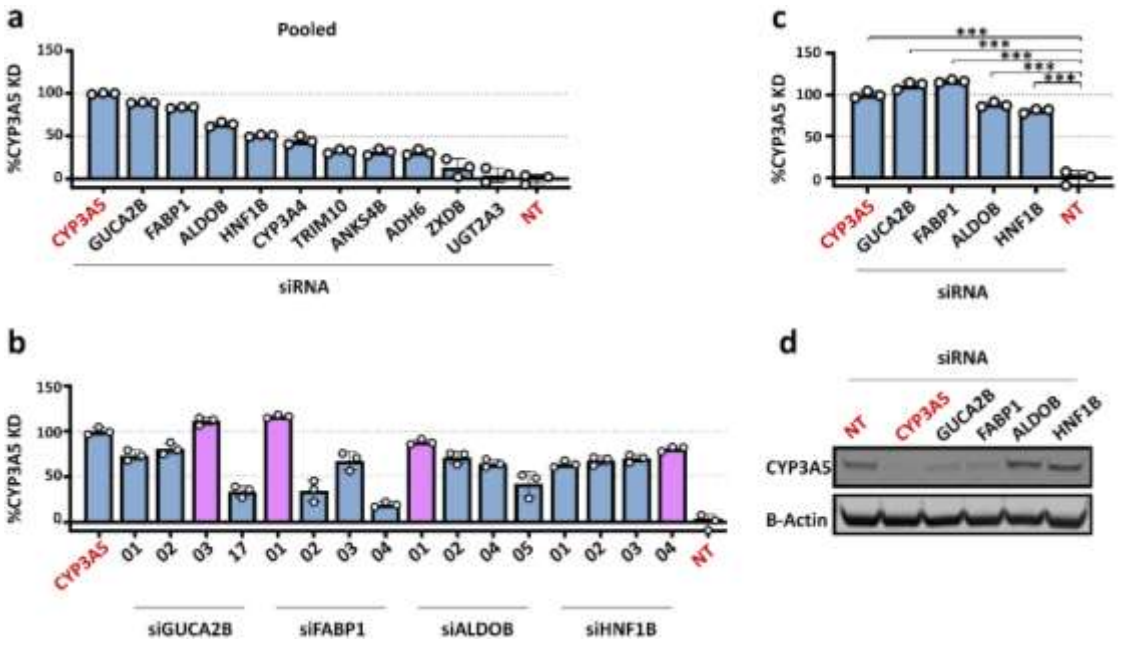

Figure 3-4. Knockdown of predicted transcriptional regulators ablates CYP3A5 mRNA expression.

(a) Normalized CYP3A5 KD upon treatment with pooled siRNAs representing top 10 screening hits. Transfection was performed in AsPC-1 cells. (b) Deconvolution of siRNA hits from panel a (defined by ≥ 50% CYP3A5 KD). Pink bars represent the individual best performing siRNA. (c) Statistical comparison of the deconvoluted siRNAs and siCYP3A5 control compared to siNT. *** $P \leq 0.0001$, one-way analysis of variance (ANOVA)

possibly indicating they act primarily on the mRNA level. Collectively, our results demonstrate that COLDSTaR successfully identified 4 transcriptional regulators of CYP3A5 in a pancreatic cancer model. These regulators are unreported in the context of regulating CYP3A5, and warrant further investigation, particularly in the case of targeting CYP3A5 in disease.

CHAPTER 4. METHODOLOGY*

Compounds Used

All compounds were obtained from commercial sources and the purity was 95% or higher. The compound name, vendor, catalog number, and analytical method used to determine purity are: Ritonavir, Toronto Research Chemicals, R535000, 1H NMR; 1-hydroxymidazolam, Cayman Chemical, 10385, 1H NMR; Clobetasol propionate, AK Scientific, F535, HPLC; Ketoconazole, Abovchem, AC513267, 1H NMR; Midazolam, U.S. Pharmacopeia, 1443599, UHPLC and LC-MS/MS.

CYP3A4 and CYP3A5 Biochemical Inhibition

To measure the inhibition of CYP3A4 or CYP3A5, the P450-Glo luminescence assay using the substrate Luciferin-IPA was purchased from Promega (Madison, WI; cat. no. V9002). Supersomes from Corning Life Sciences (Tewksbury, MA) were used as the source of purified recombinant human enzymes; they contained P450 oxidoreductase (POR), cytochrome b5, and either CYP3A4 (Corning, cat. no. 456202) or CYP3A5 (Corning, cat. no. 456256), each at 1000 pmol/mL. Insect cell control supersomes were used as a negative assay control (Corning, cat. no. 456200). The assay protocol was performed in accordance with the P450-Glo manual, using final concentrations of 0.1 pmol of enzyme, 100 mM KPO4 (pH 7.4) buffer, and 3 µM Luciferin-IPA as substrate. Upon the reactions being initiated by the addition of NADPH, the plates were incubated for 10 min at 37 °C. Reactions were then quenched for 20 min at room temperature, using the luciferin detection reagent. Luminescence was recorded with an EnVision 2102 Multilabel Plate Reader from PerkinElmer Life Sciences (Hopkinton, MA). All assays were performed using 384-well, polystyrene, white, opaque, non-treated plates (Corning, cat. no. 8850BC). The percentage inhibition was normalized to the average of six replicates containing either 30 µM ketoconazole (100% inhibition) or DMSO (0% inhibition) within each plate. The final concentration of DMSO for all compound and control wells of the assay plates was 0.1%.

For primary screening, an in-house library of bioactive compounds (n = 11,200, but some compounds are redundant) having diverse bioactivity was screened at a single concentration of 5 µM against CYP3A5. Compounds conferring at least 60% inhibition

---

* Portions of chapter from previously published article; pre-print submission reprinted with permission of American Chemical Society. Wright, W. C. et al. Clobetasol Propionate Is a Heme-Mediated Selective Inhibitor of Human Cytochrome P450 3A5. J Med Chem 63, 1415-1433, https://doi.org/10.1021/acs.jmedchem.9b02067 (2020).[180]

(n = 423; 252 unique compounds) were then screened in a dose-response format against CYP3A4 and CYP3A5 in parallel. All compounds were screened in technical triplicate as 1:2 dilutions with concentrations ranging from 0.0073 μM to 15 μM. Scale transformation, normalization, curve fitting, and inhibitory concentration calculations were performed using GraphPad Prism 8.2.0 (GraphPad Software, La Jolla, CA). Specifically, the "log(inhibitor) vs. normalized response" equation was used to fit a standard slope curve based on normalized data and to subsequently extrapolate IC50 and IC90 values. Statistical comparisons were also performed in GraphPad Prism, using one-way ANOVA assuming equal standard deviations and comparing mean values.

Clobetasol Inhibition Profiling Against a Panel of Major Human CYPs

Clobetasol propionate was prepared as a 25 mM stock solution in DMSO and stored at −20 °C. The compound was screened against a panel of major human CYPs by using the cytochrome P450 inhibition service from Cyprotex US, LLC (Watertown, MA). Serial dilutions of clobetasol were made in acetonitrile:DMSO (9:1) to yield final concentrations at 1:3 intervals ranging from 0.068 μM to 50 μM. The final DMSO concentration across all reactions was 0.2%. Clobetasol was incubated with pooled human liver microsomes (Bioreclamation-IVT, Baltimore, MD) in the presence of 2 mM NADPH in 100 mM KPO4 buffer, pH 7.4, containing 5 mM MgCl2 and the respective CYP probe substrate. The final volume of all reactions was 200 μL, and the assay was performed in technical triplicate. The probe substrate, probe concentration, microsomal protein concentration, incubation time, and positive control compound for each tested CYP were as follows: for CYP1A2: tacrine, 5 μM, 0.2 mg/mL, 10 min, α-naphthoflavone; for CYP2B6: bupropion, 100 μM, 0.25 mg/mL, 10 min, ticlopidine; for CYP2C8: amodiaquine, 5 μM, 0.25 mg/mL, 10 min, quercetin; for CYP2C9, tolbutamide, 100 μM, 0.5 mg/mL, 15 min, sulfaphenazole; for CYP2C19: mephenytoin, 100 μM, 0.25 mg/mL, 60 min, ticlopidine; for CYP2D6: dextromethorphan, 5 μM, 0.5 mg/mL, 10 min, quinidine; and for CYP3A4: midazolam, 2.5 μM, or testosterone, 50 μM, 0.25 mg/mL, 10 min, ketoconazole. Each reaction mixture was incubated at 37 °C. Reactions were terminated by adding methanol containing an internal standard for analytical quantification. Quenched samples were then incubated at 4 °C for 10 min and centrifuged at 6,102 × RCF. Supernatants were analyzed by LC-MS/MS for the following metabolites: hydroxytacrine for CYP1A2; hydroxybupropion for CYP2B6; desethylamodiaquine for CYP2C8; α-hydroxytolbutamide for CYP2C9; 4-hydroxymephenytoin for CYP2C19; dextromethorphan for CYP2D6; and 1-hydroxymidazolam or 6β-hydroxytestosterone for CYP3A4.

Samples were analyzed using a 5500 QTrap mass spectrometer (AB Sciex, Framingham, MA) in positive ionization mode, a 1290 Infinity Series autosampler and solvent delivery system (Agilent, Santa Clara, CA) at 10 °C, and an Acquity UPLC HSS T3 1.8 μm, 2.1 mm × 50 mm column (Waters, Milford, MA) at 50 °C. For the UPLC gradient, samples were collected at 0.00, 0.05, 1.00, 1.80, 1.81, and 2.80 min. At the collection times, the respective flow rates (in mL/min) were 0.6 for all times; the mobile phase A percentages were 98, 98, 5.0, 5.0, 98, and 98, respectively; and the mobile phase

B percentages were 2.0, 2.0, 95, 95, 2.0, and 2.0. Mobile phase A consisted of water containing 0.1% formic acid, and mobile phase B consisted of acetonitrile containing 0.1% formic acid. Injection volumes were 10 µL for all samples.

Data Mining to Profile CYP3A5 Expression Across Cancer Types

To determine the CYP3A5 expression levels in publicly available cancer samples, data were obtained from the UCSC TOIL recompute[210] of samples originating from the Pan-Cancer analysis project conducted by The Cancer Genome Atlas (TCGA)[163]. Expression data from 33 cancer types (10,534 samples) were loaded into the R statistical environment [www.r-project.org] in the form of gene-level counts produced as the output of RSEM[174]. The edgeR package[211], with Limma[212] and Voom[213], was used for linear modeling, empirical Bayes smoothing, and TMM normalization to produce normalized expression in units of log2(normalized CPM+1). CYP3A5 expression levels were plotted using the ggplot2 package[214] as ranked levels in descending order according to their median values. The stepwise data-mining protocol is available in the Protocol Exchange[164].

RNA Extraction and Sequencing

Total RNA was extracted from each cell line by using the Maxwell 16 LEV automation system and a Maxwell simplyRNA Purification Kit (Promega, cat. no. 1280) in accordance with the manufacturer's protocol. The extracted RNA was quantified by spectrophotometry, using a NanoDrop 8000 spectrophotometer (Thermo Fisher Scientific, Waltham, MA) to ensure a reading for OD260/OD280 between 1.8 and 2.0.

The RNA quality was further checked by TapeStation 4200 high-sensitivity RNA screen tape (Agilent, Santa Clara, CA) before library generation. Only high-quality samples with an RNA integrity number (RIN) of 8 or higher were used to construct the sequencing library. The RNA was fragmented using fragmentation reagent. For cDNA synthesis, the first-strand cDNA was generated using random hexamer-primed reverse transcription, after which the second-strand cDNA was synthesized. Libraries were prepared from total RNA with the TruSeq Stranded mRNA Library Preparation Kit (Illumina, San Diego, CA). Libraries were quantified using the Quant-iT PicoGreen dsDNA Assay (Life Technologies, Carlsbad, CA). One hundred–cycle paired-end sequencing was performed using an Illumina NovaSeq 6000 System to produce 100 bp paired-end reads.

RNA-Seq Data Analysis

Raw sequence files were merged across lanes according to sample and subjected to a first round of quality control by using the FastQC tool (http://www.bioinformatics.babraham.ac.uk/projects/fastqc/). Illumina universal adapters

were trimmed from all samples using Trim Galore (http://www.bioinformatics.babraham.ac.uk/projects/trim_galore/), and samples were then subjected to a second round of quality control. Reads were mapped to the human Hg38 reference genome by using Bowtie2[215] in sensitive mapping mode. Gene-level quantification was obtained using RSEM[174] to produce raw read counts. The edgeR package[211], with Limma[212] and Voom[213], was used for linear modeling, empirical Bayes smoothing, TMM normalization, and all statistical comparisons. All *P* values were calculated based on t statistics then adjusted with the Benjamini–Hochberg false discovery rate. RNA-seq data from all included cell lines are available at the Gene Expression Omnibus (GEO) repository (accession no. GSE138437).

Cell Culture Method

AsPC-1 wild-type (WT), AsPC-1CYP3A5−/− (3A5−/−), and SU.86.86 cells were grown in culture in RPMI 1640 medium containing phenol red (Gibco, cat. no. 11875-093) with added 10% fetal bovine serum (HyClone, cat. no. SH30071.03), 1% Glutamax (Gibco, cat. no. 35050-061), and 1% penicillin streptomycin (Gibco, cat. no. 15140-122). AsPC-1 cells with CYP3A5 overexpression (WT + 3A5OE cells), AsPC-1CYP3A5−/− cells with CYP3A5 overexpression ("3A5−/− + 3A5OE" cells), and AsPC-1CYP3A5−/−cells with CYP3A4 overexpression ("3A5−/− + 3A4OE" cells) were grown in culture in RPMI 1640 medium containing phenol red (Gibco) with added 10% tetracycline-free fetal bovine serum (Takara, cat. no. 631101), 2 µg/mL puromycin (Sigma, cat. no. P9620), 1 mg/mL G418 (Gibco, cat. no. 10131-027), and 1% Glutamax (Gibco). MIA PaCa-2 cells were grown in culture in DMEM containing phenol red (Gibco, cat. no. 11965-092) with added 10% fetal bovine serum (HyClone), 1% penicillin streptomycin (Gibco), and 2.5% horse serum (ATCC, cat. no. 30-2040). PANC-1 cells were grown in culture DMEM (Gibco) with added 10% fetal bovine serum (HyClone) and 1% penicillin streptomycin (Gibco). hTERT-HPNE cells were grown in culture in DMEM containing phenol red (Gibco) with added 5% fetal bovine serum (HyClone), 150 ng/mL puromycin (Sigma), 10 ng/mL human epidermal growth factor (Fisher Scientific, cat. no. 50400346), and 5.5 mM D-glucose (Sigma, cat. no. G8769). CFPAC-1 cells were grown in culture in IMDM containing phenol red (Life Technologies, cat. no. 12440-053) with added 10% fetal bovine serum (HyClone) and 1% penicillin streptomycin (Gibco). Capan-2 cells were grown in culture in McCoy's 5A modified medium containing phenol red (ATCC, cat. no. 30-2007) with added 10% fetal bovine serum (HyClone) and 1% penicillin streptomycin (Gibco). HPAF-II cells were grown in culture in EMEM containing phenol red (ATCC, cat. no. 30-2003) with added 10% fetal bovine serum (HyClone) and 1% penicillin streptomycin (Gibco). Panc 02.13 cells were grown in culture in RPMI containing phenol red (Gibco) with 15% fetal bovine serum (Gibco), 1% penicillin streptomycin (Gibco), and 10 units/mL insulin (Sigma, cat. no. 91077C). All cell lines were obtained from ATCC (Manassas, VA), and all were maintained at 37 °C in 5% CO2. All cell lines have been authenticated by short tandem repeat (STR) DNA profiling and were routinely verified to be free of mycoplasma contamination.

Generation of Stable AsPC-1 Cells with Inducible Overexpression of CYP3A4 and CYP3A5

pLVX-TRE3G-ZsGreen1 (cat. no. 631361) and pLVX-EF1a-TRE3G (cat. no. 631359) were obtained from Clontech Laboratories, Inc. (Mountain View, CA). CYP3A5 cDNA (OriGene RC207432) and CYP3A4 cDNA (OriGene SC125488) were obtained from OriGene Technologies Inc. (Rockville, MD). The following PCR primers were used to amplify the CYP3A5 MluI/EcoRI fragment and the CYP3A4 MluI/NdeI fragment for subcloning into the corresponding sites of the pLVX-TRE3G-ZsGreen1 vector, after gel extraction and purification using the QIAquick Gel Extraction Kit (cat. no. 28407) from Qiagen Science Inc. (Germantown, MD):Tet-ZsGreen-3A5-MluI-F: 5′-GCCCCCGGGACGCGTGATGGACCTCATCCCAAATTTGG-3′ Tet-ZsGreen-3A5-EcoRI-R: 5′-CTACCCGGTAGAATTCTCATTCTCCACTTAGGGTTCCA-3′ Tet-ZsGreen-3A4-MluI-F: 5′-GAAAACGCGTATGGCTCTCATCCCAGACTTGGCCA-3 Tet-ZsGreen-3A4-NdeI-R: 5′-AGCATATGTCAGGCTCCACTTACGGTGCCATC-3′ The resulting constructs, pLVX-TRE3G-ZsGreen1-CYP3A4 and pLVX-TRE3G-ZsGreen1-CYP3A5, were confirmed by sequencing. Lentiviruses for pLVX-TRE3G-ZsGreen1-CYP3A5 or pLVX-TRE3G-ZsGreen1-CYP3A4 and pLVX-EF1a-TRE3G transactivator were packaged and generated in 293T cells (ATCC), using medium with 10% Tet System Approved FBS (Takara Bio, Mountain View, CA; cat. no. 631101). AsPC-1 cells were transduced with lentiviral pLVX-TRE3G-ZsGreen1-CYP3A5 or pLVX-TRE3G-ZsGreen1-CYP3A4 and pLVX-EF1a-TRE3G transactivator. Treatment with 100 ng/mL doxycycline for 16 hours was sufficient to induce CYP3A4 or CYP3A5. Stable cells were selected by using 5 μg/mL puromycin and 1.5 mg/mL G418 for 2 weeks.

Western Blot Analysis

Opti-MEM (250 μL) containing siRNA (3.75 μL of 10 μM) was mixed with 250 μL Opti-MEM containing 3.75 μL Lipofectamine RNAiMAX Transfection Reagent, incubated at room temperature for 10 min, and placed in a 6-well plate. 1 mL of medium containing 7.5×10^5 cells was added to each well to make the final siRNA concentration 25 nM. The next day, 1.5 mL of medium was added to each well. After 2 additional days, cells were trypsinized, pelleted by centrifugation, washed with DPBS, and lysed with 50 μL of RIPA Lysis and Extraction Buffer (Thermo Fisher Scientific) containing Halt Protease Inhibitor Cocktail (Thermo Fisher Scientific). Samples were incubated on ice for 30 min and centrifuged at 16,000 × *g* for 10 min at 4°C. Protein in the supernatant was quantified with the Pierce BCA Protein Assay Kit (Thermo Fisher Scientific), and 100 μg of protein was loaded into NuPAGE 4%–12% Bis-Tris gels (Thermo Fisher Scientific) with NuPAGE MES SDS running buffer (Thermo Fisher Scientific). Proteins were transferred from the gels to nitrocellulose membranes with the iBlot gel-transfer system (Thermo Fisher Scientific). The membranes were blocked for 1 h with Odyssey Blocking Buffer (LI-COR Biosciences), probed overnight at 4°C with rabbit anti-CYP3A5 (Abcam, cat. # ab108624, 1:1,000 dilution) and mouse anti-β-actin (Sigma, cat. # A5441, 1:2,000 dilution), washed 3x with TBS containing 0.1% Tween-20 (TBS-T) for 10 min

each, incubated with 1:10,000 dilutions of secondary antibodies conjugated with infrared dyes (LI-COR Biosciences, goat anti-rabbit IRDye 680RD and goat anti-mouse IRDye 800CW), and washed 3x with TBS-T as above. An Odyssey infrared imager (LI-COR Biosciences) was used to visualize the protein bands. At least three independent experiments were performed, and a representative gel is shown. For quantification, gel images were imported into Image Studio Lite. Equal size quantification rectangles were placed around each band to be measured. Measurements were visually inspected to ensure the total protein band was captured. After quantification of triplicate gels, the relative intensity of each protein band was then determined by normalizing the intensity of each protein band to that of actin. The relative intensity of control was set as 1.0.

CRISPR/Cas9-Mediated Deletion of CYP3A5

AsPC-1 cells with full deletion of CYP3A5 were generated using CRISPR/Cas9 technology at the St. Jude Center for Advanced Genome Engineering (CAGE). Briefly, sgRNAs were designed with at least 2 bp of mismatch to any other site in the human genome to mitigate the risk of off-target editing. Two sets of sgRNAs were used sequentially to delete the entire ORF of both alleles (Set 1—g8: 5′-UGGCUGAAGACUGCUGUGCA-3′ and g4: 5′- UAAUGUACUGCAUGAGUAGU -3′; Set 2—g12: 5′- AACAGCAGCACUCAGCUAAA-3′ and g7: 5′-AGUUGAAAUCUCUGGUGUUC-3′). To generate the AsPC-1CYP3A5−/− line, 400,000 cells were transiently co-transfected with 100 µmol of each sgRNA (Synthego) in Set 1, 35 µmol SpCas9 protein (from the St. Jude Protein Production Core), and 200 ng of pMaxGFP via nucleofection (with a 4D-Nucleofector™ X-unit; Lonza) in a small cuvette, using solution P3 and program EN-158, in accordance with the manufacturer's recommended protocol. Five days post nucleofection, cells were single-cell sorted into 96-well plates by FACS for transfected cells based on pMaxGFP expression. After sorting, cells were clonally expanded and screened for the desired deletion by PCR-based assays and confirmed with targeted deep sequencing. Specifically, the deletion was detected using primers hCYP3A5.Del.F (5′- ACCCTTGGACTCCCCGATAACACTGA-3′) and hCYP3A5.Del.R (5′- TCTGATGAGAGCTCAGGAGGAGTTGA-3′). The nucleofection, cloning, and screening process was repeated with sgRNA Set 2 as described above, and the deletions were sequence confirmed by targeted deep sequencing. Additionally, the internal primers hCYP3A5.inner.F (5′-AGTCACAATCCCTGTGACCTG -3′) and hCYP3A5.inner.R (5′-GAAACCTCAGAACTCCCTCCC-3′) were used to verify the loss of the intervening sequence (by the absence of the band). CYP3A5 deletion was further verified by Western blot analysis, qRT-PCR, and functional testing.

LC-MS/MS Detection of Midazolam and 1-Hydroxymidazolam

Cells were plated at a concentration of 10,000 cells per well in 384-well white, opaque, tissue culture–treated microplates (Corning, cat. no. 8804BC). Overexpression cell lines were induced with 100 ng/mL doxycycline. Twenty-four hours later, the cells

were treated with clobetasol, ketoconazole, or DMSO. Both clobetasol and ketoconazole were tested in a dose-response format, using 16 concentrations in 1:2 dilutions ranging from 0.0003 μM to 10 μM. Additionally all groups were treated with 5 μM midazolam. The final DMSO concentration for all wells of the assay plates, including the controls, was 0.66%. Twenty-four hours after drug treatment, the reaction was quenched by adding acetonitrile (containing 4 μg/mL warfarin as an internal standard) to the wells in a 2:1 volume ratio. The plates were centrifuged for 20 min at 4,000 × *g*, and the reaction supernatants were diluted into an equal volume of dH_2O. Reference standards of midazolam and 1-hydroxymidazolam were also prepared in the same fashion, using culture medium and concentration ranges of 1.19×10^{-6} μM to 10 μM (for midazolam) or 1.19×10^{-7} μM to 1 μM (for 1-hydroxymidazolam). Samples were then frozen at −20 °C until analyzed by mass spectrometry.

LC-MS/MS analysis was performed using a SCIEX Triple Quad 6500 triple-quadrupole mass spectrometer (SCIEX, Forster City, CA) coupled to an ACQUITY UPLC system (Waters Corporation, Milford, MA). For each unknown sample and calibration sample, 10 μL was injected onto an Acquity UPLC HSS C18 2.1 mm × 50 mm column (particle size: 1.8 μm) (Waters Corporation). Chromatographic separation was performed by gradient elution at a constant flow rate of 1 mL/min for 2 min. The mobile phase consisted of 0.1% formic acid–water (solvent A) and 0.1% formic acid–acetonitrile (solvent B). The gradient applied was 0.0 min, 90% A–10% B; 0.3 min, 80% A–20% B; 1.35 min, 80% A–20% B; 1.65 min, 5% A–95% B; and 1.95 min, 10% A–90% B. The first 0.5 min of eluate was desalted to waste by an integrated Valco valve. The remaining eluates were directed to the triple quadrupole mass spectrometer, which was equipped with an electrospray ionization source. LC-MS/MS was performed in positive polarity (at 3000 V), and the source temperature was 650 °C. Gas 1 and gas 2 settings for nitrogen were set to 60. The curtain gas and collision gas were also nitrogen and were set to 20 and 10, respectively. Multiple reaction monitoring transitions were m/z 326 to m/z 291 for MDZ, m/z 342 to m/z 324 for 1-OH MDZ, and m/z 309 to m/z 163 for the IS (warfarin). The declustering potentials, entrance potential, collision energy, and collision cell exit potential were as follows: 120 V, 12 V, 35V, and 27 V, respectively, for MDZ; 70 V, 12 V, 30V, and 40 V for 1-OH MDZ; and 57 V, 12V, 44V, and 20 V for the IS. Data acquisition was conducted with Analyst 1.6.3 (SCIEX) and the data processes were operated with MultiQuant 2.1.1 software (SCIEX). The stepwise protocol for cell-based LC-MS/MS detection of CYP3A4 or CYP3A5 activity in cells is available in the Protocol Exchange (http://doi.org/ 10.21203/rs.2.16299/v1).

Confluence Imaging

Cells were plated at a concentration of 10,000 cells per well in 384-well, black, tissue culture–treated, clear-bottom polystyrene microplates (Corning, cat. no. 3712BC). All samples were processed in parallel with samples used for LC-MS/MS (and using the same methods) until just before the reaction-quenching stage. Cells were then imaged using a Lionheart FX Automated Live Cell Imager (BioTek, Winooski, VT). Single images of each well were acquired using phase-contrast microscopy with a 4× objective.

An LED intensity of 10 was used, with a 100-millisecond integration time and a camera gain of 6.8. The laser was set to autofocus, and the wells were scanned at a distance of 600 µm in increments of 50 µm with a 0-µm well offset. The vibration CV threshold was set to 0.01. The instrument was set to add a 30-millisecond delay after plate movement. Lionheart FX software version 3.05.11 was used to obtain the cell confluence and export the well-by-well results. Confluence data were normalized in GraphPad Prism 8.2.0, using the average of six replicates of 0.66% DMSO (set to 100% confluence) for each cell line. Nonlinear regression curves were fitted using the "log(inhibitor) vs. response (three parameters)" equation applied to normalized data and were plotted to show normalized cell confluence over the tested concentration ranges.

Ligand Docking and Molecular Dynamics Simulations

Published crystal structures of ritonavir-bound CYP3A4 (PDB: 3NXU, Chain A) or CYP3A5 (PDB: 5VEU, Chain A) were loaded into Maestro software (Schrödinger Release 2019-3). To prepare the protein for docking and simulations, the protein preparation wizard was used to assign bond orders, add hydrogens, create zero-order bonds to metals, create disulfide bonds, and fill in missing side chains and loops. Default parameters were used for the optimization of hydrogen-bond assignment (sampling of water orientations and use of pH 7.0). Waters beyond 5 Å of het groups or with fewer than three hydrogen bonds to non-waters were removed. Restrained energy minimization was applied using the OPLS3e[216] forcefield. Prepared protein systems were further checked by Ramachandran plots, ensuring there were no steric clashes. To generate receptor grids, ritonavir was selected as the grid-defining ligand for both the CYP3A4 and CYP3A5 systems. Default Van der Waals radius scaling parameters were used (scaling factor of 1, partial charge cutoff of 0.25).

For docking clobetasol into CYP3A4 and CYP3A5, the 3D structure of clobetasol was first obtained from the PubChem database (www.pubchem.ncbi.nlm.nih.gov). The virtual screening workflow panel was used to prepare clobetasol (by generating possible states at pH 7.0 ± 2.0 and retaining the specified stereochemical properties) and dock it into CYP3A4 and CYP3A5 in parallel. The most stringent docking mode (extra precision, "XP") of Glide[217] was used, with the following parameters: dock flexibly, perform post-docking minimization, and keep 100% of scoring compounds. Of note, only one pose of clobetasol was returned for each system. For molecular dynamics simulations, systems were built for clobetasol-docked CYP3A4 and CYP3A5 by using the system builder panel of Desmond (Schrödinger Release 2019-3). The SPC solvent model was used, and the forcefield was set to OPLS3e. Solvated systems were loaded into the workspace by using the molecular dynamics panel. The total simulation time for each system was set to 200 nanoseconds, with 200-picosecond trajectory recording intervals. The system energy was set to 1.2, and the ensemble class used was NPT. Simulations were set to run at 300.0 K and at 1.01325 bar. The option to relax model systems before simulations was selected.

Cloning of CYP3A4 and CYP3A5 for Bacterial Protein Expression

The cloning procedure closely followed that previously described[115,117]. Cloning was performed in pCW ori$^+$ plasmids harboring either *CYP2C8* or *CYP2C9* from Addgene: *CYP2C8* and *CYP2C9* in pCW ori$^+$ were gifts from Joyce Goldstein (Addgene plasmid # 69604; http://n2t.net/addgene:69604; RRID:Addgene_69604 and plasmid # 69554; http://n2t.net/addgene:69554; RRID:Addgene_69554). The pCW3A4His plasmid was generated by replacing the *CYP2C8* sequence of the pCW ori+-*CYP2C8* plasmid with a codon-optimized *CYP3A4* coding sequence at the *Nde*I/*Xba*I sites by GenScript (Piscataway, NJ), which expresses an N-terminal truncated version of CYP3A4 (with amino acids 3–24 truncated) with the His-4 tag at the C-terminal as previously described[115]. The pCW3A5His expression plasmid was generated by PCR from a cDNA template coding for full-length *CYP3A5* (OriGene, Rockville, MD) by using the forward and reverse primers 5′-ggattcGGCAT**ATG**GACTATCTATATGGGACCCGTACACATGGAC-3' and 5′-cggaattccgAAGCTT**TTA**GTGGTGGTGGTGTCCATCTCTTGAATCCACCTTTAGAAC-3′ (Invitrogen, Carlsbad, CA). The underlined letters in the primers indicate engineered restriction sites (*Nde*I/*Hin*dIII). The bold letters indicate engineered ATG start and stop codons. The PCR reaction was accomplished using a ProFlex PCR system (Life Technologies, Carlsbad, CA) and Fusion High-Fidelity Master Mix (New England Biolabs, Ipswitch, MA). The amplification conditions were 95 °C for 2 min followed by 30 cycles of 95 °C for 30 s, 60 °C for 30 s, and 68 °C for 5 min, with a final polymerization step of 68 °C for 5 min. The PCR product was then digested using *Nde*I/*Hin*dIII and inserted into the restriction sites in a pCW ori$^+$ plasmid (previously digested with the corresponding enzymes to remove *CYP2C9*) by using a Quick Ligation Kit (New England Biolabs). The resulting pCW3A5His construct encoded an N-terminal 3–24 trans-membrane helix amino acid deletion and a C-terminal 498–501 amino acid deletion. The C-terminal deletion in CYP3A5 produces a more soluble protein, as observed previously[117]. In addition, a His-4 tag to aid nickel affinity chromatography was engineered at the C-terminal. No other mutations were made in the enzymes. All constructs were confirmed by DNA sequencing.

Expression and Purification of CYP3A4 and CYP3A5

The expression and purification methods closely followed those previous described, albeit with a few modifications[115,117]. The cloned pCW3A4His and pCW3A5His constructs were co-transformed with a pGro7 plasmid (Takara Bio, Japan) harboring the *E. coli* chaperone proteins groES and groEL (henceforth, groESL) into *E. coli* DH5-α cells, and transformed cells were co-selected using ampicillin and chloramphenicol (Gold Biotechnology, Olivette, MO). The chaperone proteins were co-transformed to aid solubility and improve protein yield. Expression of the individual (*CYP3A4* or *CYP3A5*) gene constructs was achieved by using an isopropyl β-D-thiogalactopyranoside (IPTG) (Gold Biotechnology)–inducible *tac* promoter system in the pCW ori$^+$ plasmid.

Protein production was typically done in 12-L cultures of Terrific Broth (TB) growth medium (Fisher Scientific, Hampton, NH) distributed between six 4-L conical flasks. Each flask contained 2000 mL of growth medium supplemented with ampicillin (50 µg/mL) and chloramphenicol (35 µg/mL). The medium was then inoculated with 20 mL of transformant cells from an overnight culture in the same medium and under the same conditions. The cells were then grown at 37 °C with 200 rpm agitation to an exponential phase with an OD_{600} of 0.5, then the temperature was dropped to 28 °C and the agitation to 170 rpm. At an OD_{600} of 0.7–0.8, IPTG (1 mM) and delta-aminolevulinic acid (1 mM) (Gold Biotechnology) were added to induce P450 production and to promote heme synthesis, respectively. Approximately 3 g/L of L-(+)-arabinose (Sigma-Aldrich, St. Louis, MO) was also added to induce expression of the *E. coli* chaperone proteins groESL. The transformant cells were grown for a further 48–50 h, then the cells were harvested by centrifugation at 6000 × *g* for 10 min at 4 °C by using an F9-6X1000 LEX rotor in a Sorvall Lynx6000 centrifuge (Thermo Fisher Scientific). The supernatant was discarded, and the cell pellets were resuspended in approximately 500 mL of 0.5 M potassium phosphate (KPi, pH 7.4) containing 20% glycerol and 1 mM phenylmethanesulfonyl fluoride (PMSF) protease inhibitor (Sigma-Aldrich). A few granules of lysozyme (Sigma-Aldrich) were added to facilitate cell lysis. The cells were lysed by passing them once through a microfluidizer (Microfluidics, Newton, MA); thereafter, the resulting lysate was supplemented with 10 mM CHAPS and incubated for 2 h (for CYP3A5) or 6 h (for CYP3A4) to release the proteins from the spheroplasts. The lysates were then centrifuged at 40,000 × *g* for 60 min at 4 °C and the supernatants were collected.

Each supernatant was mixed in batch with Ni-NTA resin (Qiagen, Hilden, Germany) pre-equilibrated with buffer **A** (0.5 M potassium phosphate, pH 7.4, 1 mM PMSF, 10 mM CHAPS, 20% glycerol) and incubated overnight at 4 °C with stirring. Next day, the supernatant–Ni-NTA resin was loaded onto a column and washed with 2 bed volumes (BV) of buffer **A**. The resin was then washed/buffer exchanged with 10 BV of buffer **B** (25 mM potassium phosphate, pH 6.8, 10 mM 2-mercaptoethanol, 20 mM NaCl, 2% Tween-20, 20% glycerol), followed by another 10 BV of buffer **C** (buffer **B** supplemented with 50 mM $MgCl_2$ and 5 mM ATP) to remove the groESL chaperone proteins. The resin was next washed with 5 BV of buffer **B** to remove excess ATP. The CYPs were then eluted from the resin by using buffer **B** supplemented with 200 mM imidazole and were analyzed spectrally (at 250–800 nm) and by SDS-PAGE.

The CYPs were then subjected to a second round of purification using a cation exchange chromatography column packed with carboxymethyl (CM) sepharose fast-flow resin (GE Healthcare) pre-equilibrated with buffer **B**. The column was mounted on an automated AKTA Avant purification system (GE Healthcare) and eluted via a linear gradient of NaCl (20–500 mM) with buffer **B** and buffer **B2** (buffer **B** supplemented with 500 mM NaCl), and each fraction was analyzed by both spectroscopy and SDS-PAGE as before. Eluted fractions with high A_{420}/A_{280} (Reinheitszahl, Rz) ratios (≥ 1) were pooled and concentrated to approximately 3–5 mL by ultrafiltration with a Vivaspin 20 concentrator at 4 °C. The CYPs were then subjected to a final purification step using a Sephacryl S-200 size-exclusion chromatography column and an AKTA Avant

purification system with buffer **C** (100 mM HEPES, pH 7.4, 10 mM 2-mercaptoethanol, 200 mM NaCl, 20% glycerol). Fractions with Rz values of 1.3 or higher were pooled, concentrated, and stored at −80 °C until use.

UV-Visible Absorbance Titrations with CYP3A4 and CYP3A5

UV–visible experiments were carried out in accordance with previously described methods[218-221]. Optical titrations were performed to determine the dissociation constant (K_d) values for interactions of clobetasol, ketoconazole, and midazolam with CYP3A4 or CYP3A5. Titrations were performed using 1-cm path-length cuvettes in a SPECTRAmax PLUS[384] UV–Visible spectrophotometer (Molecular Devices, San Jose, CA). Stock solutions (10 mM) of all compounds were made in DMSO-d_6 and titrated (in 1.0 μL aliquots) in cuvettes containing either ligand-free CYP3A4/CYP3A5 (4–6 μM) or buffer alone (as a negative control). The total DMSO-d_6 concentrations after saturation of enzyme were kept below 2.2%, and the absorbance spectra of CYP3A4 and CYP3A5 were not affected by DMSO-d_6 within this range. Continuous absorbance spectra (250–800 nm) were recorded at 25 °C. The negative control spectra generated from the buffer alone were subtracted from the protein absorbance spectra to eliminate the absorbance due to optical interference from small molecules. In addition, difference spectra were generated by subtracting the initial ligand-free protein absorbance spectrum from the ligand-bound spectrum, and the maximum change in absorbance calculated from each difference spectrum was then plotted against the corresponding ligand concentration.

EPR Spectroscopic Analysis of CYP3A4 and CYP3A5

A continuous-wave X-band EPR spectrum was collected for both CYP3A4 and CYP3A5. Spectra were obtained at 10 K by using a Bruker ELEXSYS E500 EPR spectrometer equipped with an ER4122SHQ Super High Q cavity. An Oxford Instruments ESR900 cryostat connected to an ITC503 was used to control the temperature. The microwave power was set to 0.5 mW, with the frequency and modulation amplitude set to 10 GHz and 5 G, respectively. Spectra were collected for both CYPs in the ligand-free state (200 μM) and with the addition of exogenous compounds (400 μM).

Statistics for CYP Inhibition

For CYP inhibition, we performed statistical calculations by using one-way analysis of variance (ANOVA) assuming Gaussian distribution of residuals and equal standard deviation. Tuckey correction for multiple comparisons was applied. For CYP3A5 expression in RNA-seq experiments, the edgeR package with Limma and Voom was first used for linear modeling, empirical Bayes smoothing, and TMM normalization. Subsequently, all *P* values were derived from *t* statistics, then adjusted with the Benjamini-Hochberg false discovery rate (FDR) adjustment. For protein

expression we either performed unpaired, two-tailed *t* tests, assuming Gaussian distribution and all populations having equal standard deviation, or used a one-way ANOVA, assuming Gaussian distribution of residuals and equal standard deviation. The Tuckey method of adjustment for multiple comparisons was applied. Information on sample size selection is indicated in the figures and corresponding Methods section, and no data were excluded from the analyses. For all statistical analyses, *** $P \leq 0.0001$, ** $P \leq 0.005$, * $P \leq 0.05$, and ns = not significant ($P \geq 0.05$).

COLDSTaR Development and Analysis of Pancreatic Cancer

We find it best to start with data processed uniformly using well-established methods, such as the UCSC Toil recompute of TCGA data which is available in the form of Log2(gene counts). We obtained expression data in this form from the TCGA pancreatic cancer (PAAD) cohort. These counts are back-transformed into a linear scale. Then, TMM normalization and linear modelling are performed through the edgeR package[211] using limma[212] and VOOM[213].The output is expression data in units of Log2(normalized CPM). In the data preparation stage, the sum of expression is calculated for each gene across all samples. Genes whose sum is zero (completely unexpressed in all samples) are discarded. In the block-wise computation step, we employ a modified version of the bigcor package, and calculate the Spearman correlation coefficients and adjusted p-values (see bigcor function definition in code repository). Pairs of genes with correlations ≥ 0.6 and adjusted p-values ≤ 0.05 are extracted and saved as final tabular results. We then use the COLDNet package to calculate and plot a given network (detailed in code repository). We make all corresponding code available in our GitHub repository (github.com/wcharleswright).

NetBID Analysis of Pancreatic Cancer

Gene expression was obtained from the same cohort as described in the previous section, TCGA pancreatic cancer. According to NetBID methods, data were Log2-transformed into Log2(FPKM+0.1) and transcripts were filtered by IQR variance, filtering with a cutoff of 0.3 which resulted in 32,088 transcript sets representing 20,517 genes. The data quality was further assessed by the function draw.eset.QC from the NetBID2 toolkit[183] and 7 outliers were found and removed from subsequent analysis. We used SJARACNE[222] to reconstruct context-dependent signaling networks. The parameters were configured as follows: p value threshold p=1e-7, data processing inequality (DPI) tolerance $\epsilon = 0$, and number of bootstraps (NB) = 100. The CYP3A5 subnetwork was extracted and the first neighbors were considered as candidate transcriptional regulators.

siRNA Screening of Predicted CYP3A5 Regulators

75 nL of siRNA in Echo Qualified 384-Well Low Dead Volume Microplates (Labcyte, cat. # LP-0200) was transferred to 384-well clear-bottom plates (Corning, cat. # 3764) with a Labcyte Echo 655T Liquid Handler to yield a final concentration of 25 nM. 5 µL of Opti-MEM I Reduced Serum Medium (Thermo Fisher Scientific, cat. # 31985062) containing 50 nL Lipofectamine RNAiMAX Transfection Reagent (Thermo Fisher Scientific, cat. # 13778150) was added to each well and incubated for 10 min at room temperature. 25 µL of medium (RPMI + 10% FBS + 1% glutamax + Penicillin-Streptomycin) containing 104 cells was added to each well. The next day, 30 µL of medium was added to each well. After 2 additional days, plates were imaged with a Lionheart FX Automated Live Cell Imager (BioTek) as described previously[180]. Single images of each well were acquired using phase-contrast microscopy with a 4× objective and laser autofocus. BioTek Gen5 Image Prime version 3.05.11, was used to obtain the cell confluence and export the well-by-well results. After imaging, the plates were processed for Cells-to-CT assay using Cells-to-CT Bulk Lysis Reagents (Thermo Fisher Scientific, cat. # 4391851C) and Cells-to-CT Bulk Fast Advanced RT Reagents (Thermo Fisher Scientific, cat. # A39110). The medium was removed from each well, cells were washed with 50 µL cold DPBS, and the DPBS was removed. Lysis solution (25 µL) containing 0.25 µL DNase I was added to each well, and plates were shaken for 5 min at room temperature. Stop solution (2.5 µL) was added to each well, and plates were shaken for 2 min at room temperature. 5 µL of lysate was transferred to MicroAmp Optical 384-Well Reaction Plates (Thermo Fisher Scientific, cat. # 4309849) containing 2x Fast Advanced RT Buffer (10 µL), 20x Fast Advanced RT Enzyme Mix (1 µL), and nuclease-free H2O (4 µL). Plates were incubated at 37°C for 60 min and 95°C for 5 min. The resulting cDNA (2 µL) was subjected to multiplexed quantitative polymerase chain reaction (qPCR) using TaqMan Fast Advanced Master Mix (Thermo Fisher Scientific, cat. # 4444557) with a 10 µL total reaction volume in an Applied Biosystems 7900HT system. DNA was denatured at 95°C for 2 min and amplified by 40 cycles of 95°C for 1 s and 60°C for 20 s. TaqMan gene expression assays specific for CYP3A5 (Hs01070905_m1, FAM-labeled) and GAPDH (Hs03929097_g1, VIC-labeled) were purchased from Thermo Fisher Scientific. Fold induction values were calculated according to the 2-ΔΔCT method[223], where ΔCT represents the differences in cycle threshold numbers between the target gene and reference gene and ΔΔCT represents the relative change in these differences between the control and treatment groups.

qPCR-Based Validation of CYP3A5 Regulators

Opti-MEM (50 µL) containing siRNA (1 µL of 10 µM) was mixed with 50 µL Opti-MEM containing 1 µL Lipofectamine RNAiMAX Transfection Reagent, incubated at room temperature for 10 min, and placed in a 24-well plate. 300 µL of medium containing 1.5 × 105 cells was added to each well to make the final siRNA concentration 25 nM. The next day, 500 µL of medium was added to each well. After 2 additional days, total RNA was isolated from the cells with Maxwell 16 LEV SimplyRNA Tissue Kits (Promega), and cDNA was generated from 1 µg of RNA with the SuperScript VILO

cDNA Synthesis Kit (Invitrogen). The resulting cDNA (2 μL) was subjected to multiplexed qPCR as above

CHAPTER 5. DISCUSSION*

Until now, a CYP3A5 inhibitor that does not also inhibit CYP3A4 has not been identified. In addition to the difficulty arising from the fact that CYP3A5 and CYP3A4 have a high degree of structural homology, there was a lack of commercially available tools with which to screen for such a selective inhibitor by using requisite throughput. Many assays for screening CYP3A4 inhibitors are available with various readouts, such as luminescence and fluorescence, and are compatible with high-throughput screening[224], but there are no such assays for CYP3A5. We hypothesized that we could exploit the overlapping substrate specificity of the enzymes and use an assay originally intended for CYP3A4 to screen for CYP3A5 inhibitors. The luminescence-based assay from Promega that we used (as detailed in the Methods section) is advertised as having no cross-reactivity with CYPs outside the CYP3A family, with the kit being optimized for CYP3A4. Nevertheless, we hypothesized that, with proper controls and normalization, the assay would work for CYP3A5. Our hypothesis was validated when we began testing the assay. Although the higher catalytic activity of CYP3A4 was clear, the properly controlled assay produced exceptional signal windows that were suitable for parallel screening and cross-enzyme comparisons. Our screen yielded results showing both zero CYP3A5 inhibition and total CYP3A5 inhibition. Furthermore, many known inhibitors were successfully identified from the screen, and a few cross-plate duplicates that served as internal controls lined up very well and demonstrated assay reproducibility. Interestingly, our screen also identified a few CYP3A5 enzymatic activators, a phenomenon already reported in the literature for CYP3A enzymes[81,83]. Our dose-response analysis further confirmed the high performance of the assay, as indicated by the tight replicates and sigmoidal inhibitory curves. After demonstrating the potential of clobetasol to selectively inhibit CYP3A5 while avoiding CYP3A4, we used a different assay to test the effect of clobetasol on six other major human CYPs. The IC_{90} concentration of clobetasol for CYP3A5 (1.8 μM) showed no significant inhibition of these enzymes. This validated the selectivity of clobetasol not just in the context of CYP3A4. The lack of CYP3A4 inhibition observed with three different substrates and two different readouts gave us confidence that clobetasol was potent and selective for CYP3A5 in cell-free systems.

We identified a cell model that was suited to studying the *in vitro* effect of clobetasol by leveraging publicly available RNA-seq data and confirming the results with in-house sequencing experiments using a panel of cell models that we assembled. We simultaneously normalized the expression results of the entire TCGA dataset (described in detail in our stepwise protocol available in the Protocol Exchange[164]). This benefited

---

* Portions of chapter from previously published article; pre-print submission reprinted with permission of American Chemical Society. Wright, W. C. et al. Clobetasol Propionate Is a Heme-Mediated Selective Inhibitor of Human Cytochrome P450 3A5. J Med Chem 63, 1415-1433, https://doi.org/10.1021/acs.jmedchem.9b02067 (2020).[180]

our study twofold: 1) it enabled proper and confident interpretation of the results when comparing CYP3A4 and CYP3A5 expression levels, and 2) it used the same processing pipeline that we used for our own samples from our cell panel, enabling much more direct comparisons. Our transcriptomic studies culminated in the understanding that CYP3A5 was highly expressed in pancreatic cancer but CYP3A4 was not. Notably, CYP3A4 was predominantly expressed in two cancer types: liver hepatocellular carcinoma and bile duct cancer, whereas CYP3A5 was highly expressed not only in these two cancers but also in several others, including PDAC. These findings informed our decision to procure various pancreatic cancer cell lines. We performed RNA-Seq on each of these cell lines and clearly demonstrated that CYP3A5 was overexpressed in PDAC. Moreover, we sought to examine the expression of other CYPs in these models. The CYP superfamily is broad, with humans expressing 57 CYP enzymes[225]. We focused on xenobiotic-metabolizing CYPs because of their relevance to our project, and we showed that most of them, including CYP3A4, are not expressed in any of these cells. Although it is entirely plausible that CYPs outside this category are present, they are unlikely to be expressed at levels as high as those of CYP3A5 or to interfere with our selectivity studies. There is a dearth of information on CYP3A5 versus CYP3A4 expression in cancer, but these data helped us to conclude that pancreatic cancer cells were appropriate models for our cell-based selectivity studies.

We went on to demonstrate the selectivity of clobetasol *in vitro* by modulating the expression levels of CYP3A5 or CYP3A4. In WT cells that endogenously express CYP3A5 but not CYP3A4, we were surprised to see clobetasol behaving as a more potent inhibitor than ketoconazole, however slightly. Importantly, in CYP3A4-null cells with a genetic deletion of *CYP3A5*, the metabolic activity for midazolam was completely abolished, thus demonstrating that no other enzymes were catalyzing the midazolam hydroxylation. The midazolam-metabolizing activity was rescued by overexpression of CYP3A5 but was again abolished by clobetasol, confirming that the effect of clobetasol was indeed CYP3A5 dependent. Overexpression of CYP3A4 in the CYP3A5-null cells rescued the midazolam-metabolizing activity but could not be inhibited by clobetasol, thus confirming that clobetasol inhibits CYP3A5 but not CYP3A4. We were intrigued by the apparent clobetasol-induced enzymatic activation of CYP3A4 observed at high concentrations of the compound. Although our Western blot analysis indicated that clobetasol did not increase the protein levels of CYP3A4, we cannot exclude the possibility that there is an endogenous CYP3A4 inhibitor present in our cell system that was somehow replaced by clobetasol. This intriguing phenomenon warrants further investigation. We also noticed that ketoconazole increased CYP3A4 protein levels, as reported previously[226], but that this increase in protein levels did not hinder our ability to enzymatically inactivate CYP3A4. Additionally, the relative CYP3A4-specific contribution to midazolam catalysis was drastically lower than that of CYP3A5 in DMSO-treated samples, which appears to be consistent with the lower protein levels of CYP3A4, as compared to CYP3A5, in DMSO-treated samples.

In silico approaches have been used to study differential ligand interactions with CYP3A4 and CYP3A5. These reports use techniques such as ligand docking and molecular dynamics simulations to understand the differential behavior of ligands with

the two homologs, usually focusing on heme–ligand interactions[95,227,228]. We applied the same approaches to investigate how clobetasol selectively inhibited CYP3A5 but not its nearly identical homolog CYP3A4. Clobetasol formed a tight heme–ligand interaction throughout the simulation for CYP3A5 but preferred a site further from the heme in the CYP3A4 simulation. To our surprise, the simulations revealed that solvent enters the binding pocket and becomes stabilized on the heme only in CYP3A4, which is indicative of the resting (non-inhibited) enzyme state[53,172,173]. Conversely, clobetasol blocked solvent access throughout the simulation for CYP3A5, coordinating with the anchoring cysteine residue through the heme iron. We determined that the subtle differences in the shape of the active sites of the two enzymes were sufficient to cause discrete binding orientations for clobetasol, and this ultimately helped us to propose a mechanism for the selective inhibition. Furthermore, the MD simulations may be consistent with the enzymatic CYP3A4 activation that we observed at high concentrations of clobetasol. It is possible that clobetasol stabilizes CYP3A4 in an orientation that allows solvent (and, therefore, substrate) access to the heme more frequently, but this is of no significant consequence as only high concentrations produced this effect (and no concentration produced CYP3A4 inhibition).

We proceeded to experimentally test the model predicted by our MD simulations by using classical biophysical techniques for studying CYPs, namely UV–visible and EPR spectroscopy to interrogate the spin states and the overall electronic environment of the ferric heme iron in both CYPs, using recombinantly expressed proteins. With CYP3A5, UV–visible titrations distinctly showed a typical type I ligand-binding mode (indicating the displacement of the axial water ligand) for clobetasol, resulting in the formation of a five-coordinate ferric heme iron, whereas a type II spectrum shift was produced for ketoconazole, indicating the replacement of the axial water ligand with the nitrogen atom from the imidazole moiety of the azole compound to retain the six-coordinate ferric heme iron state. Both phenomena are consistent with the results of previous studies on human and bacterial CYPs[113,117,229,230]. To our surprise, clobetasol also showed a profoundly higher binding affinity for CYP3A5 when compared to ketoconazole, the pan-CYP3A inhibitor. In contrast, UV–visible titrations could not detect a significant spectral shift by which to assign a binding mode for clobetasol in CYP3A4, although minor spectral perturbations were observed with higher clobetasol concentrations. Moreover, the spectral binding data generated showed clobetasol to have a significantly weaker affinity for CYP3A4 when compared to ketoconazole. However, ketoconazole also produced a type II binding mode in CYP3A4, with binding affinities similar to those noted with CYP3A5. These findings support the prediction from the MD simulations that clobetasol occupies a site closer to the heme in CYP3A5 compared to that in CYP3A4. We further validated this heme-dependent selectivity by using EPR to monitor the effect of clobetasol on the ferric heme iron in the resting state of both enzymes. Interestingly, clobetasol induced an LS to an HS ferric heme iron spin state in only CYP3A5, maintaining an LS ferric heme iron spin state similar to the ligand-free water-ligated resting form of the protein in CYP3A4. In addition, as expected, midazolam and ketoconazole induced HS and LS spin states corresponding to typical type I and type II ligand-bound CYP species in both enzymes. A small proportion of HS was seen in the ligand-free form of CYP3A4 corresponding to a small portion of the enzyme existing

without the axial water ligand to keep it in a complete LS spin state. However, this ligand-free HS does not correspond to a typical HS produced in the presence of a true type I ligand-bound form that usually presents concurrently with a significant size reduction in the g_z and g_y signals as noticed in the midazolam-bound forms of both CYPs . This feature was also observed in other CYPs from bacteria[231,232]. Our data confirm beyond reasonable doubt that the selective type I binding mode induced by clobetasol in the heme of CYP3A5, but not in that of CYP3A4, represents a true CYP3A5-inhibitor complex. Indeed, inhibitors that mimic substrates with a type I binding mode are not novel in the CYP field. Previous studies have shown that bromocryptine displays similar atypical type I–like binding features in CYP3A4 but is arguably classified as an inhibitor for the enzyme[233,234].In addition, previous studies on bacterial CYPs involving CYP126A1 in *Mycobacterium tuberculosis* also identified potent inhibitors that displayed similar type I–like features[218]. Our proposed mechanism is that clobetasol initially presents as a substrate on approaching the heme in CYP3A5, but the enzyme fails to oxidize the compound, leading to the formation of a pseudosubstrate–CYP complex that in turn inhibits the enzyme.

Identifying a CYP3A5-selective inhibitor has been challenging for many reasons, not least of which is the 83% sequence homology between CYP3A4 and CYP3A5[235]. The potential applications for such a compound range from delineating substrates of CYP3A4 to studying the role of CYP3A5 as a mediator of drug resistance[9] or its involvement in oncogenic signaling[236]. We have identified and characterized clobetasol as being capable of potently and selectively inhibiting CYP3A5. Our work lays the foundation for developing CYP3A5-selective inhibitors and can be expanded in various ways to uncover the roles of CYP3A5 both in catalytic mechanisms and in disease-relevant contexts.

In addition to selectively targeting CYP3A5 with chemical-mediated inhibition, we also sought to target it upstream by elucidating its transcriptional regulators. The prospect of doing so was challenging since transcriptional regulation of CYP3A5 in extra-hepatic contexts is poorly understood. To this end, we developed a new computational pipeline designed to quickly and efficiently calculate co-expression data from which candidate transcriptional regulators of a given target can be identified. Our resulting tool, COLDSTaR, overcomes a handful of limitations present in existing pipelines. Namely, overcoming the need for inference, calculating all-by-all correlation matrices, computing p-values and adjusting them in one step, and quickly constructing a co-expression network. COLDSTaR automates all steps of computation including data normalization and produces an easy to interpret list of gene pairs, their correlation coefficients, and corresponding adjusted p-values. To generate the very large correlation matrices necessary for these calculations, we expanded upon research into block-wise computing. We took advantage of what is known in this area and modified it to fit our specific needs of all-by-all Spearman-based pairwise calculations. This allowed for completion of large datasets (hundreds of samples, tens of thousands of genes) to be analyzed in a matter of an hour, compared to about 1 week if the block-wise technique were not used. One of the final steps in our workflow is the application of correlation and statistical thresholds. Applying such thresholds in an application intended to predict transcriptional regulators is a double-edged sword. Setting the cutoff too high can

severely limit the number of candidates to work with. Assuming that an expression-based regulator-target relationship is more subtle than two co-regulated genes, it becomes desirable to have many candidates as opposed to few. One must also consider the other possible interpretations of co-expressed genes (**Figure 3-2a**). Conversely, setting the cutoff too low may result in overwhelming amounts of candidates, especially in the case of transcription factors controlling very large subsets of genes (potentially including other transcription factors). The lower the cutoff, the more threshold-passing correlations are detected (**Figure 3-2c**). One further theoretical limitation is the p-value cutoff. While we take the route of applying the most stringent p-value adjustment, these metrics are based on random chance assumptions, - not grounded in solid biological context. For example, p-values < 0.05 certainly do not signify a tested hypothesis is biologically important. Based on empirical testing, we assigned a cutoff of $|rho| \geq 0.6$ and adjusted p-value ≤ 0.05. This routinely produced networks with known regulator-target relationships, and the resulting subnetworks were also typically on the order of < 100 genes, compared to several hundred when testing correlation cutoffs around $|rho| \geq 0.5$.

We highlight that one of the most substantial benefits of COLDSTaR is data browsing. Other tools do not allow researchers to investigate which two genes are most tightly correlated in a dataset. This is because the only way to know such information is to calculate the pairwise relationship of every gene by every gene (all-by-all). COLDSTaR performs this one-time calculation and allows the resulting lists to be sorted. This could be particularly useful for asking which gene products in a given pathway are highest on the list (mTOR pathway, for example). We further developed the downstream complementary tool COLDNet to take this data and subsequently calculate and visualize co-expression networks. Rather than simply return a plot of all first neighbor genes in the network relative to a gene of interest, we also keep the inter-network relationships. This is especially valuable in cases where the amount of candidate regulators exceeds experimental testing capability and can be used to help narrow down a list. For example, a given network may indicate that a particular gene is strongly co-expressed with 90% of the network (in addition to the gene of interest), prioritizing it for validation. Network construction is done on the fly for each query gene but is nearly instant due to the co-expression results being pre-computed.

Upon completion of COLDSTaR development, we next sought to use it for analysis of pancreatic cancer data, as this was relevant to CYP3A5. We analyzed a cohort from TCGA of this cancer type consisting of 183 tumor samples and $> 30{,}000$ expressed genes. Extracting subnetworks of transcriptional regulators with known downstream targets produced networks that captured at least some of those targets. This was a good indication that our tool could capture biologically true relationships in a completely agnostic way, and only using expression data as input. Once the subnetwork for CYP3A5 was extracted, we obtained 72 co-expressed genes. 60 of these were commercially-available. Additionally, we tested two other methods reportedly capable of predicting transcriptional regulators (NetBID and Spearman correlation only). Each method predicted unique CYP3A5 regulator candidates. When we screened them by knocking them down in AsPC-1 cells and measuring CYP3A5 mRNA, it was evident that COLDSTaR predictions outperformed the other methods. This wasn't too surprising

however, because NetBID is designed to uncover driver genes, and the correlation only method fails to properly normalize data (leading to skewed results). Moreover, COLDSTaR started with less than half the number of candidates compared to NetBID but produced more hits in terms of CYP3A5 knockdown; it exclusively found 8 of the top 10 hits. Interestingly, only 2 of the top 10 hits were transcription factors. We validated screening hits at the qPCR level and deconvoluted the pooled siRNA hits conferring > 50% CYP3A5 knockdown. Our results were striking and indeed show that transcriptional regulators of CYP3A5 were captured. Of particular interest was that the top 2 hits were a peptide and an enzyme, neither of which is a nucleic acid-binding protein. These hits also reduced CYP3A5 at the protein level. If the experiments were started with a transcription factor siRNA library, these regulators would have been missed. The same is true for looking into ChIP-seq data; non-DNA-binding proteins are excluded. This underscores the importance of considering all classes of gene products as potential transcriptional regulators, and highlights that these can be predicted computationally with COLDSTaR.

We have successfully targeted CYP3A5 at two distinct and important levels, illuminating details into its function and regulation. We identified the first isoform-selective small molecule inhibitor of CYP3A5. This was challenging due to its wildly promiscuous ligand binding capability, structural overlap with CYP3A4, and lack of available assays for CYP3A5. Leveraging high-throughput screening led to the identification of the FDA-approved clobetasol propionate as a truly selective inhibitor. Moreover, this compound worked as potently and effectively (and sometimes better) in cells compared to the gold standard nonselective inhibitor ketoconazole – all while refraining from CYP3A4 inhibition. Based on our biophysical and computational endeavors, we demonstrated that subtle differences in active site shapes allow clobetasol to form a tight heme-ligand interaction exclusively in CYP3A5, serving as the basis for selective inhibition. This lays the foundation for designing molecules in the future that exploit these minute differences in an effort to try and overcome CYP3A5-mediated chemoresistance. We also aimed to uncover the regulators upstream of CYP3A5 in pancreatic cancer. To do this we developed the novel computational tool COLDSTaR which performed better than other methods and successfully identified a handful of CYP3A5 transcriptional regulators. These regulators of CYP3A5 mRNA consisted of a peptide, two enzymes, and a transcription factor. This is the first report of these factors as transcriptional regulators of CYP3A5, and sheds light on the poorly-understood topic of extra-hepatic CYP3A5 regulation. Strikingly, these were identified from a predicted list containing just 60 candidate genes. This comprises < 0.5% of a standard whole-genome siRNA library and was performed with publicly-available data. It stands to reason that a major factor in successful prediction came from the heterogenous input data. These patient data likely added robustness to the prediction, as any correlations surviving across the heterogenous tumors have a greater propensity of holding true in a given single model. This presents a deeper understanding of CYP3A5 regulation in cancer, and highlights targets that could be the subject of future studies into CYP3A5 in disease.

LIST OF REFERENCES

1 Zanger, U. M. & Schwab, M. Cytochrome P450 enzymes in drug metabolism: regulation of gene expression, enzyme activities, and impact of genetic variation. *Pharmacol Ther* **138**, 103-141, http://doi.org/10.1016/j.pharmthera.2012.12.007 (2013).

2 Lolodi, O., Wang, Y. M., Wright, W. C. & Chen, T. Differential Regulation of CYP3A4 and CYP3A5 and its Implication in Drug Discovery. *Curr Drug Metab* **18**, 1095-1105, http://doi.org/10.2174/1389200218666170531112038 (2017).

3 Klein, K. & Zanger, U. M. Pharmacogenomics of Cytochrome P450 3A4: Recent Progress Toward the "Missing Heritability" Problem. *Front Genet* **4**, 12, http://doi.org/10.3389/fgene.2013.00012 (2013).

4 Komori, M. *et al.* Fetus-specific expression of a form of cytochrome P-450 in human livers. *Biochemistry* **29**, 4430-4433 (1990).

5 Brandl, E. J. *et al.* Genetic variation in CYP3A43 is associated with response to antipsychotic medication. *J Neural Transm (Vienna)* **122**, 29-34, http://doi.org/10.1007/s00702-014-1298-8 (2015).

6 Han, J. H., Lee, Y. S., Kim, H. J., Lee, S. Y. & Myung, S. C. Association between cytochrome CYP17A1, CYP3A4, and CYP3A43 polymorphisms and prostate cancer risk and aggressiveness in a Korean study population. *Asian J Androl* **17**, 285-291, http://doi.org/10.4103/1008-682X.133320 (2015).

7 Dennison, J. B. *et al.* Selective metabolism of vincristine in vitro by CYP3A5. *Drug Metab Dispos* **34**, 1317-1327, http://doi.org/10.1124/dmd.106.009902 (2006).

8 Iwasaki, K. Metabolism of tacrolimus (FK506) and recent topics in clinical pharmacokinetics. *Drug Metab Pharmacokinet* **22**, 328-335 (2007).

9 Noll, E. M. *et al.* CYP3A5 mediates basal and acquired therapy resistance in different subtypes of pancreatic ductal adenocarcinoma. *Nat Med* **22**, 278-287, http://doi.org/10.1038/nm.4038 (2016).

10 Hayes, M. A., Li, X. Q., Gronberg, G., Diczfalusy, U. & Andersson, T. B. CYP3A Specifically Catalyzes 1beta-Hydroxylation of Deoxycholic Acid: Characterization and Enzymatic Synthesis of a Potential Novel Urinary Biomarker for CYP3A Activity. *Drug Metab Dispos* **44**, 1480-1489, http://doi.org/10.1124/dmd.116.070805 (2016).

11 Mao, J. *et al.* Perspective: 4beta-hydroxycholesterol as an emerging endogenous biomarker of hepatic CYP3A. *Drug Metab Rev* **49**, 18-34, http://doi.org/10.1080/03602532.2016.1239630 (2017).

12 Kasichayanula, S. *et al.* Validation of 4beta-hydroxycholesterol and evaluation of other endogenous biomarkers for the assessment of CYP3A activity in healthy subjects. *Br J Clin Pharmacol* **78**, 1122-1134, http://doi.org/10.1111/bcp.12425 (2014).

13 Wang, Y. M., Chai, S. C., Brewer, C. T. & Chen, T. Pregnane X receptor and drug-induced liver injury. *Expert Opin Drug Metab Toxicol* **10**, 1521-1532, http://doi.org/10.1517/17425255.2014.963555 (2014).

14 Diczfalusy, U., Nylen, H., Elander, P. & Bertilsson, L. 4beta-Hydroxycholesterol, an endogenous marker of CYP3A4/5 activity in humans. *Br J Clin Pharmacol* **71**, 183-189, http://doi.org/10.1111/j.1365-2125.2010.03773.x (2011).
15 Hole, K., Wollmann, B. M., Nguyen, C., Haslemo, T. & Molden, E. Comparison of CYP3A4-Inducing Capacity of Enzyme-Inducing Antiepileptic Drugs Using 4beta-Hydroxycholesterol as Biomarker. *Ther Drug Monit* **40**, 463-468, http://doi.org/10.1097/FTD.0000000000000518 (2018).
16 Xue, Y. J. *et al.* Use of 4beta-hydroxycholesterol in animal and human plasma samples as a biomarker for CYP3A induction. *Bioanalysis* **8**, 215-228, http://doi.org/10.4155/bio.15.241 (2016).
17 Waxman, D. J., Attisano, C., Guengerich, F. P. & Lapenson, D. P. Human liver microsomal steroid metabolism: identification of the major microsomal steroid hormone 6 beta-hydroxylase cytochrome P-450 enzyme. *Arch Biochem Biophys* **263**, 424-436 (1988).
18 Penzak, S. R. & Rojas-Fernandez, C. 4beta-Hydroxycholesterol as an Endogenous Biomarker for CYP3A Activity: Literature Review and Critical Evaluation. *J Clin Pharmacol*, http://doi.org/10.1002/jcph.1391 (2019).
19 Usmani, K. A. & Tang, J. Human cytochrome P450: metabolism of testosterone by CYP3A4 and inhibition by ketoconazole. *Curr Protoc Toxicol* **Chapter 4**, Unit4 13, http://doi.org/10.1002/0471140856.tx0413s20 (2004).
20 Kamdem, L. K. *et al.* Limited contribution of CYP3A5 to the hepatic 6beta-hydroxylation of testosterone. *Naunyn Schmiedebergs Arch Pharmacol* **370**, 71-77, http://doi.org/10.1007/s00210-004-0944-3 (2004).
21 Arlotto, M. P., Trant, J. M. & Estabrook, R. W. Measurement of steroid hydroxylation reactions by high-performance liquid chromatography as indicator of P450 identity and function. *Methods Enzymol* **206**, 454-462 (1991).
22 Gupta, R. P., Hollis, B. W., Patel, S. B., Patrick, K. S. & Bell, N. H. CYP3A4 is a human microsomal vitamin D 25-hydroxylase. *J Bone Miner Res* **19**, 680-688, http://doi.org/10.1359/JBMR.0301257 (2004).
23 Sakaki, T. *et al.* Dual metabolic pathway of 25-hydroxyvitamin D3 catalyzed by human CYP24. *Eur J Biochem* **267**, 6158-6165 (2000).
24 Bjorkhem-Bergman, L. *et al.* Serum levels of 25-hydroxyvitamin D and the CYP3A biomarker 4beta-hydroxycholesterol in a high-dose vitamin D supplementation study. *Drug Metab Dispos* **41**, 704-708, http://doi.org/10.1124/dmd.113.051136 (2013).
25 Fujita, K. Cytochrome P450 and anticancer drugs. *Curr Drug Metab* **7**, 23-37 (2006).
26 Zhou, X. J. *et al.* Human liver microsomal cytochrome P450 3A isozymes mediated vindesine biotransformation. Metabolic drug interactions. *Biochem Pharmacol* **45**, 853-861 (1993).
27 Preissner, S. *et al.* SuperCYP: a comprehensive database on Cytochrome P450 enzymes including a tool for analysis of CYP-drug interactions. *Nucleic Acids Res* **38**, D237-243, http://doi.org/10.1093/nar/gkp970 (2010).
28 Spratlin, J. & Sawyer, M. B. Pharmacogenetics of paclitaxel metabolism. *Crit Rev Oncol Hematol* **61**, 222-229, http://doi.org/10.1016/j.critrevonc.2006.09.006 (2007).

29 Royer, I., Monsarrat, B., Sonnier, M., Wright, M. & Cresteil, T. Metabolism of docetaxel by human cytochromes P450: interactions with paclitaxel and other antineoplastic drugs. *Cancer Res* **56**, 58-65 (1996).
30 Harris, J. W. *et al.* Isolation, structural determination, and biological activity of 6 alpha-hydroxytaxol, the principal human metabolite of taxol. *J Med Chem* **37**, 706-709 (1994).
31 Baker, S. D., Sparreboom, A. & Verweij, J. Clinical pharmacokinetics of docetaxel : recent developments. *Clin Pharmacokinet* **45**, 235-252, http://doi.org/10.2165/00003088-200645030-00002 (2006).
32 Tang, S. C. *et al.* P-glycoprotein, CYP3A, and Plasma Carboxylesterase Determine Brain Disposition and Oral Availability of the Novel Taxane Cabazitaxel (Jevtana) in Mice. *Mol Pharm* **12**, 3714-3723, http://doi.org/10.1021/acs.molpharmaceut.5b00470 (2015).
33 Jackson, K. D., Durandis, R. & Vergne, M. J. Role of Cytochrome P450 Enzymes in the Metabolic Activation of Tyrosine Kinase Inhibitors. *Int J Mol Sci* **19**, http://doi.org/10.3390/ijms19082367 (2018).
34 Fujita, K. I., Ishida, H., Kubota, Y. & Sasaki, Y. Toxicities of Receptor Tyrosine Kinase Inhibitors in Cancer Pharmacotherapy: Management with Clinical Pharmacology. *Curr Drug Metab* **18**, 186-198, http://doi.org/10.2174/1389200218666170105165832 (2017).
35 Duckett, D. R. & Cameron, M. D. Metabolism considerations for kinase inhibitors in cancer treatment. *Expert Opin Drug Metab Toxicol* **6**, 1175-1193, http://doi.org/10.1517/17425255.2010.506873 (2010).
36 Smith, D. A. *et al.* Effects of ketoconazole and carbamazepine on lapatinib pharmacokinetics in healthy subjects. *Br J Clin Pharmacol* **67**, 421-426, http://doi.org/10.1111/j.1365-2125.2009.03370.x (2009).
37 Li, X. *et al.* Characterization of dasatinib and its structural analogs as CYP3A4 mechanism-based inactivators and the proposed bioactivation pathways. *Drug Metab Dispos* **37**, 1242-1250, http://doi.org/10.1124/dmd.108.025932 (2009).
38 Ling, J. *et al.* Metabolism and excretion of erlotinib, a small molecule inhibitor of epidermal growth factor receptor tyrosine kinase, in healthy male volunteers. *Drug Metab Dispos* **34**, 420-426, http://doi.org/10.1124/dmd.105.007765 (2006).
39 Schacher-Kaufmann, S. & Pless, M. Acute Fatal Liver Toxicity under Erlotinib. *Case Rep Oncol* **3**, 182-188, http://doi.org/10.1159/000315366 (2010).
40 Li, X., Kamenecka, T. M. & Cameron, M. D. Cytochrome P450-mediated bioactivation of the epidermal growth factor receptor inhibitor erlotinib to a reactive electrophile. *Drug Metab Dispos* **38**, 1238-1245, http://doi.org/10.1124/dmd.109.030361 (2010).
41 Caba, O. *et al.* Identification of gene expression profiling associated with erlotinib-related skin toxicity in pancreatic adenocarcinoma patients. *Toxicol Appl Pharmacol* **311**, 113-116, http://doi.org/10.1016/j.taap.2016.10.003 (2016).
42 Smith, H. S. Opioid metabolism. *Mayo Clin Proc* **84**, 613-624, http://doi.org/10.1016/S0025-6196(11)60750-7 (2009).
43 Klees, T. M., Sheffels, P., Dale, O. & Kharasch, E. D. Metabolism of alfentanil by cytochrome p4503a (cyp3a) enzymes. *Drug Metab Dispos* **33**, 303-311, http://doi.org/10.1124/dmd.104.002709 (2005).

44 Kharasch, E. D. *et al.* The role of cytochrome P450 3A4 in alfentanil clearance. Implications for interindividual variability in disposition and perioperative drug interactions. *Anesthesiology* **87**, 36-50 (1997).
45 FDA.gov. *Drug Development and Drug Interactions : Table of Substrates, Inhibitors and Inducers*, <https://www.fda.gov/drugs/developmentapprovalprocess/developmentresources/druginteractionslabeling/ucm093664.htm#table1> (2017).
46 Lamb, D. C., Kelly, D. E., Baldwin, B. C. & Kelly, S. L. Differential inhibition of human CYP3A4 and Candida albicans CYP51 with azole antifungal agents. *Chem Biol Interact* **125**, 165-175 (2000).
47 Mahatthanatrakul, W. *et al.* Effect of cytochrome P450 3A4 inhibitor ketoconazole on risperidone pharmacokinetics in healthy volunteers. *J Clin Pharm Ther* **37**, 221-225, http://doi.org/10.1111/j.1365-2710.2011.01271.x (2012).
48 Boulenc, X. *et al.* CYP3A4-based drug-drug interaction: CYP3A4 substrates' pharmacokinetic properties and ketoconazole dose regimen effect. *Eur J Drug Metab Pharmacokinet* **41**, 45-54, http://doi.org/10.1007/s13318-014-0235-4 (2016).
49 Martin, P. *et al.* Effects of CYP3A4 Inhibitors Ketoconazole and Verapamil and the CYP3A4 Inducer Rifampicin on the Pharmacokinetic Parameters of Fostamatinib: Results from In Vitro and Phase I Clinical Studies. *Drugs R D* **16**, 81-92, http://doi.org/10.1007/s40268-015-0118-4 (2016).
50 Dutreix, C., Munarini, F., Lorenzo, S., Roesel, J. & Wang, Y. Investigation into CYP3A4-mediated drug-drug interactions on midostaurin in healthy volunteers. *Cancer Chemother Pharmacol* **72**, 1223-1234, http://doi.org/10.1007/s00280-013-2287-6 (2013).
51 Wiesinger, H. *et al.* Pharmacokinetic interaction between the CYP3A4 inhibitor ketoconazole and the hormone drospirenone in combination with ethinylestradiol or estradiol. *Br J Clin Pharmacol* **80**, 1399-1410, http://doi.org/10.1111/bcp.12745 (2015).
52 Townsend, R. *et al.* Pharmacokinetic Evaluation of CYP3A4-Mediated Drug-Drug Interactions of Isavuconazole With Rifampin, Ketoconazole, Midazolam, and Ethinyl Estradiol/Norethindrone in Healthy Adults. *Clin Pharmacol Drug Dev* **6**, 44-53, http://doi.org/10.1002/cpdd.285 (2017).
53 Godamudunage, M. P., Grech, A. M. & Scott, E. E. Comparison of Antifungal Azole Interactions with Adult Cytochrome P450 3A4 versus Neonatal Cytochrome P450 3A7. *Drug Metab Dispos* **46**, 1329-1337, http://doi.org/10.1124/dmd.118.082032 (2018).
54 Hariparsad, N. *et al.* Induction of CYP3A4 by efavirenz in primary human hepatocytes: comparison with rifampin and phenobarbital. *J Clin Pharmacol* **44**, 1273-1281, http://doi.org/10.1177/0091270004269142 (2004).
55 Martinez-Jimenez, C. P., Jover, R., Donato, M. T., Castell, J. V. & Gomez-Lechon, M. J. Transcriptional regulation and expression of CYP3A4 in hepatocytes. *Curr Drug Metab* **8**, 185-194 (2007).

56 Wang, K., Chen, S., Xie, W. & Wan, Y. J. Retinoids induce cytochrome P450 3A4 through RXR/VDR-mediated pathway. *Biochem Pharmacol* **75**, 2204-2213, http://doi.org/10.1016/j.bcp.2008.02.030 (2008).
57 Josephson, F. *et al.* CYP3A induction and inhibition by different antiretroviral regimens reflected by changes in plasma 4beta-hydroxycholesterol levels. *Eur J Clin Pharmacol* **64**, 775-781, http://doi.org/10.1007/s00228-008-0492-8 (2008).
58 Hossain, M. A., Tran, T., Chen, T., Mikus, G. & Greenblatt, D. J. Inhibition of human cytochromes P450 in vitro by ritonavir and cobicistat. *J Pharm Pharmacol* **69**, 1786-1793, http://doi.org/10.1111/jphp.12820 (2017).
59 Liddy, A. M., McLaughlin, G., Schmitz, S., D'Arcy, D. M. & Barry, M. G. The pharmacokinetic interaction between ivacaftor and ritonavir in healthy volunteers. *Br J Clin Pharmacol* **83**, 2235-2241, http://doi.org/10.1111/bcp.13324 (2017).
60 Wang, P., Shehu, A. I., Liu, K., Lu, J. & Ma, X. Biotransformation of Cobicistat: Metabolic Pathways and Enzymes. *Drug Metab Lett* **10**, 111-123 (2016).
61 Nguyen, T., McNicholl, I., Custodio, J. M., Szwarcberg, J. & Piontkowsky, D. Drug Interactions with Cobicistat- or Ritonavir-Boosted Elvitegravir. *AIDS Rev* **18**, 101-111 (2016).
62 Sherman, E. M., Worley, M. V., Unger, N. R., Gauthier, T. P. & Schafer, J. J. Cobicistat: Review of a Pharmacokinetic Enhancer for HIV Infection. *Clin Ther* **37**, 1876-1893, http://doi.org/10.1016/j.clinthera.2015.07.022 (2015).
63 Granfors, M. T. *et al.* Differential inhibition of cytochrome P450 3A4, 3A5 and 3A7 by five human immunodeficiency virus (HIV) protease inhibitors in vitro. *Basic Clin Pharmacol Toxicol* **98**, 79-85, http://doi.org/10.1111/j.1742-7843.2006.pto_249.x (2006).
64 Bailey, D. G., Spence, J. D., Munoz, C. & Arnold, J. M. Interaction of citrus juices with felodipine and nifedipine. *Lancet* **337**, 268-269 (1991).
65 Bailey, D. G., Dresser, G. & Arnold, J. M. Grapefruit-medication interactions: forbidden fruit or avoidable consequences? *CMAJ* **185**, 309-316, http://doi.org/10.1503/cmaj.120951 (2013).
66 Schmiedlin-Ren, P. *et al.* Mechanisms of enhanced oral availability of CYP3A4 substrates by grapefruit constituents. Decreased enterocyte CYP3A4 concentration and mechanism-based inactivation by furanocoumarins. *Drug Metab Dispos* **25**, 1228-1233 (1997).
67 Lin, H. L., Kenaan, C. & Hollenberg, P. F. Identification of the residue in human CYP3A4 that is covalently modified by bergamottin and the reactive intermediate that contributes to the grapefruit juice effect. *Drug Metab Dispos* **40**, 998-1006, http://doi.org/10.1124/dmd.112.044560 (2012).
68 Holmberg, M. T. *et al.* Grapefruit juice inhibits the metabolic activation of clopidogrel. *Clin Pharmacol Ther* **95**, 307-313, http://doi.org/10.1038/clpt.2013.192 (2014).
69 Holmberg, M. T. *et al.* Effect of grapefruit juice on the bioactivation of prasugrel. *Br J Clin Pharmacol* **80**, 139-145, http://doi.org/10.1111/bcp.12581 (2015).
70 Iwata, H., Tezuka, Y., Kadota, S., Hiratsuka, A. & Watabe, T. Mechanism-based inactivation of human liver microsomal CYP3A4 by rutaecarpine and limonin from Evodia fruit extract. *Drug Metab Pharmacokinet* **20**, 34-45 (2005).

71 Manda, V. K. *et al.* Inhibition of CYP3A4 and CYP1A2 by Aegle marmelos and its constituents. *Xenobiotica* **46**, 117-125, http://doi.org/10.3109/00498254.2015.1053006 (2016).
72 Liu, R. *et al.* In vitro activity of Lycium barbarum (Goji) against major human phase I metabolism enzymes. *J Complement Integr Med* **13**, 257-265, http://doi.org/10.1515/jcim-2015-0038 (2016).
73 Hidaka, M. *et al.* Potent inhibition by star fruit of human cytochrome P450 3A (CYP3A) activity. *Drug Metab Dispos* **32**, 581-583, http://doi.org/10.1124/dmd.32.6.581 (2004).
74 Sato, Y., Sasaki, T., Takahashi, S., Kumagai, T. & Nagata, K. Development of a highly reproducible system to evaluate inhibition of cytochrome P450 3A4 activity by natural medicines. *J Pharm Pharm Sci* **18**, 316-327 (2015).
75 Zhao, J. *et al.* Inhibition of human CYP3A4 and CYP3A5 enzymes by gomisin C and gomisin G, two lignan analogs derived from Schisandra chinensis. *Fitoterapia* **119**, 26-31, http://doi.org/10.1016/j.fitote.2017.03.010 (2017).
76 Roby, C. A., Anderson, G. D., Kantor, E., Dryer, D. A. & Burstein, A. H. St John's Wort: effect on CYP3A4 activity. *Clin Pharmacol Ther* **67**, 451-457, http://doi.org/10.1067/mcp.2000.106793 (2000).
77 Mannel, M. Drug interactions with St John's wort : mechanisms and clinical implications. *Drug Saf* **27**, 773-797, http://doi.org/10.2165/00002018-200427110-00003 (2004).
78 Zhou, S., Chan, E., Pan, S. Q., Huang, M. & Lee, E. J. Pharmacokinetic interactions of drugs with St John's wort. *J Psychopharmacol* **18**, 262-276, http://doi.org/10.1177/0269881104042632 (2004).
79 Davydov, D. R. *et al.* Peripheral ligand-binding site in cytochrome P450 3A4 located with fluorescence resonance energy transfer (FRET). *J Biol Chem* **287**, 6797-6809, http://doi.org/10.1074/jbc.M111.325654 (2012).
80 Davydov, D. R., Baas, B. J., Sligar, S. G. & Halpert, J. R. Allosteric mechanisms in cytochrome P450 3A4 studied by high-pressure spectroscopy: pivotal role of substrate-induced changes in the accessibility and degree of hydration of the heme pocket. *Biochemistry* **46**, 7852-7864, http://doi.org/10.1021/bi602400y (2007).
81 Blobaum, A. L. *et al.* Heterotropic activation of the midazolam hydroxylase activity of CYP3A by a positive allosteric modulator of mGlu5: in vitro to in vivo translation and potential impact on clinically relevant drug-drug interactions. *Drug Metab Dispos* **41**, 2066-2075, http://doi.org/10.1124/dmd.113.052662 (2013).
82 Pourdjabbar, A. *et al.* A pharmacodynamic analysis for the co-administration of inducers of CYP3A with ticagrelor: A cautionary tale in managing patients with acute coronary syndromes. *Int J Cardiol* **214**, 423-425, http://doi.org/10.1016/j.ijcard.2016.03.153 (2016).
83 Blobaum, A. L. *et al.* A Screen of Approved Drugs Identifies the Androgen Receptor Antagonist Flutamide and Its Pharmacologically Active Metabolite 2-Hydroxy-Flutamide as Heterotropic Activators of Cytochrome P450 3A In Vitro and In Vivo. *Drug Metab Dispos* **43**, 1718-1726, http://doi.org/10.1124/dmd.115.064006 (2015).

84 Teng, R. & Butler, K. The effect of ticagrelor on the metabolism of midazolam in healthy volunteers. *Clin Ther* **35**, 1025-1037, http://doi.org/10.1016/j.clinthera.2013.06.003 (2013).
85 Polic, V. & Auclair, K. Allosteric Activation of Cytochrome P450 3A4 via Progesterone Bioconjugation. *Bioconjug Chem* **28**, 885-889, http://doi.org/10.1021/acs.bioconjchem.6b00604 (2017).
86 Zhuang, X. *et al.* Allosteric activation of midazolam CYP3A5 hydroxylase activity by icotinib - Enhancement by ketoconazole. *Biochem Pharmacol* **121**, 67-77, http://doi.org/10.1016/j.bcp.2016.09.012 (2016).
87 Li, X., Song, X., Kamenecka, T. M. & Cameron, M. D. Discovery of a highly selective CYP3A4 inhibitor suitable for reaction phenotyping studies and differentiation of CYP3A4 and CYP3A5. *Drug Metab Dispos* **40**, 1803-1809, http://doi.org/10.1124/dmd.112.046144 (2012).
88 Walsky, R. L. *et al.* Selective mechanism-based inactivation of CYP3A4 by CYP3cide (PF-04981517) and its utility as an in vitro tool for delineating the relative roles of CYP3A4 versus CYP3A5 in the metabolism of drugs. *Drug Metab Dispos* **40**, 1686-1697, http://doi.org/10.1124/dmd.112.045302 (2012).
89 Ekins, S., Stresser, D. M. & Williams, J. A. In vitro and pharmacophore insights into CYP3A enzymes. *Trends Pharmacol Sci* **24**, 161-166 (2003).
90 Williams, J. A., Cook, J. & Hurst, S. I. A significant drug-metabolizing role for CYP3A5? *Drug Metab Dispos* **31**, 1526-1530, http://doi.org/10.1124/dmd.31.12.1526 (2003).
91 Li, X. *et al.* Characterization of T-5 N-oxide formation as the first highly selective measure of CYP3A5 activity. *Drug Metab Dispos* **42**, 334-342, http://doi.org/10.1124/dmd.113.054726 (2014).
92 Dennison, J. B., Jones, D. R., Renbarger, J. L. & Hall, S. D. Effect of CYP3A5 expression on vincristine metabolism with human liver microsomes. *J Pharmacol Exp Ther* **321**, 553-563, http://doi.org/10.1124/jpet.106.118471 (2007).
93 Bosilkovska, M. *et al.* Severe Vincristine-induced Neuropathic Pain in a CYP3A5 Nonexpressor With Reduced CYP3A4/5 Activity: Case Study. *Clin Ther* **38**, 216-220, http://doi.org/10.1016/j.clinthera.2015.10.017 (2016).
94 Kayilioglu, H. *et al.* Association of CYP3A5 Expression and Vincristine Neurotoxicity in Pediatric Malignancies in Turkish Population. *J Pediatr Hematol Oncol* **39**, 458-462, http://doi.org/10.1097/MPH.0000000000000910 (2017).
95 Saba, N., Bhuyan, R., Nandy, S. K. & Seal, A. Differential Interactions of Cytochrome P450 3A5 and 3A4 with Chemotherapeutic Agent-Vincristine: A Comparative Molecular Dynamics Study. *Anticancer Agents Med Chem* **15**, 475-483 (2015).
96 Kamdem, L. K. *et al.* Contribution of CYP3A5 to the in vitro hepatic clearance of tacrolimus. *Clin Chem* **51**, 1374-1381, http://doi.org/10.1373/clinchem.2005.050047 (2005).
97 Quteineh, L. *et al.* Influence of CYP3A5 genetic polymorphism on tacrolimus daily dose requirements and acute rejection in renal graft recipients. *Basic Clin Pharmacol Toxicol* **103**, 546-552, http://doi.org/10.1111/j.1742-7843.2008.00327.x (2008).

98 Soars, M. G., Grime, K. & Riley, R. J. Comparative analysis of substrate and inhibitor interactions with CYP3A4 and CYP3A5. *Xenobiotica* **36**, 287-299, http://doi.org/10.1080/00498250500446208 (2006).
99 Wu, J. J. *et al.* Gomisin A is a Novel Isoform-Specific Probe for the Selective Sensing of Human Cytochrome P450 3A4 in Liver Microsomes and Living Cells. *AAPS J* **18**, 134-145, http://doi.org/10.1208/s12248-015-9827-4 (2016).
100 Wan, C. K. *et al.* Inhibition of cytochrome P450 3A4 activity by schisandrol A and gomisin A isolated from Fructus Schisandrae chinensis. *Phytomedicine* **17**, 702-705, http://doi.org/10.1016/j.phymed.2009.12.005 (2010).
101 Hong, M. *et al.* A Network Pharmacology-Based Study on the Hepatoprotective Effect of Fructus Schisandrae. *Molecules* **22**, http://doi.org/10.3390/molecules22101617 (2017).
102 Teraoka, R., Shimada, T. & Aburada, M. The molecular mechanisms of the hepatoprotective effect of gomisin A against oxidative stress and inflammatory response in rats with carbon tetrachloride-induced acute liver injury. *Biol Pharm Bull* **35**, 171-177 (2012).
103 Cali, J. J. CYP3A4 P450-Glo® Assays with Luciferin-IPA: The Most Sensitive and Selective Bioluminescent CYP3A4 Assay. *Cell Notes*, 17-19 (2006).
104 Wakuri, S. *et al.* Correlation between luminescence intensity and cytotoxicity in cell-based cytotoxicity assay using luciferase. *Anal Biochem* **522**, 18-29, http://doi.org/10.1016/j.ab.2017.01.015 (2017).
105 Li, A. P. & Doshi, U. Higher throughput human hepatocyte assays for the evaluation of time-dependent inhibition of CYP3A4. *Drug Metab Lett* **5**, 183-191 (2011).
106 Anzenbacher, P. & Hudecek, J. Differences in flexibility of active sites of cytochromes P450 probed by resonance Raman and UV-Vis absorption spectroscopy. *J Inorg Biochem* **87**, 209-213 (2001).
107 Ohkura, K. *et al.* Flexible structure of cytochrome P450: promiscuity of ligand binding in the CYP3A4 heme pocket. *Anticancer Res* **29**, 935-942 (2009).
108 Teixeira, V. H., Ribeiro, V. & Martel, P. J. Analysis of binding modes of ligands to multiple conformations of CYP3A4. *Biochim Biophys Acta* **1804**, 2036-2045, http://doi.org/10.1016/j.bbapap.2010.06.008 (2010).
109 Sevrioukova, I. F. & Poulos, T. L. Structural and mechanistic insights into the interaction of cytochrome P4503A4 with bromoergocryptine, a type I ligand. *J Biol Chem* **287**, 3510-3517, http://doi.org/10.1074/jbc.M111.317081 (2012).
110 Sevrioukova, I. F. & Poulos, T. L. Anion-Dependent Stimulation of CYP3A4 Monooxygenase. *Biochemistry* **54**, 4083-4096, http://doi.org/10.1021/acs.biochem.5b00510 (2015).
111 Ekroos, M. & Sjogren, T. Structural basis for ligand promiscuity in cytochrome P450 3A4. *Proc Natl Acad Sci U S A* **103**, 13682-13687, http://doi.org/10.1073/pnas.0603236103 (2006).
112 Sevrioukova, I. F. & Poulos, T. L. Dissecting cytochrome P450 3A4-ligand interactions using ritonavir analogues. *Biochemistry* **52**, 4474-4481, http://doi.org/10.1021/bi4005396 (2013).

113 Sevrioukova, I. F. & Poulos, T. L. Structural basis for regiospecific midazolam oxidation by human cytochrome P450 3A4. *Proc Natl Acad Sci U S A* **114**, 486-491, http://doi.org/10.1073/pnas.1616198114 (2017).
114 Otyepka, M., Berka, K. & Anzenbacher, P. Is there a relationship between the substrate preferences and structural flexibility of cytochromes P450? *Curr Drug Metab* **13**, 130-142 (2012).
115 Yano, J. K. *et al.* The structure of human microsomal cytochrome P450 3A4 determined by X-ray crystallography to 2.05-A resolution. *J Biol Chem* **279**, 38091-38094, http://doi.org/10.1074/jbc.C400293200 (2004).
116 Sevrioukova, I. F. & Poulos, T. L. Pyridine-substituted desoxyritonavir is a more potent inhibitor of cytochrome P450 3A4 than ritonavir. *J Med Chem* **56**, 3733-3741, http://doi.org/10.1021/jm400288z (2013).
117 Hsu, M. H., Savas, U. & Johnson, E. F. The X-Ray Crystal Structure of the Human Mono-Oxygenase Cytochrome P450 3A5-Ritonavir Complex Reveals Active Site Differences between P450s 3A4 and 3A5. *Mol Pharmacol* **93**, 14-24, http://doi.org/10.1124/mol.117.109744 (2018).
118 Sevrioukova, I. F. High-Level Production and Properties of the Cysteine-Depleted Cytochrome P450 3A4. *Biochemistry* **56**, 3058-3067, http://doi.org/10.1021/acs.biochem.7b00334 (2017).
119 Krauser, J. A. & Guengerich, F. P. Cytochrome P450 3A4-catalyzed testosterone 6beta-hydroxylation stereochemistry, kinetic deuterium isotope effects, and rate-limiting steps. *J Biol Chem* **280**, 19496-19506, http://doi.org/10.1074/jbc.M501854200 (2005).
120 Nebert, D. W., Wikvall, K. & Miller, W. L. Human cytochromes P450 in health and disease. *Philos Trans R Soc Lond B Biol Sci* **368**, 20120431, http://doi.org/10.1098/rstb.2012.0431 (2013).
121 Raunio, H. *et al.* Expression of xenobiotic-metabolizing CYPs in human pulmonary tissue. *Exp Toxicol Pathol* **51**, 412-417, http://doi.org/10.1016/S0940-2993(99)80031-1 (1999).
122 Shimada, T. & Fujii-Kuriyama, Y. Metabolic activation of polycyclic aromatic hydrocarbons to carcinogens by cytochromes P450 1A1 and 1B1. *Cancer Sci* **95**, 1-6 (2004).
123 D'Uva, G., Baci, D., Albini, A. & Noonan, D. M. Cancer chemoprevention revisited: Cytochrome P450 family 1B1 as a target in the tumor and the microenvironment. *Cancer Treat Rev* **63**, 1-18, http://doi.org/10.1016/j.ctrv.2017.10.013 (2018).
124 Raccor, B. S. & Kaspera, R. Extra-hepatic isozymes from the CYP1 and CYP2 families as potential chemotherapeutic targets. *Curr Top Med Chem* **13**, 1441-1453 (2013).
125 Nebert, D. W. Aryl hydrocarbon receptor (AHR): "pioneer member" of the basic-helix/loop/helix per-Arnt-sim (bHLH/PAS) family of "sensors" of foreign and endogenous signals. *Prog Lipid Res* **67**, 38-57, http://doi.org/10.1016/j.plipres.2017.06.001 (2017).
126 Chen, C. & Wang, D. W. Cytochrome P450-CYP2 Family-Epoxygenase Role in Inflammation and Cancer. *Adv Pharmacol* **74**, 193-221, http://doi.org/10.1016/bs.apha.2015.04.005 (2015).

127 Hedrich, W. D., Hassan, H. E. & Wang, H. Insights into CYP2B6-mediated drug-drug interactions. *Acta Pharm Sin B* **6**, 413-425, http://doi.org/10.1016/j.apsb.2016.07.016 (2016).
128 Zanger, U. M. & Klein, K. Pharmacogenetics of cytochrome P450 2B6 (CYP2B6): advances on polymorphisms, mechanisms, and clinical relevance. *Front Genet* **4**, 24, http://doi.org/10.3389/fgene.2013.00024 (2013).
129 Kikuta, Y. *et al.* Purification and characterization of recombinant human neutrophil leukotriene B4 omega-hydroxylase (cytochrome P450 4F3). *Arch Biochem Biophys* **355**, 201-205, http://doi.org/10.1006/abbi.1998.0724 (1998).
130 Edson, K. Z. & Rettie, A. E. CYP4 enzymes as potential drug targets: focus on enzyme multiplicity, inducers and inhibitors, and therapeutic modulation of 20-hydroxyeicosatetraenoic acid (20-HETE) synthase and fatty acid omega-hydroxylase activities. *Curr Top Med Chem* **13**, 1429-1440 (2013).
131 Ortiz de Montellano, P. R. Mechanism and role of covalent heme binding in the CYP4 family of P450 enzymes and the mammalian peroxidases. *Drug Metab Rev* **40**, 405-426, http://doi.org/10.1080/03602530802186439 (2008).
132 Eun, H. S., Cho, S. Y., Lee, B. S., Seong, I. O. & Kim, K. H. Profiling cytochrome P450 family 4 gene expression in human hepatocellular carcinoma. *Mol Med Rep* **18**, 4865-4876, http://doi.org/10.3892/mmr.2018.9526 (2018).
133 Guengerich, F. P., Waterman, M. R. & Egli, M. Recent Structural Insights into Cytochrome P450 Function. *Trends Pharmacol Sci* **37**, 625-640, http://doi.org/10.1016/j.tips.2016.05.006 (2016).
134 McDonnell, A. M. & Dang, C. H. Basic review of the cytochrome p450 system. *J Adv Pract Oncol* **4**, 263-268 (2013).
135 Liu, Y. T., Hao, H. P., Liu, C. X., Wang, G. J. & Xie, H. G. Drugs as CYP3A probes, inducers, and inhibitors. *Drug Metab Rev* **39**, 699-721, http://doi.org/10.1080/03602530701690374 (2007).
136 Guengerich, F. P. Cytochrome p450 and chemical toxicology. *Chem Res Toxicol* **21**, 70-83, http://doi.org/10.1021/tx700079z (2008).
137 Achour, B., Barber, J. & Rostami-Hodjegan, A. Expression of hepatic drug-metabolizing cytochrome p450 enzymes and their intercorrelations: a meta-analysis. *Drug Metab Dispos* **42**, 1349-1356, http://doi.org/10.1124/dmd.114.058834 (2014).
138 Shimada, T., Yamazaki, H., Mimura, M., Inui, Y. & Guengerich, F. P. Interindividual variations in human liver cytochrome P-450 enzymes involved in the oxidation of drugs, carcinogens and toxic chemicals: studies with liver microsomes of 30 Japanese and 30 Caucasians. *J Pharmacol Exp Ther* **270**, 414-423 (1994).
139 Wright, W. C. C., Jude; Chen, Taosheng. Structural perspectives of the CYP3A family and their small molecule modulators in drug metabolism. *Liver Research*, http://doi.org/https://doi.org/10.1016/j.livres.2019.08.001 (2019).
140 Bui, K., Zhou, D., Sostek, M., She, F. & Al-Huniti, N. Effects of CYP3A Modulators on the Pharmacokinetics of Naloxegol. *J Clin Pharmacol* **56**, 1019-1027, http://doi.org/10.1002/jcph.693 (2016).
141 Gupta, N. *et al.* Effects of Strong CYP3A Inhibition and Induction on the Pharmacokinetics of Ixazomib, an Oral Proteasome Inhibitor: Results of Drug-

Drug Interaction Studies in Patients With Advanced Solid Tumors or Lymphoma and a Physiologically Based Pharmacokinetic Analysis. *J Clin Pharmacol* **58**, 180-192, http://doi.org/10.1002/jcph.988 (2018).

142 Dong, P. P. *et al.* Substrate-dependent modulation of the catalytic activity of CYP3A by erlotinib. *Acta Pharmacol Sin* **32**, 399-407, http://doi.org/10.1038/aps.2010.218 (2011).

143 Wandel, C. *et al.* Effect of CYP3A inhibition on vesnarinone metabolism in humans. *Clin Pharmacol Ther* **63**, 506-511, http://doi.org/10.1016/S0009-9236(98)90101-1 (1998).

144 US-FDA. *Drug Development and Drug Interactions : Table of Substrates, Inhibitors, and Inducers*, <https://www.fda.gov/drugs/drug-interactions-labeling/drug-development-and-drug-interactions-table-substrates-inhibitors-and-inducers> (2017).

145 Huang, S. M., Temple, R., Throckmorton, D. C. & Lesko, L. J. Drug interaction studies: study design, data analysis, and implications for dosing and labeling. *Clin Pharmacol Ther* **81**, 298-304, http://doi.org/10.1038/sj.clpt.6100054 (2007).

146 Vermeer, L. M., Isringhausen, C. D., Ogilvie, B. W. & Buckley, D. B. Evaluation of Ketoconazole and Its Alternative Clinical CYP3A4/5 Inhibitors as Inhibitors of Drug Transporters: The In Vitro Effects of Ketoconazole, Ritonavir, Clarithromycin, and Itraconazole on 13 Clinically-Relevant Drug Transporters. *Drug Metab Dispos* **44**, 453-459, http://doi.org/10.1124/dmd.115.067744 (2016).

147 Sudo, M., Nishihara, M., Takahashi, J. & Asahi, S. Long-Term Stability of Cryopreserved Human Hepatocytes: Evaluation of Phase I and II Drug-Metabolizing Enzyme Activities and CYP3A4/5 Induction for More than a Decade. *Drug Metab Dispos* **45**, 734-736, http://doi.org/10.1124/dmd.117.075234 (2017).

148 Xiao, K. *et al.* CYP3A4/5 Activity Probed with Testosterone and Midazolam: Correlation between Two Substrates at the Microsomal and Enzyme Levels. *Mol Pharm* **16**, 382-392, http://doi.org/10.1021/acs.molpharmaceut.8b01043 (2019).

149 Dhaini, H. R. *et al.* Cytochrome P450 CYP3A4/5 expression as a biomarker of outcome in osteosarcoma. *J Clin Oncol* **21**, 2481-2485, http://doi.org/10.1200/JCO.2003.06.015 (2003).

150 Zhu, Y. *et al.* Amlodipine metabolism in human liver microsomes and roles of CYP3A4/5 in the dihydropyridine dehydrogenation. *Drug Metab Dispos* **42**, 245-249, http://doi.org/10.1124/dmd.113.055400 (2014).

151 Tseng, E. *et al.* Relative contributions of cytochrome CYP3A4 versus CYP3A5 for CYP3A-cleared drugs assessed in vitro using a CYP3A4-selective inactivator (CYP3cide). *Drug Metab Dispos* **42**, 1163-1173, http://doi.org/10.1124/dmd.114.057000 (2014).

152 Pitre, A. *et al.* An unexpected protein interaction promotes drug resistance in leukemia. *Nat Commun* **8**, 1547, http://doi.org/10.1038/s41467-017-01678-y (2017).

153 Ippagunta, S. K. *et al.* Identification of Toll-like receptor signaling inhibitors based on selective activation of hierarchically acting signaling proteins. *Sci Signal* **11**, 543-553, http://doi.org/10.1126/scisignal.aaq1077 (2018).

154 Sevrioukova, I. F. & Poulos, T. L. Structure and mechanism of the complex between cytochrome P4503A4 and ritonavir. *Proc Natl Acad Sci U S A* **107**, 18422-18427, http://doi.org/10.1073/pnas.1010693107 (2010).
155 Ernest, C. S., 2nd, Hall, S. D. & Jones, D. R. Mechanism-based inactivation of CYP3A by HIV protease inhibitors. *J Pharmacol Exp Ther* **312**, 583-591, http://doi.org/10.1124/jpet.104.075416 (2005).
156 Moore, C. D. *et al.* Metabolic pathways of inhaled glucocorticoids by the CYP3A enzymes. *Drug Metab Dispos* **41**, 379-389, http://doi.org/10.1124/dmd.112.046318 (2013).
157 Zhao, P. *et al.* Quantitative evaluation of pharmacokinetic inhibition of CYP3A substrates by ketoconazole: a simulation study. *J Clin Pharmacol* **49**, 351-359, http://doi.org/10.1177/0091270008331196 (2009).
158 Westerink, W. M. & Schoonen, W. G. Cytochrome P450 enzyme levels in HepG2 cells and cryopreserved primary human hepatocytes and their induction in HepG2 cells. *Toxicol In Vitro* **21**, 1581-1591, http://doi.org/10.1016/j.tiv.2007.05.014 (2007).
159 Choi, J. M. *et al.* HepG2 cells as an in vitro model for evaluation of cytochrome P450 induction by xenobiotics. *Arch Pharm Res* **38**, 691-704, http://doi.org/10.1007/s12272-014-0502-6 (2015).
160 Xuan, J., Chen, S., Ning, B., Tolleson, W. H. & Guo, L. Development of HepG2-derived cells expressing cytochrome P450s for assessing metabolism-associated drug-induced liver toxicity. *Chem Biol Interact* **255**, 63-73, http://doi.org/10.1016/j.cbi.2015.10.009 (2016).
161 Yu, T. *et al.* The prognostic value of differentially expressed CYP3A subfamily members for hepatocellular carcinoma. *Cancer Manag Res* **10**, 1713-1726, http://doi.org/10.2147/CMAR.S159425 (2018).
162 Kirby, G. M. *et al.* Overexpression of cytochrome P-450 isoforms involved in aflatoxin B1 bioactivation in human liver with cirrhosis and hepatitis. *Toxicol Pathol* **24**, 458-467, http://doi.org/10.1177/019262339602400408 (1996).
163 Cancer Genome Atlas Research, N. *et al.* The Cancer Genome Atlas Pan-Cancer analysis project. *Nat Genet* **45**, 1113-1120, http://doi.org/10.1038/ng.2764 (2013).
164 Wright, W. C. C., Taosheng. *Reprocessing of RNA-sequencing samples from publicly-available data to yield normalized and comparable expression results.*, <https://dx.doi.org/10.21203/rs.2.16081/v1> (2019).
165 Paulson, S. K. *et al.* The Pharmacokinetics of the CYP3A Substrate Midazolam After Steady-state Dosing of Delafloxacin. *Clin Ther* **39**, 1182-1190, http://doi.org/10.1016/j.clinthera.2017.04.009 (2017).
166 Mooiman, K. D. *et al.* Development and validation of a LC-MS/MS method for the in vitro analysis of 1-hydroxymidazolam in human liver microsomes: application for determining CYP3A4 inhibition in complex matrix mixtures. *Biomed Chromatogr* **27**, 1107-1116, http://doi.org/10.1002/bmc.2913 (2013).
167 Hsu, M. H. & Johnson, E. F. Active-site differences between substrate-free and ritonavir-bound cytochrome P450 (CYP) 3A5 reveal plasticity differences between CYP3A5 and CYP3A4. *J Biol Chem* **294**, 8015-8022, http://doi.org/10.1074/jbc.RA119.007928 (2019).

168 Mak, P. J. & Denisov, I. G. Spectroscopic studies of the cytochrome P450 reaction mechanisms. *Biochim Biophys Acta Proteins Proteom* **1866**, 178-204, http://doi.org/10.1016/j.bbapap.2017.06.021 (2018).
169 Luthra, A., Denisov, I. G. & Sligar, S. G. Spectroscopic features of cytochrome P450 reaction intermediates. *Arch Biochem Biophys* **507**, 26-35, http://doi.org/10.1016/j.abb.2010.12.008 (2011).
170 Sevrioukova, I. F. & Poulos, T. L. Understanding the mechanism of cytochrome P450 3A4: recent advances and remaining problems. *Dalton Trans* **42**, 3116-3126, http://doi.org/10.1039/c2dt31833d (2013).
171 Greenblatt, D. J. *et al.* Mechanism of cytochrome P450-3A inhibition by ketoconazole. *J Pharm Pharmacol* **63**, 214-221, http://doi.org/10.1111/j.2042-7158.2010.01202.x (2011).
172 Conner, K. P. *et al.* Strength of axial water ligation in substrate-free cytochrome P450s is isoform dependent. *Biochemistry* **53**, 1428-1434, http://doi.org/10.1021/bi401547j (2014).
173 Shakunthala, N. New cytochrome P450 mechanisms: implications for understanding molecular basis for drug toxicity at the level of the cytochrome. *Expert Opin Drug Metab Toxicol* **6**, 1-15, http://doi.org/10.1517/17425250903329095 (2010).
174 Li, T., Bonkovsky, H. L. & Guo, J. T. Structural analysis of heme proteins: implications for design and prediction. *BMC Struct Biol* **11**, 13, http://doi.org/10.1186/1472-6807-11-13 (2011).
175 Fonvielle, M. *et al.* Substrate and reaction specificity of Mycobacterium tuberculosis cytochrome P450 CYP121: insights from biochemical studies and crystal structures. *J Biol Chem* **288**, 17347-17359, http://doi.org/10.1074/jbc.M112.443853 (2013).
176 Mast, N., Zheng, W., Stout, C. D. & Pikuleva, I. A. Antifungal Azoles: Structural Insights into Undesired Tight Binding to Cholesterol-Metabolizing CYP46A1. *Mol Pharmacol* **84**, 86-94, http://doi.org/10.1124/mol.113.085902 (2013).
177 Streetman, D. S., Bertino, J. S., Jr. & Nafziger, A. N. Phenotyping of drug-metabolizing enzymes in adults: a review of in-vivo cytochrome P450 phenotyping probes. *Pharmacogenetics* **10**, 187-216, http://doi.org/10.1097/00008571-200004000-00001 (2000).
178 Krusekopf, S., Roots, I. & Kleeberg, U. Differential drug-induced mRNA expression of human CYP3A4 compared to CYP3A5, CYP3A7 and CYP3A43. *Eur J Pharmacol* **466**, 7-12, http://doi.org/10.1016/s0014-2999(03)01481-x (2003).
179 Ghose, R., Mallick, P., Taneja, G., Chu, C. & Moorthy, B. In Vitro Approaches to Study Regulation of Hepatic Cytochrome P450 (CYP) 3A Expression by Paclitaxel and Rifampicin. *Methods Mol Biol* **1395**, 55-68, http://doi.org/10.1007/978-1-4939-3347-1_4 (2016).
180 Wright, W. C. *et al.* Clobetasol Propionate Is a Heme-Mediated Selective Inhibitor of Human Cytochrome P450 3A5. *J Med Chem* **63**, 1415-1433, http://doi.org/10.1021/acs.jmedchem.9b02067 (2020).

181 Davis, C. A. *et al.* The Encyclopedia of DNA elements (ENCODE): data portal update. *Nucleic Acids Res* **46**, D794-D801, http://doi.org/10.1093/nar/gkx1081 (2018).
182 Margolin, A. A. *et al.* ARACNE: an algorithm for the reconstruction of gene regulatory networks in a mammalian cellular context. *BMC Bioinformatics* **7 Suppl 1**, S7, http://doi.org/10.1186/1471-2105-7-S1-S7 (2006).
183 Du, X. *et al.* Hippo/Mst signalling couples metabolic state and immune function of CD8alpha(+) dendritic cells. *Nature* **558**, 141-145, http://doi.org/10.1038/s41586-018-0177-0 (2018).
184 Zhu, M., Liu, C. C. & Cheng, C. REACTIN: regulatory activity inference of transcription factors underlying human diseases with application to breast cancer. *BMC Genomics* **14**, 504, http://doi.org/10.1186/1471-2164-14-504 (2013).
185 Langfelder, P. & Horvath, S. WGCNA: an R package for weighted correlation network analysis. *BMC Bioinformatics* **9**, 559, http://doi.org/10.1186/1471-2105-9-559 (2008).
186 Serin, E. A., Nijveen, H., Hilhorst, H. W. & Ligterink, W. Learning from Co-expression Networks: Possibilities and Challenges. *Front Plant Sci* **7**, 444, http://doi.org/10.3389/fpls.2016.00444 (2016).
187 Liesecke, F. *et al.* Ranking genome-wide correlation measurements improves microarray and RNA-seq based global and targeted co-expression networks. *Sci Rep* **8**, 10885, http://doi.org/10.1038/s41598-018-29077-3 (2018).
188 Kumari, S. *et al.* Evaluation of gene association methods for coexpression network construction and biological knowledge discovery. *PLoS One* **7**, e50411, http://doi.org/10.1371/journal.pone.0050411 (2012).
189 Spiess, A.-N. *bigcor : creating very large correlation/covariance matrices*.
190 Jafari, M. & Ansari-Pour, N. Why, When and How to Adjust Your P Values? *Cell J* **20**, 604-607, http://doi.org/10.22074/cellj.2019.5992 (2019).
191 Chen, S. Y., Feng, Z. & Yi, X. A general introduction to adjustment for multiple comparisons. *J Thorac Dis* **9**, 1725-1729, http://doi.org/10.21037/jtd.2017.05.34 (2017).
192 Akoglu, H. User's guide to correlation coefficients. *Turk J Emerg Med* **18**, 91-93, http://doi.org/10.1016/j.tjem.2018.08.001 (2018).
193 Abel, E. V. *et al.* HNF1A is a novel oncogene that regulates human pancreatic cancer stem cell properties. *Elife* **7**, http://doi.org/10.7554/eLife.33947 (2018).
194 Yu, Y. *et al.* HNF1A/CASC2 regulates pancreatic cancer cell proliferation through PTEN/Akt signaling. *J Cell Biochem* **120**, 2816-2827, http://doi.org/10.1002/jcb.26395 (2019).
195 Hoskins, J. W. *et al.* Transcriptome analysis of pancreatic cancer reveals a tumor suppressor function for HNF1A. *Carcinogenesis* **35**, 2670-2678, http://doi.org/10.1093/carcin/bgu193 (2014).
196 Shukla, S. *et al.* Aberrant Activation of a Gastrointestinal Transcriptional Circuit in Prostate Cancer Mediates Castration Resistance. *Cancer Cell* **32**, 792-806 e797, http://doi.org/10.1016/j.ccell.2017.10.008 (2017).
197 Lau, H. H., Ng, N. H. J., Loo, L. S. W., Jasmen, J. B. & Teo, A. K. K. The molecular functions of hepatocyte nuclear factors - In and beyond the liver. *J Hepatol* **68**, 1033-1048, http://doi.org/10.1016/j.jhep.2017.11.026 (2018).

198 Dittmer, J. The biology of the Ets1 proto-oncogene. *Mol Cancer* **2**, 29, http://doi.org/10.1186/1476-4598-2-29 (2003).
199 De Val, S. *et al.* Mef2c is activated directly by Ets transcription factors through an evolutionarily conserved endothelial cell-specific enhancer. *Dev Biol* **275**, 424-434, http://doi.org/10.1016/j.ydbio.2004.08.016 (2004).
200 Shiota, M. *et al.* Ets regulates peroxiredoxin1 and 5 expressions through their interaction with the high-mobility group protein B1. *Cancer Sci* **99**, 1950-1959, http://doi.org/10.1111/j.1349-7006.2008.00912.x (2008).
201 Sinh, N. D., Endo, K., Miyazawa, K. & Saitoh, M. Ets1 and ESE1 reciprocally regulate expression of ZEB1/ZEB2, dependent on ERK1/2 activity, in breast cancer cells. *Cancer Sci* **108**, 952-960, http://doi.org/10.1111/cas.13214 (2017).
202 Heubach, J. *et al.* The long noncoding RNA HOTAIR has tissue and cell type-dependent effects on HOX gene expression and phenotype of urothelial cancer cells. *Mol Cancer* **14**, 108, http://doi.org/10.1186/s12943-015-0371-8 (2015).
203 Rinn, J. L. *et al.* Functional demarcation of active and silent chromatin domains in human HOX loci by noncoding RNAs. *Cell* **129**, 1311-1323, http://doi.org/10.1016/j.cell.2007.05.022 (2007).
204 Xiang, Z. *et al.* A novel human zinc finger protein ZNF540 interacts with MVP and inhibits transcriptional activities of the ERK signal pathway. *Biochem Biophys Res Commun* **347**, 288-296, http://doi.org/10.1016/j.bbrc.2006.06.076 (2006).
205 Wang, J., Chen, W., Wei, W. & Lou, J. Oncogene TUBA1C promotes migration and proliferation in hepatocellular carcinoma and predicts a poor prognosis. *Oncotarget* **8**, 96215-96224, http://doi.org/10.18632/oncotarget.21894 (2017).
206 Cerami, E. *et al.* The cBio cancer genomics portal: an open platform for exploring multidimensional cancer genomics data. *Cancer Discov* **2**, 401-404, http://doi.org/10.1158/2159-8290.CD-12-0095 (2012).
207 Tsherniak, A. *et al.* Defining a Cancer Dependency Map. *Cell* **170**, 564-576 e516, http://doi.org/10.1016/j.cell.2017.06.010 (2017).
208 Brenna, O. *et al.* The guanylate cyclase-C signaling pathway is down-regulated in inflammatory bowel disease. *Scand J Gastroenterol* **50**, 1241-1252, http://doi.org/10.3109/00365521.2015.1038849 (2015).
209 Guzman, C. *et al.* The human liver fatty acid binding protein (FABP1) gene is activated by FOXA1 and PPARalpha; and repressed by C/EBPalpha: Implications in FABP1 down-regulation in nonalcoholic fatty liver disease. *Biochim Biophys Acta* **1831**, 803-818, http://doi.org/10.1016/j.bbalip.2012.12.014 (2013).
210 Vivian, J. *et al.* Toil enables reproducible, open source, big biomedical data analyses. *Nat Biotechnol* **35**, 314-316, http://doi.org/10.1038/nbt.3772 (2017).
211 Robinson, M. D., McCarthy, D. J. & Smyth, G. K. edgeR: a Bioconductor package for differential expression analysis of digital gene expression data. *Bioinformatics* **26**, 139-140, http://doi.org/10.1093/bioinformatics/btp616 (2010).
212 Ritchie, M. E. *et al.* limma powers differential expression analyses for RNA-sequencing and microarray studies. *Nucleic Acids Res* **43**, e47, http://doi.org/10.1093/nar/gkv007 (2015).

213 Law, C. W., Chen, Y., Shi, W. & Smyth, G. K. voom: Precision weights unlock linear model analysis tools for RNA-seq read counts. *Genome Biol* **15**, R29, http://doi.org/10.1186/gb-2014-15-2-r29 (2014).
214 Wickham, H. *ggplot2 Elegant Graphics for Data Analysis*. 213 (Springer-Verlag New York, 2009).
215 Langmead, B. & Salzberg, S. L. Fast gapped-read alignment with Bowtie 2. *Nat Methods* **9**, 357-359, http://doi.org/10.1038/nmeth.1923 (2012).
216 Harder, E. *et al.* OPLS3: A Force Field Providing Broad Coverage of Drug-like Small Molecules and Proteins. *J Chem Theory Comput* **12**, 281-296, http://doi.org/10.1021/acs.jctc.5b00864 (2016).
217 Friesner, R. A. *et al.* Extra precision glide: docking and scoring incorporating a model of hydrophobic enclosure for protein-ligand complexes. *J Med Chem* **49**, 6177-6196, http://doi.org/10.1021/jm051256o (2006).
218 Chenge, J. T. *et al.* Structural Characterization and Ligand/Inhibitor Identification Provide Functional Insights into the Mycobacterium tuberculosis Cytochrome P450 CYP126A1. *J Biol Chem* **292**, 1310-1329, http://doi.org/10.1074/jbc.M116.748822 (2017).
219 Bui, S. H. *et al.* Unusual spectroscopic and ligand binding properties of the cytochrome P450-flavodoxin fusion enzyme XplA. *J Biol Chem* **287**, 19699-19714, http://doi.org/10.1074/jbc.M111.319202 (2012).
220 Morrison, J. F. Kinetics of the reversible inhibition of enzyme-catalysed reactions by tight-binding inhibitors. *Biochim Biophys Acta* **185**, 269-286, http://doi.org/10.1016/0005-2744(69)90420-3 (1969).
221 Gustafsson, M. C. *et al.* Expression, purification, and characterization of Bacillus subtilis cytochromes P450 CYP102A2 and CYP102A3: flavocytochrome homologues of P450 BM3 from Bacillus megaterium. *Biochemistry* **43**, 5474-5487, http://doi.org/10.1021/bi035904m (2004).
222 Khatamian, A., Paull, E. O., Califano, A. & Yu, J. SJARACNe: a scalable software tool for gene network reverse engineering from big data. *Bioinformatics* **35**, 2165-2166, http://doi.org/10.1093/bioinformatics/bty907 (2019).
223 Livak, K. J. & Schmittgen, T. D. Analysis of relative gene expression data using real-time quantitative PCR and the 2(-Delta Delta C(T)) Method. *Methods* **25**, 402-408, http://doi.org/10.1006/meth.2001.1262 (2001).
224 Ung, Y. T., Ong, C. E. & Pan, Y. Current High-Throughput Approaches of Screening Modulatory Effects of Xenobiotics on Cytochrome P450 (CYP) Enzymes. *High Throughput* **7**, 4-29, http://doi.org/10.3390/ht7040029 (2018).
225 Seliskar, M. & Rozman, D. Mammalian cytochromes P450--importance of tissue specificity. *Biochim Biophys Acta* **1770**, 458-466, http://doi.org/10.1016/j.bbagen.2006.09.016 (2007).
226 Novotna, A. *et al.* Dual effects of ketoconazole cis-enantiomers on CYP3A4 in human hepatocytes and HepG2 Cells. *PLoS One* **9**, e111286, http://doi.org/10.1371/journal.pone.0111286 (2014).
227 Xue, Y. *et al.* Computational insights into the different catalytic activities of CYP3A4 and CYP3A5 toward schisantherin E. *Chem Biol Drug Des* **93**, 854-864, http://doi.org/10.1111/cbdd.13475 (2019).

228 Niwa, T., Yasumura, M., Murayama, N. & Yamazaki, H. Comparison of catalytic properties of cytochromes P450 3A4 and 3A5 by molecular docking simulation. *Drug Metab Lett* **8**, 43-50 (2014).
229 Sevrioukova, I. F. & Poulos, T. L. Current Approaches for Investigating and Predicting Cytochrome P450 3A4-Ligand Interactions. *Adv Exp Med Biol* **851**, 83-105, http://doi.org/10.1007/978-3-319-16009-2_3 (2015).
230 McLean, K. J. *et al.* Azole antifungals are potent inhibitors of cytochrome P450 mono-oxygenases and bacterial growth in mycobacteria and streptomycetes. *Microbiology* **148**, 2937-2949, http://doi.org/10.1099/00221287-148-10-2937 (2002).
231 Rajput, S. *et al.* Structure-Activity Relationships of cyclo(l-Tyrosyl-l-tyrosine) Derivatives Binding to Mycobacterium tuberculosis CYP121: Iodinated Analogues Promote Shift to High-Spin Adduct. *J Med Chem* **62**, 9792-9805, http://doi.org/10.1021/acs.jmedchem.9b01199 (2019).
232 Matthews, S. *et al.* Catalytic Determinants of Alkene Production by the Cytochrome P450 Peroxygenase OleTJE. *J Biol Chem* **292**, 5128-5143, http://doi.org/10.1074/jbc.M116.762336 (2017).
233 Fernando, H., Halpert, J. R. & Davydov, D. R. Resolution of multiple substrate binding sites in cytochrome P450 3A4: the stoichiometry of the enzyme-substrate complexes probed by FRET and Job's titration. *Biochemistry* **45**, 4199-4209, http://doi.org/10.1021/bi052491b (2006).
234 Wynalda, M. A. & Wienkers, L. C. Assessment of potential interactions between dopamine receptor agonists and various human cytochrome P450 enzymes using a simple in vitro inhibition screen. *Drug Metab Dispos* **25**, 1211-1214 (1997).
235 de Wildt, S. N., Kearns, G. L., Leeder, J. S. & van den Anker, J. N. Cytochrome P450 3A: ontogeny and drug disposition. *Clin Pharmacokinet* **37**, 485-505, http://doi.org/10.2165/00003088-199937060-00004 (1999).
236 Jiang, F. *et al.* CYP3A5 Functions as a Tumor Suppressor in Hepatocellular Carcinoma by Regulating mTORC2/Akt Signaling. *Cancer Res* **75**, 1470-1481, http://doi.org/10.1158/0008-5472.CAN-14-1589 (2015).

VITA

William ("Charlie") Wright was born in 1989 in Memphis, TN to Mike and Stephanie Wright. He grew up in Olive Branch, Mississippi and graduated from Olive Branch High School in 2008. He went on to NorthWest Mississippi Community College in Senatobia Mississippi and received his Associate degree of Biology in 2010. He earned his Bachelor of Science in 2013 from the University of Memphis, also in Biology. During his undergraduate career, Charlie gained wet and dry lab experience in the Department of Bioinformatics. He then pursued graduate education at the University of Tennessee Health Science Center. He graduated with a Master of Science in 2016 in Laboratory Research and Management. During this time, he began his research focusing on drug metabolism proteins and cancer in the laboratory of Dr. Taosheng Chen at St. Jude Children's Research Hospital in the Department of Chemical Biology and Therapeutics. He stayed in the Chen lab to pursue his terminal degree, studying ways to selectively target CYP3A5 in cancer. He was admitted into the Ph.D. program at UTHSC in January of 2017, in the Biomedical Sciences program with a concentration in Cancer and Developmental Biology. Charlie anticipates graduation with a Doctor of Philosophy degree in June 2020.